SUBMARINE GROUNDWATER DISCHARGE AND NUTRIENT INPUT TO A SEMIARID AND HYPERSALINE ESTUARY: BAFFIN BAY, TEXAS

A Thesis

by

CODY V. LOPEZ

BS, Texas A&M University – Corpus Christi, 2016

Submitted in Partial Fulfillment of the Requirements for the Degree of

MASTER OF SCIENCE

in

ENVIRONMENTAL SCIENCE

Texas A&M University-Corpus Christi
Corpus Christi, Texas

December 2018

December 2018

SUBMARINE GROUNDWATER DISCHARGE AND NUTRIENT INPUT TO A SEMIARID AND HYPERSALINE ESTUARY: BAFFIN BAY, TEXAS

A Thesis

by

CODY V. LOPEZ

This thesis meets the standards for scope and quality of
Texas A&M University-Corpus Christi and is hereby approved.

Dorina Murgulet, PhD
Chair

Joseph Felix, PhD
Committee Member

Xinping Hu, PhD
Committee Member

December 2018

ABSTRACT

This study evaluates the role of submarine groundwater discharge (SGD)-derived nutrients to Baffin Bay, a semi-arid, hypersaline bay in south Texas. SGD can be equivalent to riverine input in some places, making SGD's role in nutrient input important. Dissolved inorganic nitrogen (DIN), and total alkalinity combined with SGD measurements, using two different geochemical tracers (radium-226 [^{226}Ra], radium 224 [^{224}Ra] and radon [^{222}Rn]) and geophysical investigations were conducted. SGD rates were found to have slight spatial variation with higher rates near the shoreline around areas characterized by course-grained sediments and relic serpulid reefs. The^{222}Rn and ^{226}Ra-based SGD estimates produced agreeable results, within the range of uncertainties, and no significant changes in SGD from July to November, within the same year, were observed. However, ^{226}Ra and ^{224}Ra activities decreased from July to November and are associated with large decreases in porewater DIN concentrations. July and November ^{222}Rn-derived SGD rates were 31.4±32.7 and 30.0±30.9 cm·d^{-1}, respectively while those derived from ^{226}Ra were 16.6±1.7 and 13.2±1.3 cm·d^{-1}, respectively. Given the lack of change in SGD between the two seasons, organic matter (OM) decay may be the driving force for changes in radium activities as it can lead to reducing conditions that enhance radium solubility from sediments. In addition to OM remineralization from phytoplankton, a shift from a seawater to a terrestrial groundwater source in the subterranean estuary is also likely to be responsible for the larger porewater radium activities and nutrient concentrations in July. A comparison of bay-wide solute fluxes indicates that DIN inputs, mainly in the form of ammonium (NH_4^+), are almost five orders of magnitude higher in the SGD component than the surface runoff. Therefore, regardless of the magnitude of SGD and its nature (i.e. fresh or saline; groundwater or recirculated saline), the associated nutrient input is likely significant in this shallow bay system in warmer months. This study helps provide an understanding of the possible effects of OM decay on radium and DIN fluctuations and inputs in a hypersaline estuary. Studying these relationships is important as hypersalinity is a developing problem in freshwater-limited environments.

TABLE OF CONTENTS

LIST OF FIGURES

FIGURES PAGE

LIST OF TABLES

TABLES PAGE

1. INTRODUCTION

In many arid and semiarid regions, wetlands and estuaries experience prolonged periods of hypersalinity (Jolly et al., 2008), in part due to anthropogenic impacts (i.e. limited freshwater inflows due to stream impairments) (Conley et al., 2009; Folk and Siedlecka, 1974; Jolly et al., 2008), which could hinder their ability to cycle nutrients (e.g., slowing the rate of nitrification) leading to eutrophication (Folk and Siedlecka, 1974; Jolly et al., 2008). Some nutrient cycling processes are expected to decrease as salinities change from below (fresh or brackish) to above (hypersaline) the average salinity of seawater (salinities are reported in practical salinity units using the global ocean seawater average salinity of 35 as reference (Millero, 1993)) (Conley et al., 2009; Loáiciga, 2006). For instance, apart from some rare cases, planktonic nitrogen (N) fixation is reported to be insignificant in coastal estuaries with salinities above 10 (Conley et al., 2009) and salinities above 10 can reduce nitrification/denitrification in sediments by 50% compared to salinities of 0 (Rysgaard et al., 1999). However, during removal of N from wastewater, denitrification has been found to occur at 40°C and a salinity of approximately 54 in a bioreactor (Glass and Silverstein, 1999; Kristensen and Jepsen, 1991), conditions that may occur naturally in semiarid estuaries. For instance, within this study's area, Baffin Bay, Texas, historic climate data for the past decade shows that though rare (0.3% of the year) the temperature reached or exceeded 40°C (NAAS, 2017). In addition, bay salinity ranges from monthly averages of 40 to 50 to as high as 85 during a historic drought (Behrens, 1966), with (seldom) flood events bringing salinity to as low as 1.4 (Folk and Siedlecka, 1974).

Nitrogen enters estuarine systems through a variety of pathways including: atmospheric deposition, surface runoff (land and riverine), biological fixation, remineralization of decaying organic matter (OM), and submarine groundwater discharge (SGD). Moore (2010) described

SGD as, “any and all flow of water on continental margins from the seabed to the coastal ocean, with scale lengths of meters to kilometers, regardless of fluid composition or driving force.” Thus, SGD includes terrestrial groundwater and recirculated seawater (Santos et al., 2012). In the estuarine and coastal ocean setting, groundwater can be a significant source of inorganic N to local ecosystems (Chaillou et al., 2014; Matson, 1993; Paerl, 1997) and may provide up to 30% of the non-recycled N (or new N) in the nutrient budget (Paerl, 1997). Giblin and Gaines (1990) found that N inputs from groundwater were similar in magnitude to riverine inputs in a river-dominated estuary. Even under low magnitudes of groundwater input (i.e. terrestrial), recirculated seawater can be a significant source of nutrients and anoxic waters to the water column (Santos et al., 2012). In bays with limited freshwater inflows and poor connection to a larger body of water, or rainfall that is significantly less than the local evaporation rate (i.e. Baffin Bay, Texas), submarine groundwater discharge (SGD) could influence the salinity of the local environment (Jolly et al., 2008) in addition to being an important source of nutrients.

Semiarid estuarine systems receive limited riverine inflows and in the absence of nutrient inputs from surface runoff, SGD could control primary productivity and lead to excessive algal growth or harmful algal blooms, especially in systems with long residence times (Hu et al., 2006; Jolly et al., 2008; Kroeger et al., 2007). For instance, anoxic conditions in the porewater coincident with low SGD conditions could lead to the buildup of ammonium (NH_4^+) from organic matter remineralization, or dissimilatory nitrate reduction to ammonia (DNRA) (Brandes et al., 2007; Prokopenko et al., 2011; Schulz et al., 1994). NH_4^+ can later be released to the water column as SGD rates increase (including both groundwater/terrestrial and recirculated seawater) (Brock, 2001; Moore, 1996). Increasing salinity levels in semiarid estuaries can affect the N cycle (Giblin et al., 2010; Holmes et al., 2000). For instance, NH_4^+ release from sediment is

dependent on salinity, with lower salinities effectively storing NH_4^+ in sediments and higher salinities releasing NH_4^+, which may enhance summertime primary productivity (Giblin et al., 2010; Holmes et al., 2000) as observed in areas with increasing salinities from 0-20 (Giblin et al., 2010). Nevertheless, the role SGD plays on N cycling in these semiarid, hypersaline environments is not fully known. This study hypothesizes that in hypersaline estuaries with almost no surface inflows, porewater contributions via SGD are significant sources of nutrients, and thus primary productivity.

The extent of SGD and its role in releasing nutrients of terrestrial or remineralized origin is not fully understood in estuaries experiencing limited surface runoff, high evaporation rates and hypersaline conditions for most of the year. Since nutrient cycling rates and bioavailability in semiarid bays with long residence times can be highly influenced by SGD derived nutrients and salinity levels, among other factors, it is important to understand the role SGD plays as a source of nutrients of terrestrial or remineralized origin. This study evaluates the effects of porewater flushing rates and SGD magnitudes (both quality, i.e. saline versus fresh, and quantity) on nutrient sources to Baffin Bay, Texas, a hypersaline, semi-enclosed estuary, which has previously experienced a harmful algal bloom that lasted eight years (Buskey et al., 2001). The relative abundances of nutrients in the bay and porewater, such as phosphorus, silica, and the different forms of nitrogen were examined to evaluate types of nutrient inputs, i.e. terrestrial versus remineralized.

More specifically, the main objectives of this study were to: 1) measure sediment flushing and SGD rates, 2) determine the role of SGD-derived nutrient fluxes to the bay in relation to surface inputs, and 3) determine the effect of sediment flushing and SGD rates on the dominant form and amount of nutrients discharging into the bay. This work is critically

important for understanding nutrient dynamics not only in Texas estuaries but in semiarid and hypersaline estuaries in general.

2. STUDY AREA

This study focused on the shallow, well-mixed Baffin Bay system, located in southern Texas (**Figure 1**), bordered by Kleberg County to the north and Kennedy County to the south, on the semiarid Texas coastal plain in the northwestern Gulf of Mexico (Dalrymple, 1964; Simms et al., 2010). The bay is often considered a reverse estuary (i.e. more saline than the bay it drains into) due to limited freshwater inflows from surface runoff, high evaporation rates, and limited connection with the Gulf of Mexico, which result in long residence times, greater than 1 year, and extreme salinities, up to 75-85 (Behrens, 1966; Folk and Siedlecka, 1974; Wetz et al., 2017). The bay is considered a schizohaline environment in that it changes from freshwater salinities to hypersaline conditions repeatedly over time (Folk and Siedlecka, 1974). The effects that hypersalinity has in this environment are applicable to other semiarid or schizohaline environments where salinity is likely to be high for prolonged periods due to limited freshwater inflows or the lack of precipitation and/or high evaporation rates (Jolly et al., 2008).

The estuary provides essential habitat for numerous commercially and recreationally important marine species. The predominantly undeveloped land use surrounding Baffin Bay results in more pristine conditions compared to the Nueces Estuary system. However, there are emerging concerns that the ecological health of this vital habitat is threatened by water quality degradation, specifically pertaining to persistent brown tides (Wetz et al., 2017).

A previous study by Rebich et al. (2011) in a large area that included Baffin Bay ranked, from largest to smallest, the sources of external N to the area as: 1) atmospheric deposition, 2) fertilizer, 3) manure from livestock, 4) urban runoff from developed land, and 5) industrial and

municipal point sources. This study did not account for groundwater inputs although it has been shown to be a likely contributor of external N to the bay (Breier et al., 2010; Santos et al., 2012; Uddameri et al., 2013). The relative contributions of each source are dependent on hydroclimatic conditions and thus are expected to shift with changes in precipitation and return flows. For instance, during drought conditions some of the tributaries often run dry while others, such as the San Fernando Creek, which has 12 permitted wastewater facilities and likely is dominated by point source N (Wetz et al., 2017), flow perpetually and could contribute a continuous source of N and other nutrients. The typical concentrations of NO_x (NO_2+NO_3) in Baffin Bay range from <0.3 µM to 35 µM with an average concentration of <1-4 µM, and NH_4^+ concentrations ranged from 7 µM to 92 µM in surface water over the years 2013-2015 (Wetz, 2015). According to Wetz (2015), surface water DON regularly exceeded 35 µM.

2.1. HYDROCLIMATIC CHARACTERISTICS

In the area of Baffin Bay, the coastal plain gradient is very gentle, approximately 0.8 $m \cdot km^{-1}$ (Simms et al., 2010), leading to low land runoff and likely high infiltration rates into soils and recharge to the water table aquifer (Fetter, 2001). The shoreline in the upper reaches of Baffin Bay consists of bluffs 2 to 4 m high that grade down to tidal flats along the lower portion of the shoreline. The bay is isolated from the Gulf of Mexico by Padre Island and is further insulated from the contiguous Laguna Madre System by shallow reefs at the mouth of the bay (Simms et al., 2010). The nearest inlets that allow for exchange between Baffin Bay and the Gulf of Mexico are Packery Channel and Aransas Pass (~41 km and ~70 km north of Baffin Bay, respectively) and Port Mansfield (~80 km south) (Wetz et al., 2017). Three creeks discharge into Baffin Bay: the San Fernando flowing into Cayo del Grullo, the Petronila flowing into Alazan Bay, and the Los Olmos into Laguna Salada (**Figure 1**). These creeks are believed to have

carved the valley that now forms Baffin Bay in response to the last sea level drop approximately 20,000 years ago (Behrens, 1963; Fisk, 1959; Simms et al., 2010).

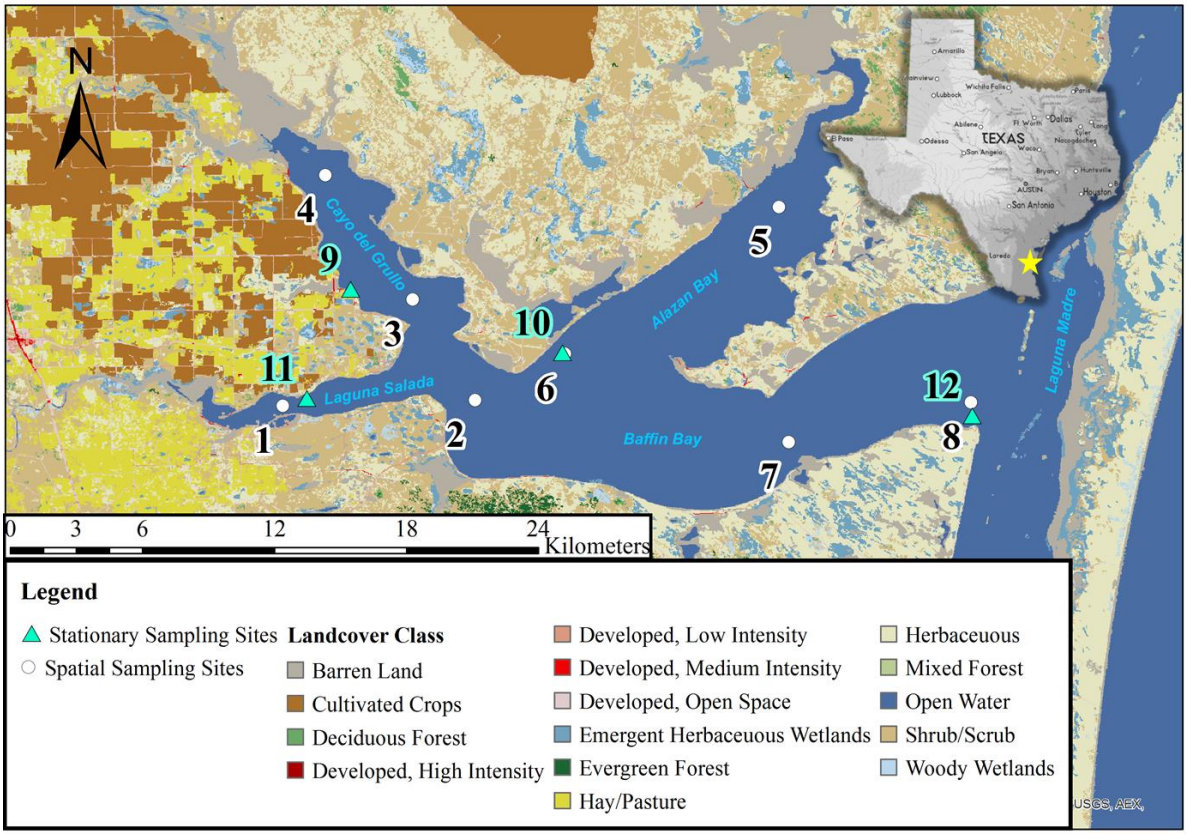

Figure 1: Study area location map including: the land use and land cover data for the Baffin Bay surroundings and the spatial (stations 1-8) and time series (9-12) sampling stations.

The semiarid area of south Texas is characterized by high evaporation rates that exceed precipitation (60-80 cm·yr^{-1}) by 60 cm annually (Behrens, 1966). This leads to average salinities of 40-50 and extremes as high as 85 during droughts and as low as 1.4 during the seldom significant precipitation events (Behrens, 1966; Simms et al., 2010). Streamflow discharge data to Baffin Bay from its tributaries is limited; however, the freshwater inflow to and from the creeks is infrequent, thus contributing to the generally high salinities and long residence times (**Figure 2**). Data from 1967-2017 (collected approximately 40 km inland from the bay) indicates that the Los Olmos Creek discharges on average 0.004 m^3·s^{-1} (min: 0.0 m^3·s^{-1}, max: 1.33 m^3·s^{-1})

(USGS, 2017b). From 1965 to 2017, streamflow data collected from a stream gauge approximately 60 km inland from the bay, an average of 0.02 $m^3 \cdot s^{-1}$ (min: 0.00 $m^3 \cdot s^{-1}$, max: 0.34 $m^3 \cdot s^{-1}$) discharged from the San Fernando Creek (USGS, 2017a) to the bay. No data were found for Petronila Creek.

Strong southeast winds of 16 to 32 $km \cdot h^{-1}$ are dominant from February to August (Dalrymple, 1964; Rusnak, 1960); however, from September to February, the dominant wind direction shifts to the northwest with an average speed of 18 $km \cdot h^{-1}$ (Lohse, 1955; TCOON, 2016). Baffin Bay is a shallow estuary with an average depth of 2 m (max: 3 m) (Simms et al., 2010) that experiences only small astronomical tides (<0.1 m) (Simms et al., 2010). With the strong, persistent winds and shallow depths, the tides are mainly controlled by wind and precipitation events (Breuer, 1957; Militello, 1998). Consequently, the semi-enclosed estuary is generally well-mixed with little stratification under normal conditions.

The major sediment types found in Baffin Bay are black-mud, ooids, quartz-mollusk sands, and coated grains (Alaniz and Goodwin, 1974; Dalrymple, 1964). The well-laminated carbonate and siliciclastic open-bay muds, ooid beaches, shelly internal spits and barrier islands, serpulid worm tube reefs, and prograding upper-bay mudflats depositional environments differentiate this system from other northern Gulf of Mexico bays (Simms et al., 2010). Sediment transport to Baffin Bay by modern aeolian dunes is limited to the seldom intense precipitation events, especially along the south shore (Simms et al., 2010). Calcite formation around the shoreline acts as a shoreline stabilizer (Behrens, 1963; Driese et al., 2005; Price, 1936) that allowed Baffin Bay to retain its dendritic shape (**Figure 1**).

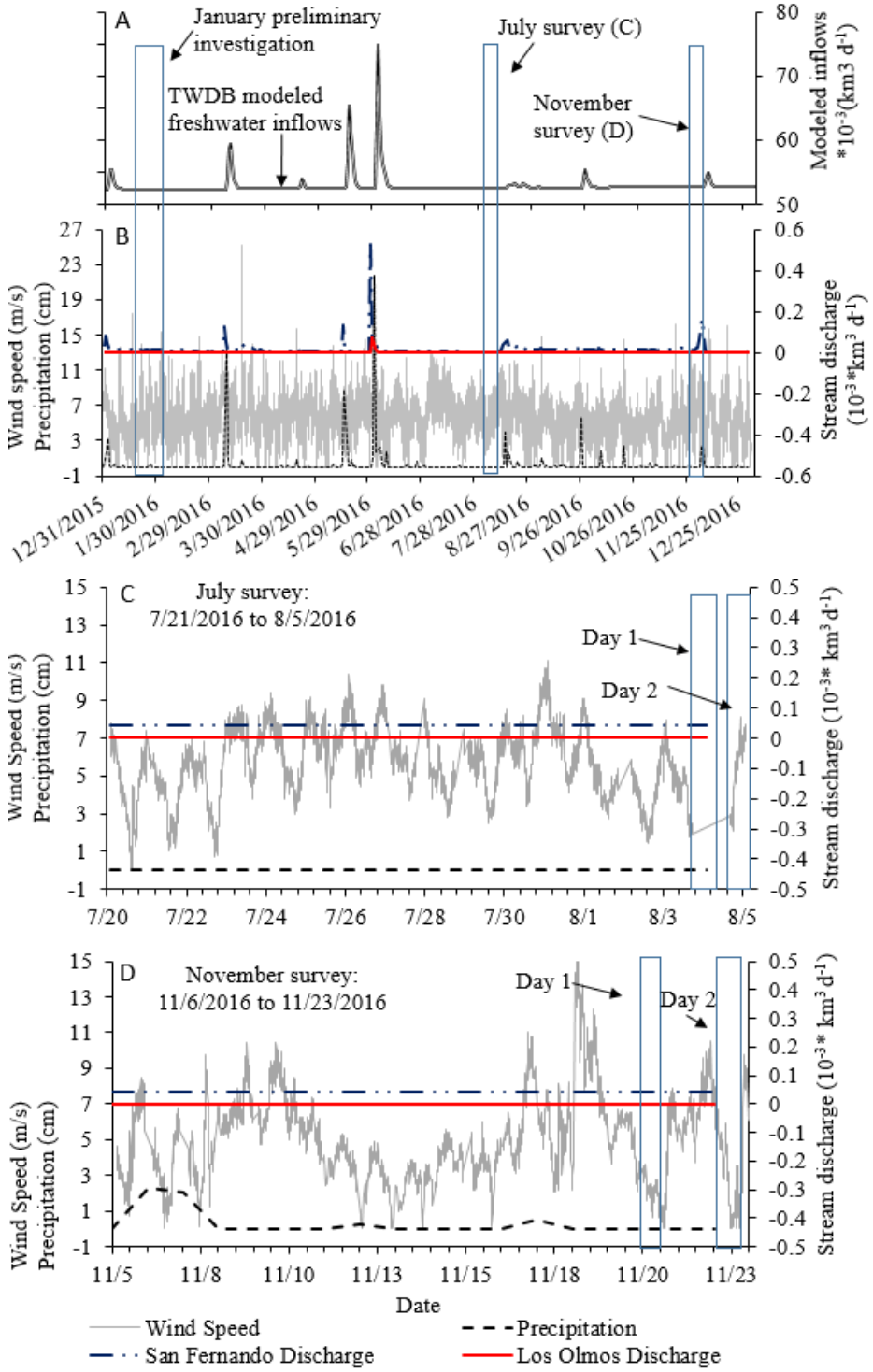

Figure 2: A) and B) (top graph) Wind speed ($m \cdot s^{-1}$), precipitation (mm), discharge from San Fernando Creek ($km^3 \cdot d^{-1}$), and discharge from Los Olmos Creek plotted versus time (i.e. 2016). C) (middle graph) The two weeks leading up to and including the days of the July sampling event were dry and had steadily rising winds. D) (bottom graph) The two weeks leading up to and including the days of the November sampling event were slightly wetter than July and sampling was performed during days of lower wind speed. Data from USGS 2017a, 2017b.

Previous studies in the South Texas area (Breier et al., 2010; Nyquist et al., 2008; USDA, 2012; Waterstone and Parsons, 2003) as well as the hydraulic conditions indicate that groundwater flows toward the coast, eventually discharging into the bays and estuaries; however, Baffin Bay receives significantly less precipitation than systems further north and when associated with the significant groundwater drawdown around Kingsville (Shafer and Baker, 1973), deeper groundwater flow toward the coast may be limited. The Gulf Coast Aquifer (GCA) is a leaky artesian aquifer comprised of a complex of clays, silts, sands, and gravels (Ashworth and Hopkins, 1995) that form the Chicot, Evangeline, and Jasper aquifers (Waterstone and Parsons, 2003). The Baffin Bay estuary and the surrounding systems are generally in direct contact with the Chicot aquifer, which is the shallowest of the mentioned aquifers. The stratigraphic units of the Chicot aquifer consist of an overlying alluvial formation preceded by Beaumont and Lissie formations (Ashworth and Hopkins, 1995), which are generally composed of clays and clayey silts with intermittent sand and gravel lenses that continue out into the Gulf of Mexico (Waterstone and Parsons, 2003). The maximum total sand thickness of the GCA ranges from 200 m in the south to 400 m in the north with an average freshwater saturated thickness of about 300 m (George et al., 2011). Brackish groundwater is more common than fresh groundwater in the southern GCA where water quality declines and total dissolved solids of 1,000 $mg \cdot L^{-1}$ or more are common (George et al., 2011).

3. METHODS

3.1 PRELIMINARY INVESTIGATION

The project started with a reconnaissance survey of the study area in which water-based continuous electrical resistivity profiling (CRP) was used to locate possible groundwater upwelling zones (or SGD). For a detailed description of the CRP methodology see Douglas et al.

(2017) and Murgulet et al. (2016). In brief, the Advanced Geosciences, Inc. SuperStingR8 Marine system with patented graphite electrodes and induced polarization imaging system and geophysical interpretive tools were used to evaluate the types of lithology and porewater with differing resistivity/electrical conductivity, to map out groundwater seepage faces. The system was equipped with a 112 m cable consisting of 56 graphite electrodes spaced 2 m apart. The depth of penetration for this system is about 20% of the total length of the electrode cable, or ~ 22 m deep, with a resolution of 50% of the electrode spacing (i.e. 2 m spacing and 1 m spatial resolution) (Advanced Geosciences, 2017). CRPs were collected in January 2016 along three transects: 1) Laguna Madre to the head of Laguna Salada through the southern half of the bay, 2) the length of Alazan Bay, and 3) the length of Cayo del Grullo (**Figure 3**). These images helped determine the location and possible extents of SGD zones and aided in selecting eight spatial surface and porewater sampling and four SGD monitoring sites.

3.2 WATER SAMPLE COLLECTION

Aqueous samples were collected at eight stations during spatial and time-series sampling events in January, July and November 2016, from both surface water and porewater, whenever possible, to capture nutrient and biomass distribution and concentrations under different environmental conditions. Water samples from the surface (0.2 m below air-water interface) and bottom (0.2 m above sediment-water interface) were collected in compliance with standard sampling techniques (Brown et al., 1970; RCRA SOP, 2009; Wood, 1976). The water depth was measured at each location using a pre-labeled line attached to a weight. Field parameters were measured before sample collection using a YSI multiparameter water quality meter, which was placed at each sampling depth within the water column for several minutes to reach stable

conditions (i.e. stable temperature, dissolved oxygen, or DO, pressure, etc.) before parameters were recorded.

Surface water samples were collected with a Van Dorn bottle deployed to the desired depth and given a few minutes to allow water to circulate through the cartridge, according to standard operating procedures (TCEQ, 2012). All sampling bottles were rinsed three times and then overfilled, capped, and placed on ice, depending on the required procedure for each analyte. For dissolved gas samples (i.e. ^{222}Rn, DIC, TA) a rubber tube used to transfer the sample was placed at the bottom of the bottle to minimize air exposure. Porewater was collected at each site by inserting a push-tip piezometer (AMS Retract-a-Tip) connected through silicone tubing to a peristaltic pump about 0.7 to 3.2 m below the sediment-water interface (i.e. deep enough to prevent bottom waters from contaminating porewater sample (RCRA SOP, 2009). Before sample collection, the tubing was flushed until the sample was clear (or a minimum amount of sediment was present in the sample) and the field parameters (i.e. salinity, temperature, pH) stabilized. Groundwater samples were collected from available wells within the local watershed screened at depths between 187-383 m. Before sample collection, the wells were purged of three well volumes or until field parameters stabilized.

3.2.1 TOTAL ALKALINITY AND DISSOLVED INORGANIC CARBON

Total alkalinity (TA) and dissolved inorganic carbon (DIC) samples were collected in 250 mL borosilicate bottles (with gas-tight caps) with no head space and preserved using 100 µL of saturated $HgCl_2$ (Kattner, 1999). Measurements of TA were conducted using a Titrando automatic titrator (Metrohm, Switzerland) with a pH electrode. Hydrochloric acid (HCl) was used as the titrant with a concentration of approximately 0.1 M. Multiple runs were conducted to reach a precision of 0.1% (Cyronak et al., 2013). DIC samples, measured by an Apollo SciTech

DIC analyzer, were brought to a temperature of 22°C by a water bath and the concentration was calculated using standard curve based on certified reference material, and by quantifying carbon dioxide released through reactions with acid (Dickson et al., 2007).

3.2.2 NUTRIENT AND CHLOROPHYLL-A SAMPLING

Nutrient and chlorophyll-α (chl-α) water samples were collected in acid-washed amber polycarbonate bottles using the techniques mentioned above. Bottles were stored on ice until return to a shore-based facility where processing of samples occurred, and analyses were conducted for chlorophyll-α (surface water) and inorganic nutrients (nitrate (NO_3^-), nitrite (NO_2^-), ammonium (NH_4^+), orthophosphate (HPO_4^{2-}), silicate ($HSiO_3^-$)) and organic nutrients (dissolved organic carbon (DOC))(surface water and porewater). Chl-α was determined from samples collected on, and extracted from, Whatman GF/F filters (nominal pore size 0.7 µm). Chl-α was extracted using methanol and analyzed fluorometrically (Welschmeyer, 1994). All nutrient samples were filtered with Whatman nuclepore track-etched hydrophilic polycarbonate membranes (nominal pore size 0.2 µm) and kept frozen until analysis.

Inorganic nutrients were determined from the filtrate using a Seal QuAAtro autoanalyzer. The method detection limit (MDL) was determined for each analyte and matrix by the EPA method detailed in 40 CFR Part 136, Appendix B (EPA, 2011), which is defined as the Student's t for 99% confidence level, times the standard deviation (σ) of seven replicate measurements of the same low level sample or spiked sample. The applicable concentration ranges of this method are defined by the concentration range of the calibration solution adjusted to the expected sample concentrations. Samples with concentrations exceeding the linear range (i.e. porewaters) were diluted and reanalyzed. The MDL (in µM) for the inorganic nutrients are: 0.11 for NO_3^-, 0.012 for NO_2^-, 0.057 for NH_4^+, 0.025 for HPO_4^{2-}, and 0.14 for $HSiO_3^-$.

Dissolved organic carbon (DOC) and total dissolved nitrogen (TDN) were determined from the filtrate using a Shimadzu TOC-V analyzer with nitrogen module. Dissolved organic nitrogen (DON) was estimated as the difference between TDN and inorganic nitrogen. The method detection limit is approximately 70 μM.

3.2.3 RADIOGENIC ISOTOPES

Samples for radium (Ra, radium-224 (^{224}Ra), radium-226 (^{226}Ra)) analysis were collected from surface water, porewater and groundwater. Surface water, when in reference to radium, was collected in three 20 L jugs (approximately 45 to 60 L total volume) at each of the spatial sampling sites using a sump pump positioned ~0.2 m above the sediment-water interface. Porewater and groundwater samples were collected in 2 L jugs using techniques presented in section 3.2. Radium was extracted by passing the samples through ~15 g manganese dioxide (MnO_2) impregnated acrylic fibers two times at a flow rate <1 L·min^{-1} (Dimova et al., 2007; Kim et al., 2001). The Mn-fibers were then rinsed thoroughly with Ra-free water to eliminate any salts or particulates. Next, the fibers were squeezed to reduce the water content to a water to fiber ratio of 0.3-1 g (i.e. 20-30 g wet weight) (Sun and Torgersen, 1998), placed in gas-tight cartridges and tested for ^{223}Ra (half-life, $t_{½}$: 11.4 days) and ^{224}Ra ($t_{½}$: 3.6 days) on a Radium Delayed Coincidence Counter (RaDeCC).

Activities of ^{224}Ra were measured within three days of collection, given the short half-life (Moore, 2006). After measurement of the short-lived isotopes, the fibers were flushed with nitrogen gas to remove any preexisting ^{222}Rn and sealed for >21 days to reach secular equilibrium before measurements of ^{226}Ra ($t_{½}$: 1,600 years) using a RAD-7 (Kim et al., 2001). The expected measurement uncertainty of radium isotopes using the RAD7 and RaDeCC is ≤10%. The resulting activities were corrected using a calibration curve determined from five standards provided by Dr. Peterson's laboratory at Coastal Carolina University.

Measurements of ^{222}Rn in surface water were conducted as both in-situ (i.e. on station time-series) and mobile continuous formats (moving along the same transects as the CRP, **Figure 4**) in July and November 2016. In-situ ^{222}Rn measurements were conducted at four stations (i.e. 9-12) each event at locations identified as areas of interest using images from the CRP (**Figure 3, Figure 4**) and based on accessibility.

Local groundwater wells and porewater were sampled for ^{222}Rn measurements to be used as possible endmembers for the SGD mass balance. The wells are part of the Baffin Bay watershed and are described further in section 4.3.1. Measurements of ^{222}Rn from 250 mL grab samples (porewater and terrestrial groundwater) were conducted using a Durridge RAD7 radon-in-air monitor with the soda bottle and WAT250 accessories and protocols, respectively (Lee and Kim, 2006). The accessories are used to sparge the gas from the water bringing it into a closed air loop and to the detector.

3.3 SUBMARINE GROUNDWATER DISCHARGE ESTIMATES

Rates of SGD were calculated from time-series ^{222}Rn, continuous ^{222}Rn (see section 3.1), and ^{226}Ra activities as described below. Estimates derived from the ^{222}Rn time-series offer in situ measurements of SGD over time while those from the continuous ^{222}Rn and spatial radium surveys provide a bay-wide estimate. Continuous ^{222}Rn estimates also help analyze the spatial distribution of SGD within the bay, but do not capture changes with time unless surveys are repeated over the same areas.

3.3.1 ^{222}*RN-DERIVED SUBMARINE GROUNDWATER DISCHARGE*

Radon is much more enriched in groundwater when compared to surface waters (typically 1,000-fold or greater) (Dimova et al., 2011). Because of its unreactive nature and short half-life ($t_{1/2}$ = 3.83 d), ^{222}Rn is an excellent tracer to identify areas of significant groundwater

discharge (Burnett and Dulaiova, 2003). Recent studies demonstrate that continuous radon measurements at one location over time (or time-series) could provide reasonably high-resolution data to evaluate temporal changes on surface water radon activities (Burnett and Dulaiova, 2003; Burnett et al., 2001).

Time-series measurements of ^{222}Rn were conducted at 4 selected locations. The automated radon system (RAD-7 and the RAD AQUA accessories) was placed at the end of each resistivity transect on the deck of the research vessel or pier. The monitoring system measures ^{222}Rn from a constant stream of water (driven by a peristaltic pump) which has an inlet held down in the moving water by a weight attached to the tubing, passing through an air-water exchanger. The exchanger distributes radon from a running flow of water to a closed air loop that feeds to the RAD-7 radon-in-air monitor. For continuous/spatial ^{222}Rn measurements, water from ~0.3 m above the sediment-water interface was pumped via a peristaltic pump to a RAD AQUA air-water exchanger and air was then pumped from the exchanger to three Durridge RAD-7 Radon-in-air detectors connected in sequence. The RAD-7s were set to 30-minute integration times and were offset by 10 minutes to allow for high spatial resolution (i.e. a ^{222}Rn measurement every 10 minutes) with moderate uncertainty. The water sample inlet was placed on the side of a boat, moving at a speed less than 4.0 km·hr^{-1}, to continuously sample and measure ^{222}Rn along the traveled path.

The continuous and time-series ^{222}Rn measurements were used to construct a mass balance to estimate SGD as described in detail by Burnett and Dulaiova (2003); Lambert and Burnett (2003); Smith and Robbins (2012), and references therein. Expressed mathematically, the total ^{222}Rn flux (F_{total}) at the station equals:

$$F_{total} = [z(\lambda A_{Rn} - \lambda A_{Ra})] + F_o - F_i - F_{sed} + F_{atm} \pm F_{mix} \quad (4)$$

where λA_{Rn} is the decay corrected activity of ^{222}Rn in water column, λA_{Ra} is the activity of ^{222}Rn due to production ^{226}Ra in the water column, z is the water depth, F_o is the offshore flux (flood tide), F_i is the inshore/nearshore flux (ebb tide), F_{sed} is the sediment flux, F_{atm} is the losses due to atmospheric evasion, and F_{mix} is the losses due to mixing processes. The main principle behind using continuous radon measurements to quantify groundwater discharge rates to surface waters is based on the inventory of ^{222}Rn over time accounting for losses/gains due to mixing with waters of different radon concentrations (i.e. low activity offshore waters), atmospheric evasion, and sediment inputs. Thus, changes over time, if any, can be converted to radon fluxes. Using the total flux (F_{total}) and the excess ^{222}Rn of the advecting fluids ($^{222}Rn_{GW}$) (which here is the activity of ^{222}Rn in porewater or local groundwater which is presumably discharging into the system), ^{222}Rn fluxes are converted to water fluxes (ω, $m \cdot s^{-1}$) (Burnett and Dulaiova, 2003):

$$\omega = \frac{F_{total}}{^{222}Rn_{GW}} \quad (5)$$

^{222}Rn-derived SGD Estimates. Monitoring of radon extended over 6 to 10 hours depending on location and weather conditions (e.g., at winds of more than 12 miles per hour bay conditions become very difficult for sampling and data collection). Consequently, tidal effects could not be fully addressed using the presented methods; however, given the microtidal characteristics of this system, tidal effects are expected to be minimal compared to wind-driven circulation (Santos et al., 2012). Nevertheless, changes in water levels of no more than 0.3 m within a day are recorded in this area due to tidal fluctuations (NOAA, 2014). It is assumed that the lower radon fluxes observed during the monitoring time are due to mixing with offshore waters of lower activity. The maximum absolute values of the observed negative fluxes during each time-series event at each location are used to correct radon fluxes for losses via mixing (Burnett and Dulaiova, 2003; Dulaiova et al., 2006).

Sediment-supported radon activities were measured using laboratory equilibration experiments from sediment cores (ranging from 21 cm to 62 cm deep) collected at each time-series station. The upper 50 cm of the sediment cores were sectioned in 10 cm increments. The first 2 cm of each section were used in sediment supported ^{222}Rn equilibration experiments as described by Corbett et al. (2000) and the next 5 cm were used for bulk density porosity measurements as described by (Fetter, 2001). The remaining sample from each increment was dried and kept for reference. Briefly, for sediment-supported ^{222}Rn measurements, sediment samples were placed into a 500 mL Erlenmeyer flask, with 400 mL of Ra-free bay water, sealed, allowed to reach equilibrium ^{222}Rn activity, and kept on a shaker table for >21days (5 times the $t_{1/2}$: 3.8 days). Afterward, samples were analyzed for ^{222}Rn activities, or sediment-supported ^{222}Rn used in calculation of both time-series and continuous SGD rates.

3.3.2 RADIUM SGD RATES

The ^{226}Ra-based SGD estimates, representative of the entire bay (Charette et al., 2001), were determined using the ^{226}Ra-based water ages, surface runoff (i.e. freshwater inflow estimates (TWDB, 2016), and the porewater ^{226}Ra measurements.

3.3.2.1 ACTIVITY RATIOS

Activity ratios (AR) for each station in Baffin Bay were determined by dividing the ^{224}Ra by ^{226}Ra activities as these isotopes had the most complete dataset and have been used in the past (Peterson et al., 2008). The activity ratios show which isotope was more abundant in the sampled waters (**Table 1)**.

3.3.2.2 RADIUM AGES

The laboratory experiments conducted using sediment cores show that the flux of dissolved Ra from bottom sediment alone are negligible for this study (see section 4.3.1).

Therefore, we can assume that the major input of Ra comes from SGD rather than from sediment diffusion or resuspension. Relative Ra age of the surface water, or the relative time (T_r) that has passed since the Ra first entered the system in a well-mixed estuary, and therefore has been separated from its radionuclide source, was calculated using the ratio of the short-lived (^{224}Ra) to the long-lived (^{226}Ra) isotopes using equation 1 from (Knee et al., 2011a):

$$T_r = \frac{AR_{GW} - AR_{CO}}{AR_{CO} \times \lambda_{224}} \quad (1)$$

where AR_{GW} is the initial activity ratio of discharging groundwater, AR_{CO} is the measured activity ratio at the station of interest, and λ_{224} is the decay constant (d^{-1}) for the short-lived ^{224}Ra isotope.

This equation assumes Ra activities and ARs are greatest in the Ra source (i.e. groundwater and sediment containing Ra) and in the receiving nearshore water, relative to offshore due to SGD input and desorption from sediments. Consequently, Ra activities and ARs should be decreasing as the water mass is moving away from the discharge point. This could occur due to two reasons: radioactive decay and mixing with more dilute offshore waters. This equation also assumes that Ra additions are occurring continuously over a wide area, in this case the Baffin Bay estuary with multiple groundwater discharge locations. The short-lived isotope (i.e. ^{224}Ra) is normalized to the long-lived isotope (i.e. ^{226}Ra) with activities that are expected to only decrease due to dilution. Because the half-life of ^{226}Ra is much longer ($t_{½}$ = 1,600 yr) with respect to mixing time, its decay rate may be neglected. Using the groundwater activity ratios as the source of Ra (i.e. water source), an estimate of the time since SGD occurred is provided.

The Ra age is not to be confused with the bay water residence time, which reflects the amount of time water resides in the bay before it is flushed out. They can however, provide some

knowledge related to how fast water moves through the porous media as they are used to calculate SGD rates as described by Swarzenski et al. (2007).

3.3.2.3 RADIUM MASS-BALANCE AND SUBMARINE GROUNDWATER DISCHARGE ESTIMATES

To estimate SGD from ^{226}Ra observations in Baffin Bay, an estuarine mass balance was developed to determine the excess ^{226}Ra (due to groundwater flux) in the bay. This includes all sources of radium other than groundwater, including tidal exchange, riverine input, desorption from riverine suspended sediments, and diffusion from bay bottom sediments (Moore, 1996). Expressed mathematically, excess ^{226}Ra ($^{226}Ra_{ex}$ [Bq·d^{-1}]) in the bay equals:

$$^{226}Ra_{ex} = \left[\frac{(^{226}Ra_{BB} - ^{226}Ra_{sea}) \times V_{bay}}{T_r}\right] - [^{226}Ra_r Q_r] - [^{226}Ra_{des} Q_r] \qquad (2)$$

where $^{226}Ra_{BB}$ is the average measured ^{226}Ra activity in Baffin Bay; $^{226}Ra_{sea}$ is the average ^{226}Ra activity in the offshore water body (i.e. Laguna Madre), which exchanges tidally with Baffin Bay; V_{bay} is the volume of Baffin Bay; T_r is the residence time, or flushing rate, estimated from the apparent Ra water ages (i.e. equation 1); Q_r is the average total discharge rate of the tributaries to the bay; $^{226}R_r$ is the average ^{226}Ra activity of the tributaries; and $^{226}Ra_{des}$ is the activity of ^{226}Ra desorbed by the sediments in the bay (Swarzenski, 2007). After accounting for all the previously mentioned sources of ^{226}Ra, it is assumed that the excess activity from equation (2) is the result of SGD. Thus, using a porewater endmember activity ($^{226}Ra_{PW}$), SGD is calculated from:

$$SGD_{^{226}Ra} = \frac{^{226}Ra_{ex}}{^{226}Ra_{PW}} \qquad (3)$$

Radium desorption experiments were conducted using riverbed sediment samples (i.e. 0-10 cm) from what could be considered the freshwater portion of each creek. Los Olmos Creek had a consistently high salinity (>60), which should cause desorption of any sediment bound

^{226}Ra and was therefore not considered as a source for suspended sediment-bound ^{226}Ra (Webster et al., 1995). Low salinity creek water (San Fernando: 2.63 and Petronila: 9.85) samples and high salinity bay water (55) were filtered through Whatman GF/F filters to remove suspended solids and processed through MnO_2 fibers to reach Ra-free status. Different salinity solutions of Ra-free creek and bay water were prepared to match bay salinities at the time of sample collection (January: 32, July: 37, November: 51). A known mass of dried sediments was added to a known volume of the Ra-free solutions in proportions mimicking naturally occurring total suspended solids (TSS) expected for the study area (40-100 $mg \cdot L^{-1}$, with 100 $mg \cdot L^{-1}$ used for all events to produce a conservative estimate of SGD) (Ward and Armstrong, 1997). Sample solutions were stirred for one hour before passing through MnO_2 fibers to extract the desorbed Ra. Processing and measurements of radium isotopes were conducted as described above for bay samples. To determine contribution of ^{226}Ra from the tributary creeks into the bay, the total ^{226}Ra activity was normalized to the sediment mass and then multiplied by the sediment flux from the creeks using the freshwater inflow data from (TWDB, 2016). It should be noted that the model includes surface runoff for the watersheds feeding into the bay, and not just the creek discharges. As of the completion of this work, the model does not include diversions and return flows to and from the creeks (TWDB, 2016). Stream discharge rates for two of the three creeks (i.e. the San Fernando and Los Olmos Creeks) (USGS, 2017a, b, 2018) are available at long distances inland, and thus these data are likely not representative of the actual discharge to the bay.

4. RESULTS

4.1 PRELIMINARY INVESTIGATION

The inverted CRPs collected along the northern and southern shorelines of Baffin Bay (**Figure 3**), were examined in conjunction with local geology to determine likely locations of SGD. Resistivities measured during the CRP ranged from 0.18-1.1 Ω-m (**Figure 4**), which is indicative of sediments saturated with high salinity water (Murgulet

et al., 2016), and likely absent freshwater. The typical average resistivities for freshwater saturated sediments like clay or sandy loam are 38 Ω-m and 51 Ω-m, respectively (Nyquist et al., 2008). In this study, the hypersaline nature of porewaters as depicted in **Figure 6,** and the presence of sediments ranging from coarse to black muds (Dalrymple, 1964) (**Figure 3**) result in the narrow electrical resistivity range.

Areas of higher electrical resistivity (0.45-0.90 Ω-m) located in close proximity to potential connections between the subsurface and surface water were deemed areas of interest (**Figure 3)**, these have been correlated with groundwater seepage faces in other studies (Dimova et al., 2012; Nyquist et al., 2008). A total of eight locations were selected for spatial assessments of groundwater influences and nutrient sources to Baffin Bay (**Figure 1**) extending from the westernmost edge of the southern CRP, into Laguna Salada (station 1), to the center of the bay (station 2), eastward along the southern CRP towards the mouth of Baffin Bay (station 7) and then very near to the mouth of Baffin Bay (station 8). Along the northwestern most point of the northern CRP (station 4), near the mouth of Cayo del Grullo (station 3), where Cayo del Grullo meets Alazan Bay (station 6), and the headwaters of Alazan Bay (station 5) (**Figure 3**).

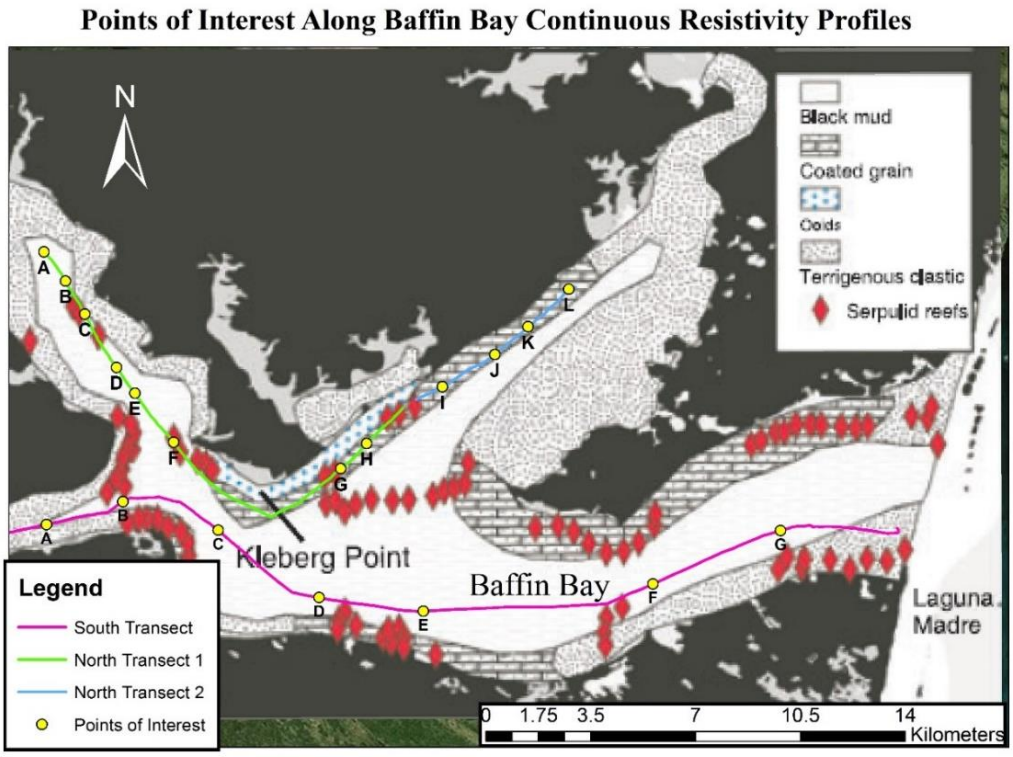

Figure 3: Map of continuous resistivity surveys in Baffin Bay. Areas of interest are marked with letters A-L on the northern shore and A-G on the southern shore (Dalrymple, 1964).

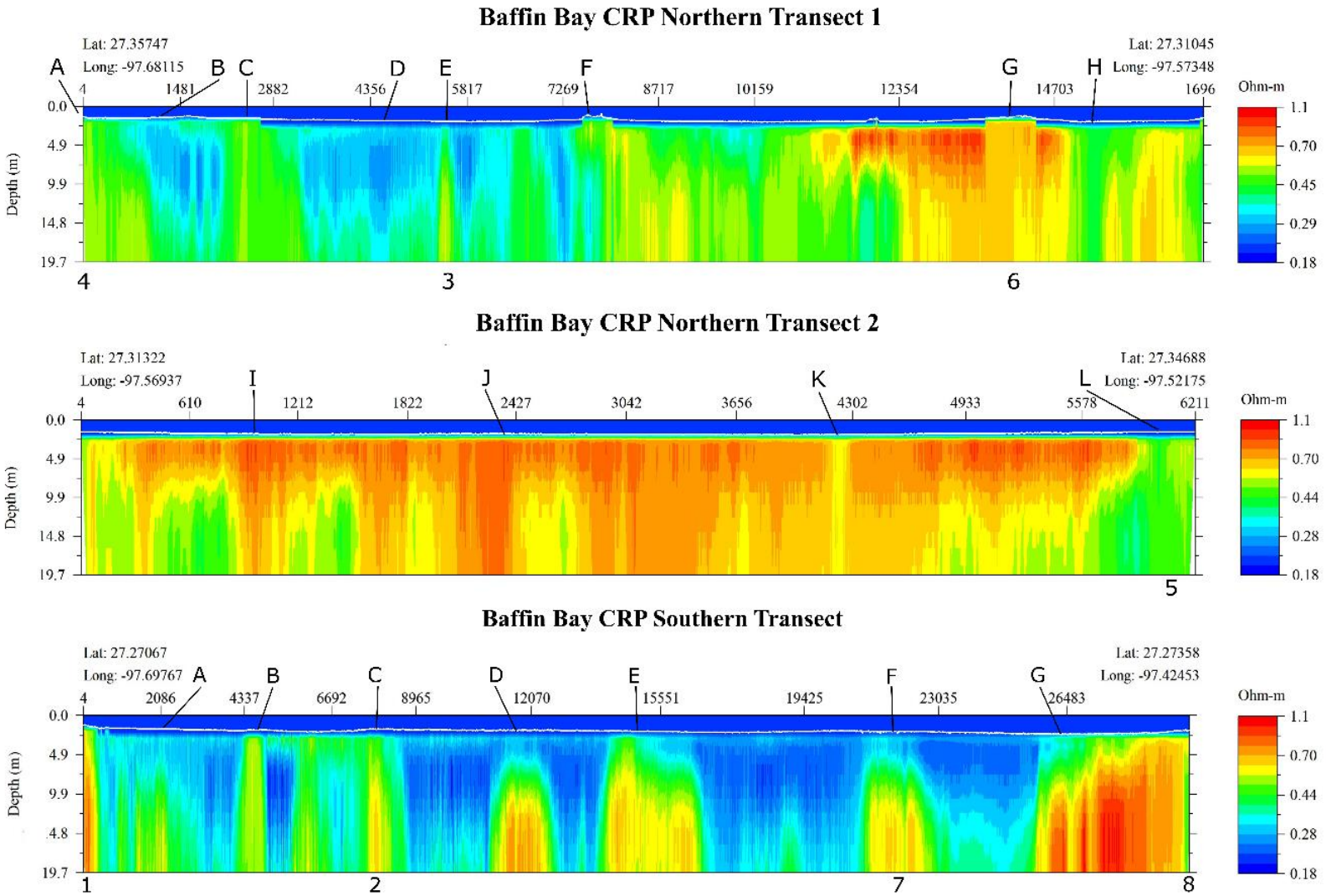

Figure 4: CRP profile images from the northern and southern transects. Images show resistivity in Ohm-m ranging from 0.18 to 1.1. Refer to **Figure 4** for the location of transects. Points of interest are labeled above each image with letters A-H, I-L, and A-G. Stations are labeled below each image with numbers (1-8).

Areas of interest such as points F and G on the northern transect 1 (**Figures 3 and 4**) revealed subsurface features that coincided with descriptions of the locations of serpulid reefs by Dalrymple (1964). The change in bathymetric elevation and resistivity at these locations is unique and not observed at other locations along the CRPs. The existence of the serpulid reef is also evidenced by the retrieval of a piece of remnant reef rock from the sediment core collected at station 6 (area of interest G along the northern transect 1) (**Figures 3 and 4**) as shown in **Figure 5**. Serpulid reefs in the area were known to grow on sandy substrates (Simms et al., 2010) which would provide a preferential flow path for groundwater. In general more coarse-grained sediments can be found in the shallower water along the coastlines (**Figure 3**) (Dalrymple, 1964), where more SGD is likely to occur, especially near the sandy pockets that the serpulid reefs prefer (Simms et al., 2010).

The center parts of the bay which have been found to be dominated by black mud, a muddy facies that is reducing and contains few benthic organisms (Dalrymple, 1964), are represented in the CRPs by higher conductivities, indicative of low permeability sediments and/or high salinity porewater (**Figure 4**). The coarser grained sediments have lower porosities compared to the black mud that was shown to have reached a maximum water content of 78% water by weight (Dalrymple, 1964) meaning that more saline pore fluid would reside in the muds leading to low resistivities (Nyquist et al., 2008) as also seen in the southern transect CRP.

Figure 5: Serpulid Reef rock found in sediment core taken at station 6 (coincident with area of interest G along northern transect 1).

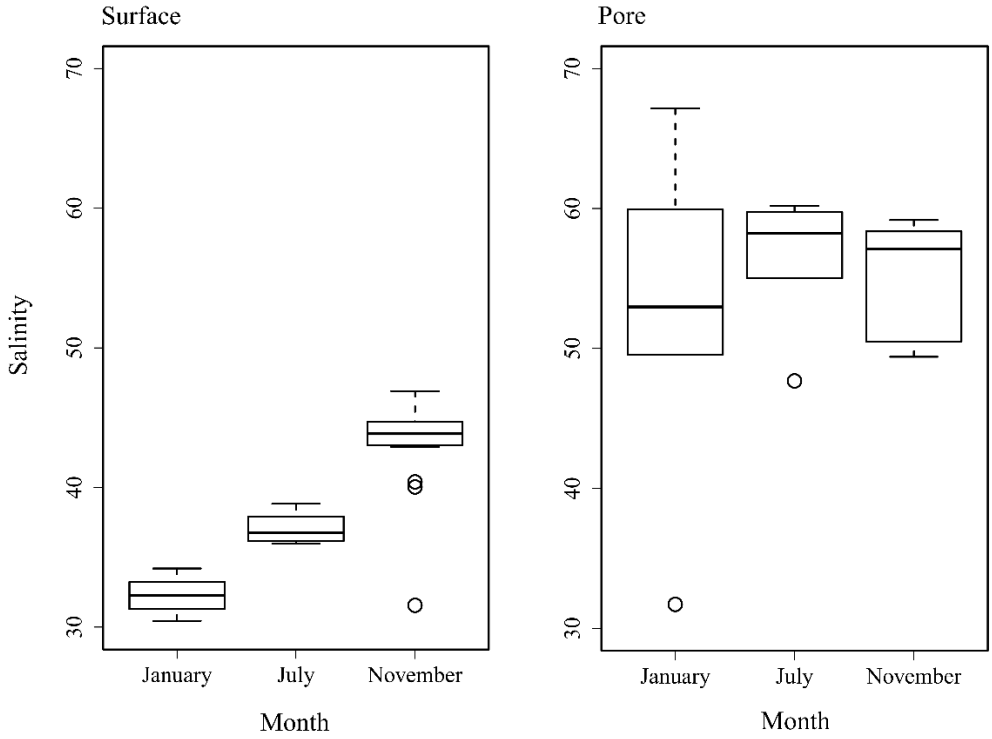

Figure 6: Salinity box plot for surface and porewater samples. Surface water salinities increase each sampling event while porewater salinities remain similar. Tukey test results show that while surface water salinities are all significantly different from one another from January to July, July

to November, and November to January (p-values in order: $1.5x10^{-6}$, 0, 0), there is no significant difference between porewater salinities (p-values in order: 0.6558, 0.9172, 0.8525).

4.2 WATER SAMPLES

4.2.1 TOTAL ALKALINITY AND DISSOLVED INORGANIC CARBON

The average TA of Baffin Bay across all events was 3,159±371 µM (n=48) in the surface water and 6,004±4,656 µM in porewater (n=18). The highest surface water TA (3,853 µM) was measured at station 1, near the head of Laguna Salada in November while the lowest (2,664 µM) was observed at the head of Alazan Bay in July. The highest porewater TA (15,715 µM) was measured at station 1, in Laguna Salada, in November while the lowest (2,789 µM) was observed at station 3 in July, at the mouth of Cayo del Grullo. The highest alkalinities measured each event occurred in surface water at the mouth of Cayo del Grullo (station 3), with each concentration being more than 2σ greater than the mean of all the surface water alkalinity samples.

DIC follows a similar trend with TA, higher in porewater and lower in surface water (**Figure 7**). The average DIC of Baffin Bay across all events was 2,669±236 µM (n=44) in the surface water and 5,508±4,605 µM in porewater (n=18). The highest surface water DIC (3,073 µM) was measured at station 1, in Laguna Salada in November and the lowest (2,092 µM) was measured at station 6 near the middle of Baffin Bay in Alazan Bay in July. The highest porewater DIC (14,715 µM) was measured in Laguna Salada at station 1 in July, while the lowest (2,312 µM) was observed at station 2 where Laguna Salada and Cayo del Grullo meet.

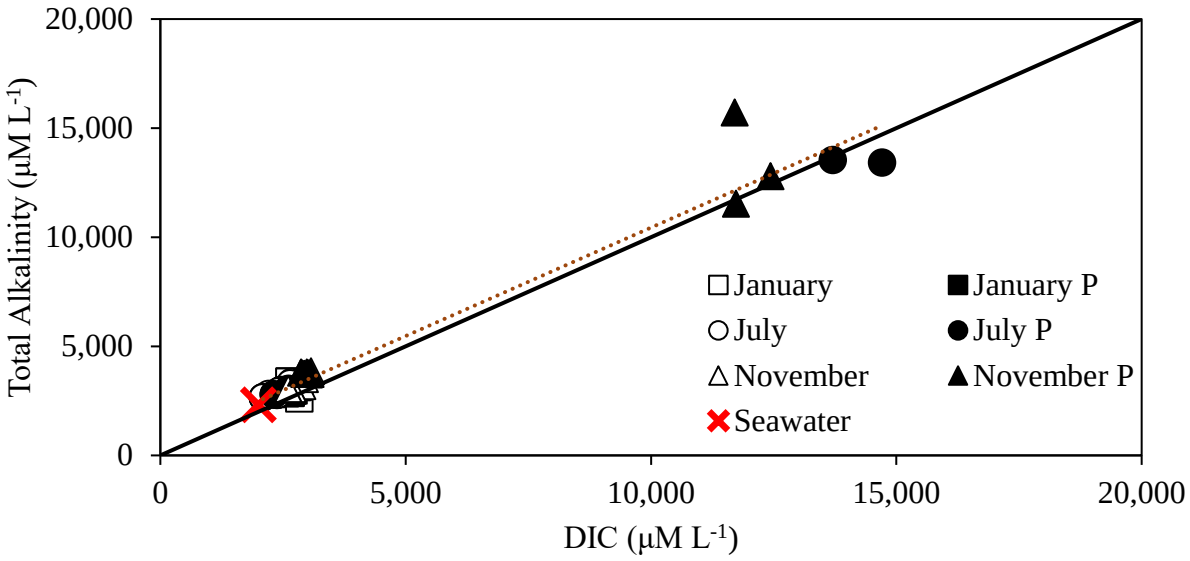

Figure 7: Graph of DIC versus total alkalinity, the relationship between total alkalinity and DIC is nearly 1:1 (represented by the solid black line), the average DIC:TA ratio for surface water (hollow shapes) and porewater (filled shapes) is 0.87. The dotted trendline represents all sampling events surface and porewater with a slightly more positive relationship between DIC and TA (R^2: 0.96 a p-value $<2.2x10^{-16}$).

Total alkalinity exceeds DIC for 95.2% of the samples, for both surface and porewater. DIC only exceeds TA 3 times, at stations 1 and 4 in pore water during July, and in the porewater at station 8 in November. Nevertheless, alkalinity and DIC levels in surface water are in general much larger than those of seawater at salinity 35 (2,322 µM for alkalinity (Takahashi et al., 1981) and approximately 2,000 µM DIC (Winn et al., 1998)) indicative of in-situ production of both, or groundwater input. The positive relationship between DIC and TA are an indication of a similar source of carbonate and the potential of limited TA consumption **(Figure 7)**. Organic matter degradation by microbes or photooxidation could be sources of alkalinity and DIC (Minor et al., 2006).

4.2.2 NUTRIENTS AND CHLOROPHYLL-A

4.2.2.1 CHLOROPHYLL-A

In the surface of the water column, the highest chl-α concentration in January ($\bar{x}$: 13.0 $\mu g \cdot L^{-1}$; σ: 5.3) was measured at station 1 (25.1 $\mu g \cdot L^{-1}$) and the lowest at station 5 (7.0 $\mu g \cdot L^{-1}$). The highest chl-α measured in July ($\bar{x}$: 15.6 $\mu g \cdot L^{-1}$, σ: 5.7) was at station 1 (26.0 $\mu g \cdot L^{-1}$) and the lowest was at station 4 (6.6 $\mu g \cdot L^{-1}$). The highest concentration of chl-α in November ($\bar{x}$: 10.9 $\mu g \cdot L^{-1}$, σ: 2.0) was at station 1 (14.9 $\mu g \cdot L^{-1}$) and the lowest was at station 3 (7.8 $\mu g \cdot L^{-1}$). The average concentration of chl-α in the bottom of the water column, in January, was 14.4 $\mu g \cdot L^{-1}$ with a maximum and minimum concentration of 23.8 $\mu g \cdot L^{-1}$ and 6.7 $\mu g \cdot L^{-1}$ (σ: 5.6) at stations 1 and 6, respectively. In July, the average bottom chl-α concentration was 14.4 $\mu g \cdot L^{-1}$ (σ: 5.5), with a maximum and minimum of 28.4 $\mu g \cdot L^{-1}$ and 6.8 $\mu g \cdot L^{-1}$ at stations 1 and 4, respectively (**Figure 8**).

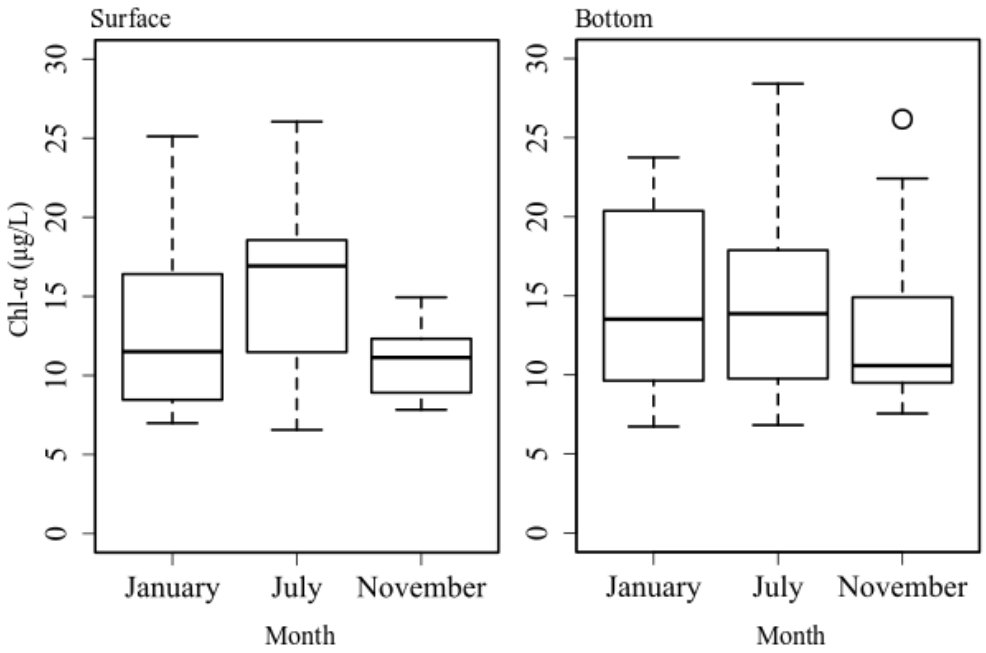

Figure 8: Chl-α concentrations for Surface and Bottom water displayed as boxplots. Chl-α concentrations did not vary much from season to season or between surface and bottom.

The average concentration of chl-α in November bottom waters was 13.1 $\mu g \cdot L^{-1}$ (σ: 5.3), with a maximum and minimum of 26.2 $\mu g \cdot L^{-1}$ and 7.6 $\mu g \cdot L^{-1}$ at stations 2 and 6, respectively. When compared to other estuaries in south Texas, primary productivity occurs in high levels year-round for the period of study. For instance, in Aransas Bay, chl-α levels were the highest in July and much lower in January and November (Douglas et al., 2017). For this study, maxima of chl-α in Baffin Bay exceed the July Aransas Bay in both, January and July, and closely match in November.

Station 1 had consistently the highest chl-α concentrations each event with the exception of November in bottom waters. Overall, the lowest concentrations were found at several locations throughout Cayo del Grullo and Alazan Bay, including Stations 4, 6, 5, and 3, in the order of increasing concentration. The consistently high chl-α at Station 1, close to the head of the Laguna Salada, coincides with some of the highest DIN (858.2, 5538.5, 1011.6 µM) and DOC (1152.3, 1630.2, 3126.3 µM) each sampling event for January, July and November, respectively. The average DIN and DOC for January, July and November were: 553.7, 2230.0, 729.1 µM and 696.0, 818.7, 1080.4 µM, respectively.

4.2.2.2 NUTRIENTS

The average NO_3^- concentration across all events was 2.5 µM (n=48) in the surface water and 0.2 µM in porewater (n=18). The highest surface water NO_3^- concentration (14.1 µM) was measured at station 1 in July while below detection limit concentrations (<0.11 µM) occurred at multiple sites, including 3, 5, and 7 in January, July, and November, respectively (**Figure 9a**). NO_3^- concentrations were consistently below the detection limit at station 7 in surface water (**Figure 1**). The highest NO_3^- concentrations measured each event occurred in surface water at station 1, or station 5. The highest porewater NO_3^- (2.0 µM) was measured at station 8 in July

while concentrations below the detection limit were consistent across events at multiple locations: in January at station 1; in July at stations 1-4 and 6; and in November at stations 1-6 and 8 (**Figures 1 and 9b**).

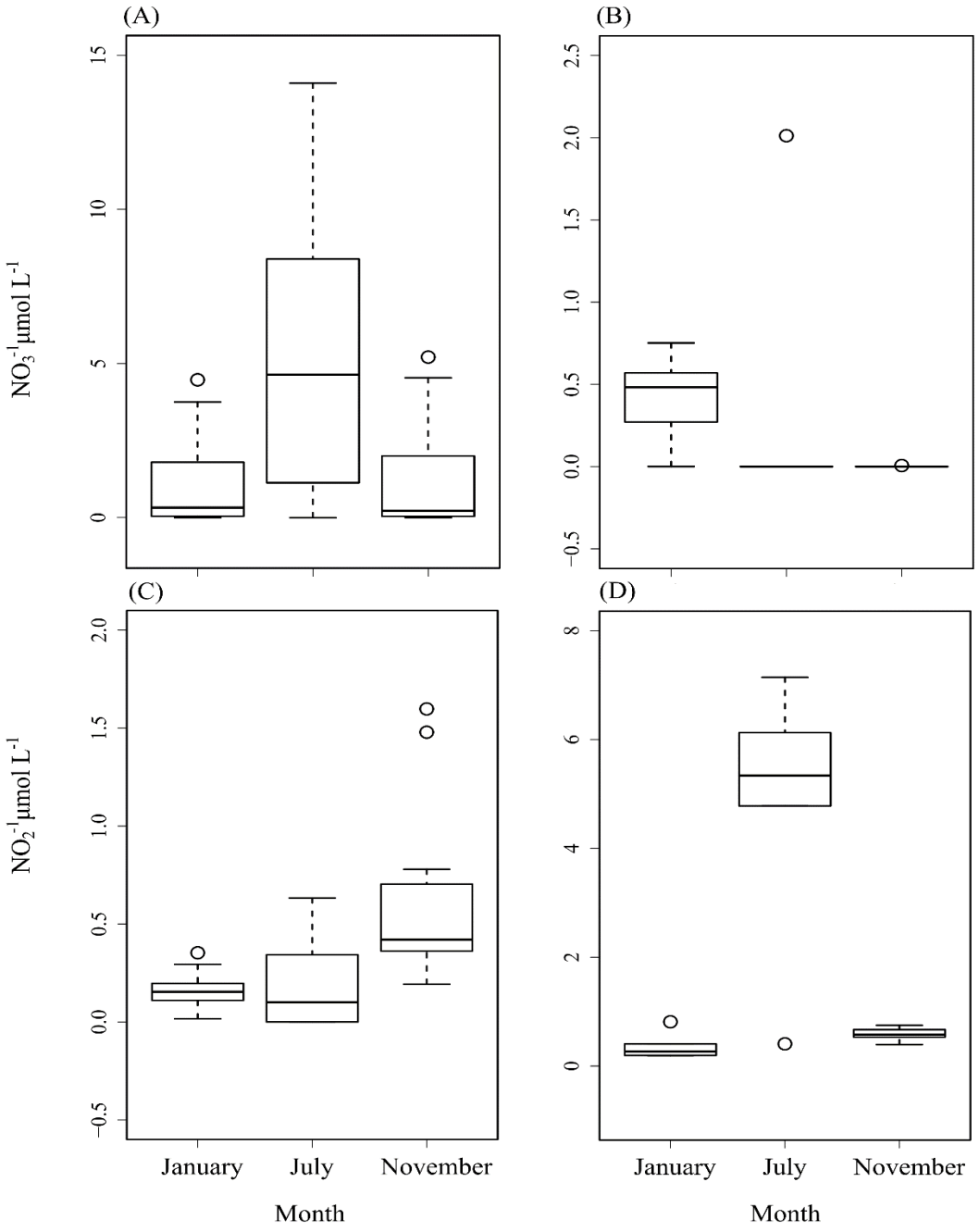

Figure 9: NO_3^- and NO_2^- concentrations (µM) for all events in surface and porewater. A) Surface water NO_3^-. B) Porewater NO_3^-. C) Surface water NO_2^-. D) Porewater NO_2^-.

The average NO_2^- concentration across all events was 0.3 µM (n=48) in the surface water (which is lower than that of NO_3^-) and 2.0 µM in porewater (n=18) (which is higher than that of NO_3^-, **Figure 9**). The highest surface water NO_2^- concentration (1.6 µM) was measured at station 6 in November while the lowest/or below the detection limit (0.012 µM) occurred at multiple sites including stations 1, 3, and 5 in July (**Figure 1, Figure 9c**). The highest porewater NO_2^- (7.2 µM) was measured at station 1 in July while the lowest (0.2 µM) at station 3 in January (**Figure 1, Figure 9d**). Similar to NO_3^-, the highest NO_2^- concentrations measured each event occurred in surface water at station 5, or station 8 (**Figures 1, 9**). Station 1 had porewater NO_2^- among the highest concentration (0.81, 7.1, 0.58 µM for January, July and November) each event (overall $\bar{x}$: 0.4, 4.9, 0.59 µM for January, July, and November respectively) (**Figure 2**).

Concentrations of NH_4^+ were extremely high in porewater. The average NH_4^+ concentration across all events in surface water was 6.2 µM (n=48) and $1.18x10^3$ µM in porewater (n=18) (**Figure 10**). The highest and lowest surface water NH_4^+ concentrations (18.7 and 0.1 µM, respectively) were measured at station 1 in July and January, respectively. The highest porewater NH_4^+ ($5.5x10^3$ µM) was also measured at station 1 in July while the lowest (38.6 µM) at station 3 in January (**Figure 1, Figure 10b**). Notably, the highest NH_4^+ concentrations measured in surface water each event occurred at stations 1, 6, and 8 (**Figure 11, Figure 12, Figure 13**). NH_4^+ is typically thought to be a preferred nitrogen source for phytoplankton (Dortch, 1990), so its preferential uptake may be heightened during times of severe N-limitation. Dissolved inorganic nitrogen (DIN) is comprised of nitrate plus nitrite and ammonium (DIN= $NO_3^- + NO_2^- + NH_4^+$). These forms of N are readily available to phytoplankton and often control the formation of blooms. In this study, in porewater, NH_4^+ makes up most of the DIN pool (**Table 6**). Thus, in this study, DIN follows the same trends as NH_4^+ in terms of

both concentrations and fluxes to the surface water (see section 4.4). NH_4^+ (µM) was also noted to correlate with alkalinity as shown in **Figure 14**.

Similar to NH_4^+, HPO_4^{2-} is much more concentrated in porewater when compared to surface water (**Figure 10**). The average HPO_4^{2-} concentration across all events was 0.7 µM (n=48) in surface water and 16.0 µM in porewater (n=18). The highest surface water HPO_4^{2-} concentration (1.5 µM) was measured at station 7 in November while the lowest (0.1 µM) at station 8, in January (**Figure 1, Figure 10c**). The highest porewater HPO_4^{2-} (43.7 µM) was measured at station 1 in July while the lowest (1.6 µM) at station 3 in January (**Figure 1, Figure 10d**). The highest HPO_4^{2-} concentrations measured each event in surface water occurred at stations 4, 1, and 7. Although HPO_4^{2-} concentrations are in low levels in surface water, the larger porewater concentrations, particularly in July, are an indication that Baffin Bay could receive significant amounts of terrigenous, anthropogenic and/or remineralized nutrients (especially phosphorous and N). This is particularly true for Laguna Salada, where the largest concentrations of most nutrients were measured, accompanied by persistently larger chl-a levels, a relationship also observed by other studies (Khalil and Rifaat, 2013).

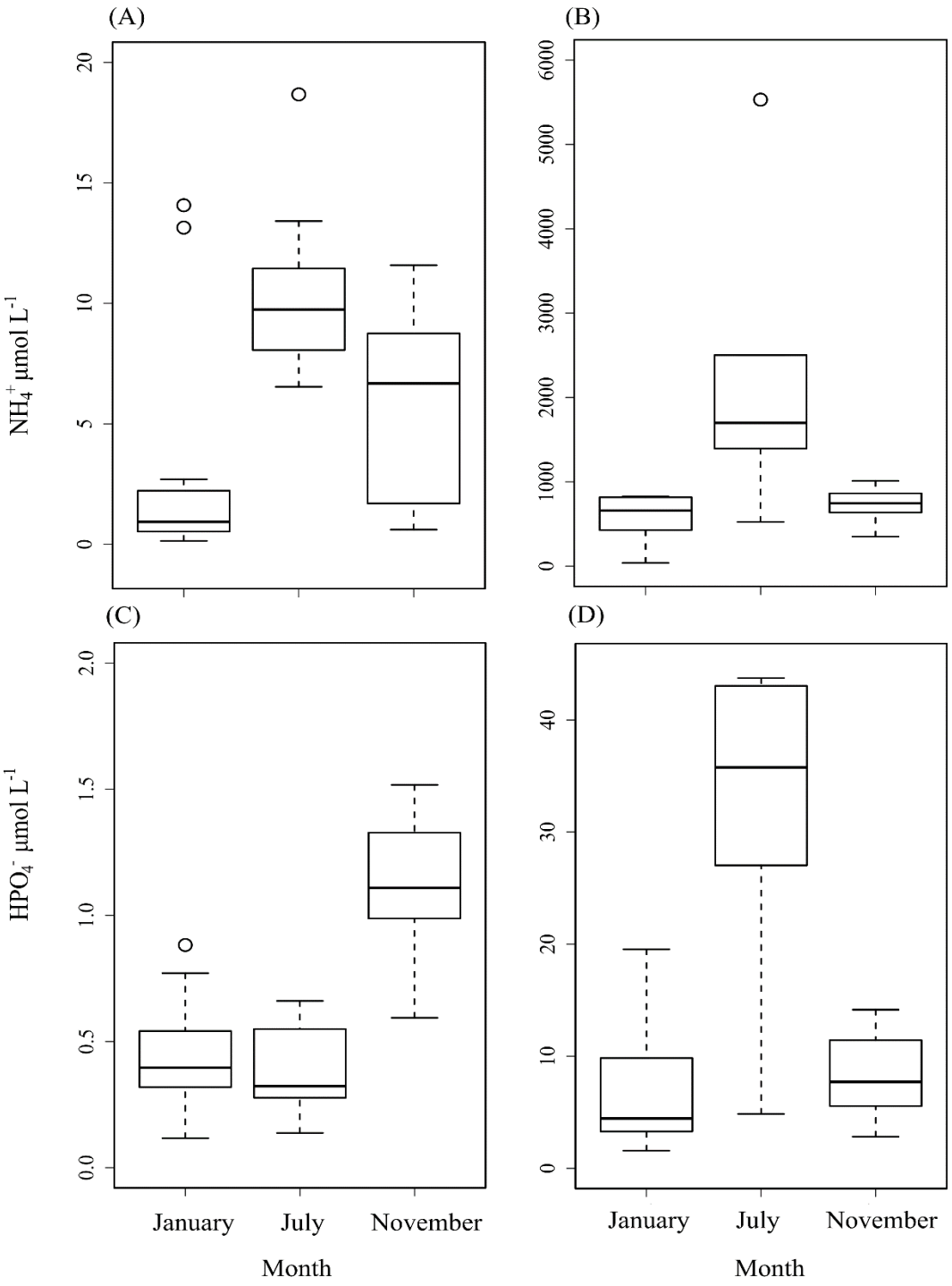

Figure 10: A) NH_4^+ concentrations for surface water spatial sampling B) NH_4^+ concentrations for porewater spatial sampling C) HPO_4^{2-} concentrations for surface water samples D) HPO_4^{2-} concentrations for porewater samples. Note that the scales between surface and porewater are different for NO_3^- and NO_2^-.

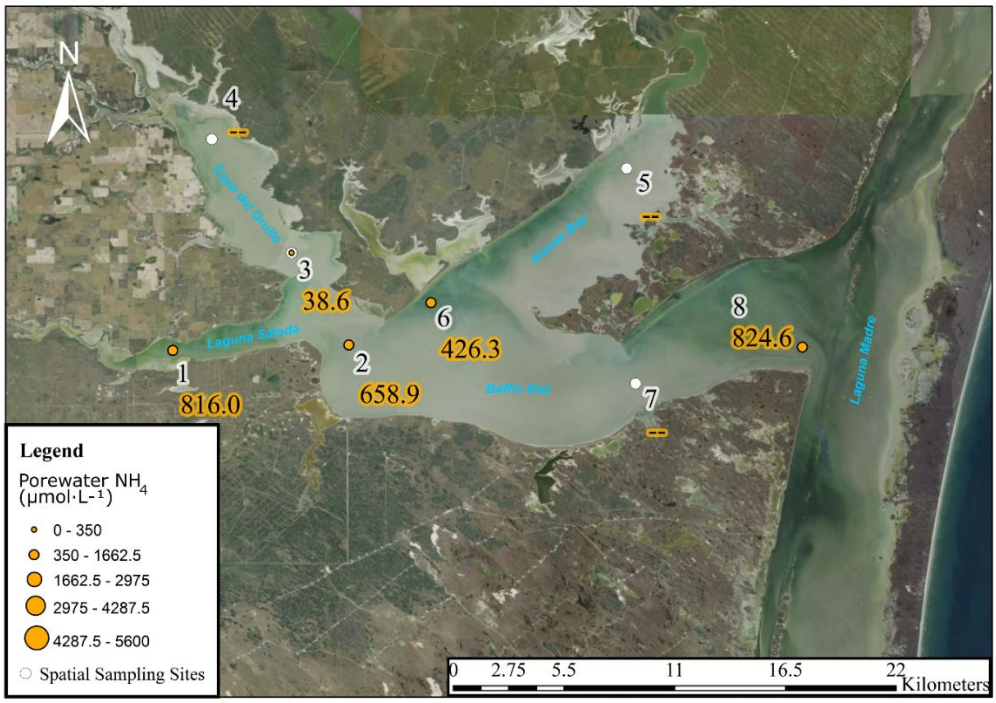

Figure 11: Porewater NH_4^+ in µmol L^{-1} for January. The data points are labeled following the format: station number (white mask labels), NH_4^+ concentration in µM (orange mask labels). Sites with no available data (i.e. 4, 5, and 7) are marked with, "--".

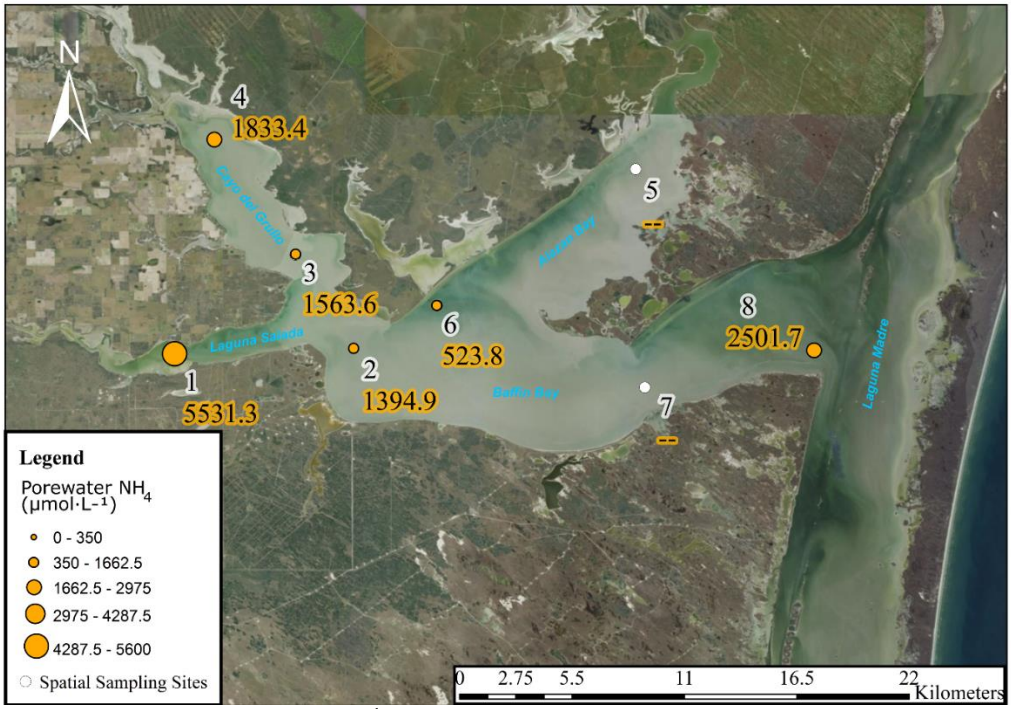

Figure 12: Porewater NH_4^+in µmol L^{-1} for July. The data points are labeled following the format: station number (white mask labels) and NH_4^+ concentration in µM (orange mask labels). Sites with no data available (i.e. 5 and 7) are marked with, "--".

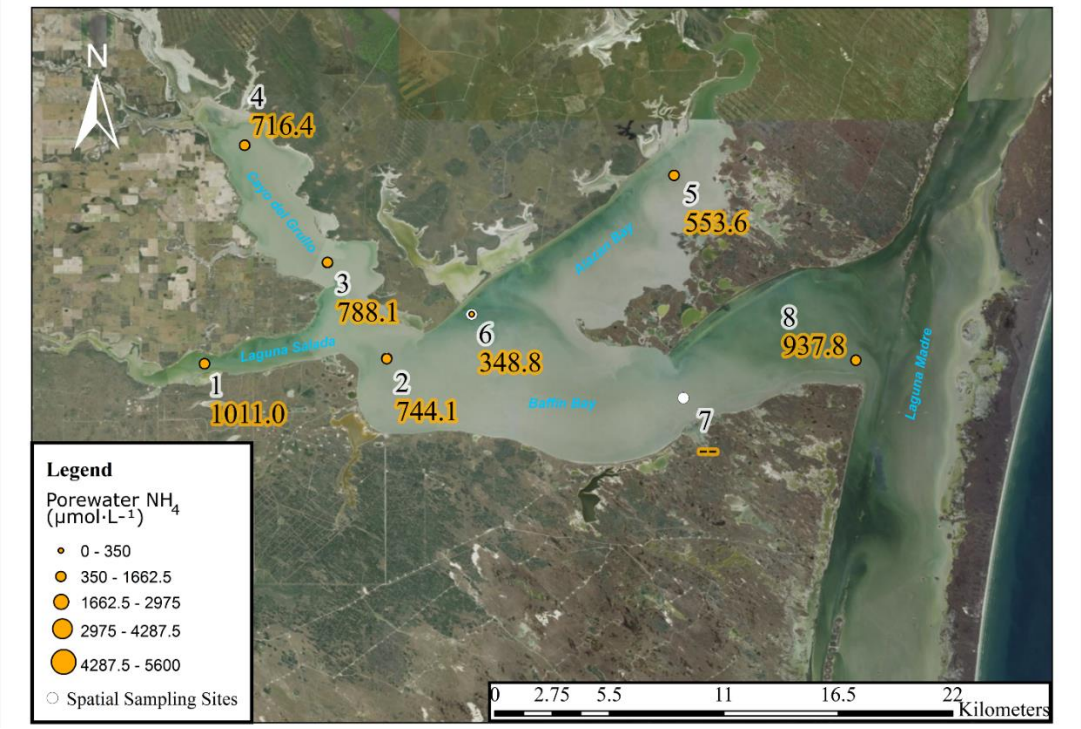

Figure 13: Porewater NH_4^+ in µmol L^{-1} for November. The data points are labeled following the format: station number (white mask labels), NH_4^+ concentration in µM (orange mask labels). Sites with no data available (i.e., 5 and 7) are marked with, "--".

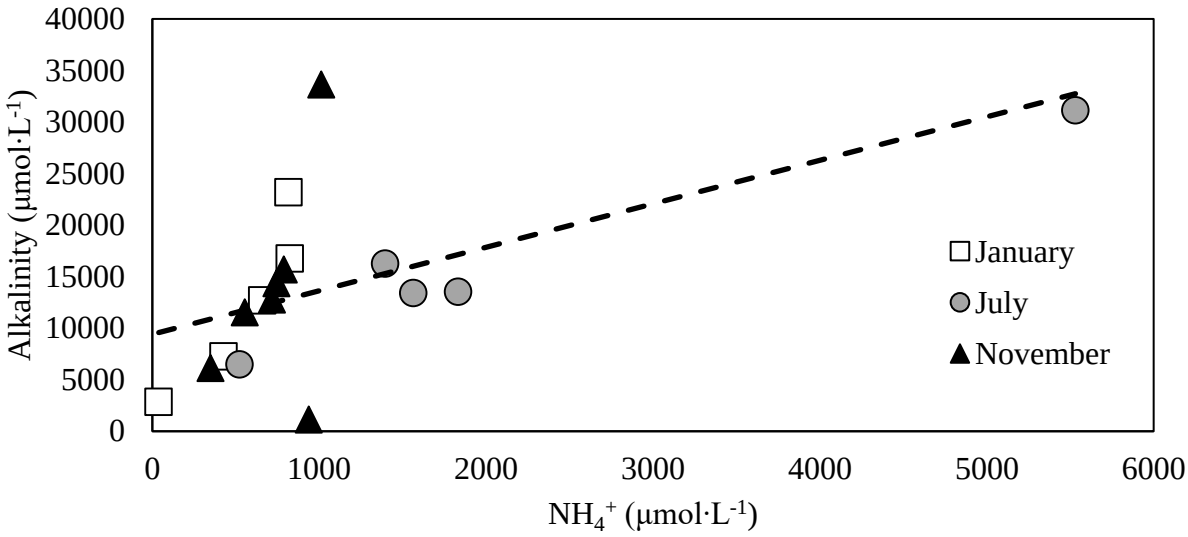

Figure 14: Graph of porewater Alkalinity (µM) vs. porewater NH_4^+ (µM) showing the correlation between the two (R^2: 0.34; p-value: 0.01336).

Larger enrichment of porewaters over surface water is also observed for $HSiO_3^-$ (**Figure 15**) but surface water concentrations are larger when compared to other nutrients presented

herein. The average $HSiO_3^-$ concentration across all events was 101.4 µM (n=48) in surface water and 275.4 µM (n=18) in porewater. The highest surface water $HSiO_3^-$ concentration (188.3 µM) was measured at station 8 in November while the lowest (13.0 µM) at station 7 in January (**Figure 1, Figure 15**). The highest porewater $HSiO_3^-$ (559.0 µM) was measured at station 1 in July while the lowest (56.7 µM) at station 3 in January (**Figure 1, Figure 15**). The highest $HSiO_3^-$ concentrations measured in surface water during each event occurred at stations 4, 7, 1 (**Figure 1**). Although, average concentrations of $HSiO_3^-$ in surface water increased from January to July to November, the chl-α level does not show a similar pattern, indicating that an increase in available silica did not play an important role on diatomaceous algae growth (Buskey et al., 2001).

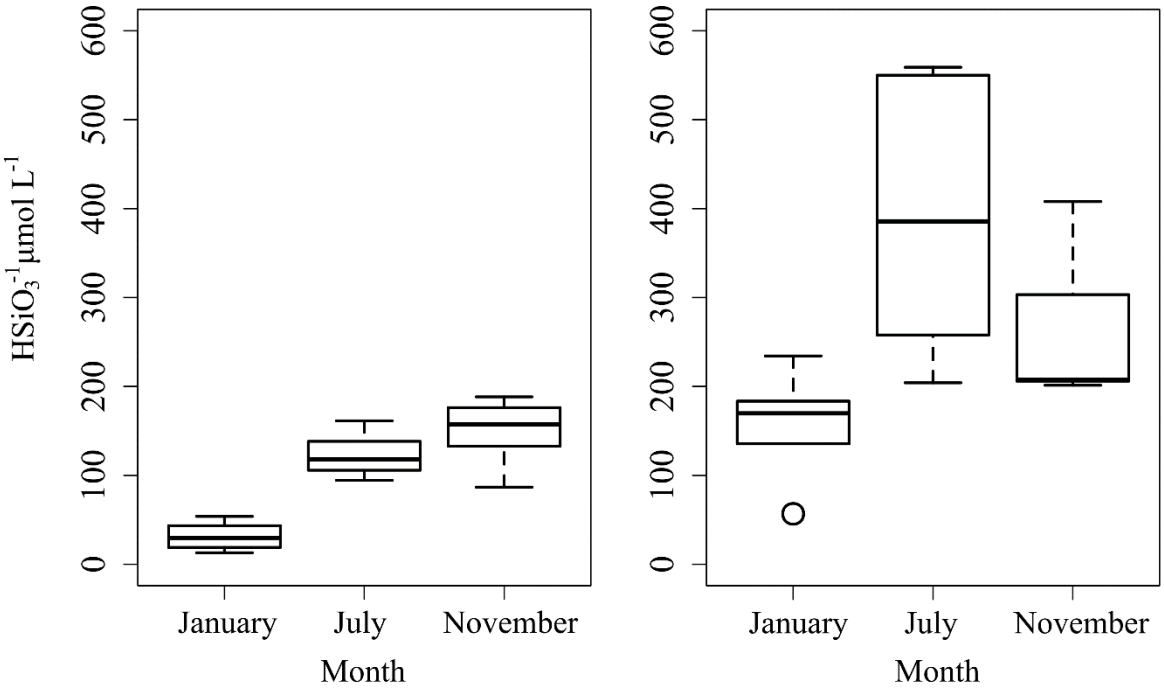

Figure 15: Surface (left) and porewater (right) $HSiO_3^-$ concentrations.

Slightly larger enrichment of surface waters over porewater is observed for DOC (**Figure 16**) but surface water concentrations are larger when compared to other nutrients presented herein. The average DOC concentration across all events was 969.8 µM (n=48) in surface water

and 886.4 µM (n=18) in porewater. The highest surface water DOC concentration (1502.4 µM) was measured at station 1 in November while the lowest (486.0 µM) at station 8 in November (**Figure 1, Figure 16**). The highest porewater DOC (3126.4 µM) was measured at station 1 in November while the lowest (387.8 µM) at station 6 in July (**Figure 1, Figure 16**). The highest DOC concentrations measured in surface water during each event occurred at stations 6 (January), and 1 (July and November) (**Figure 1**).

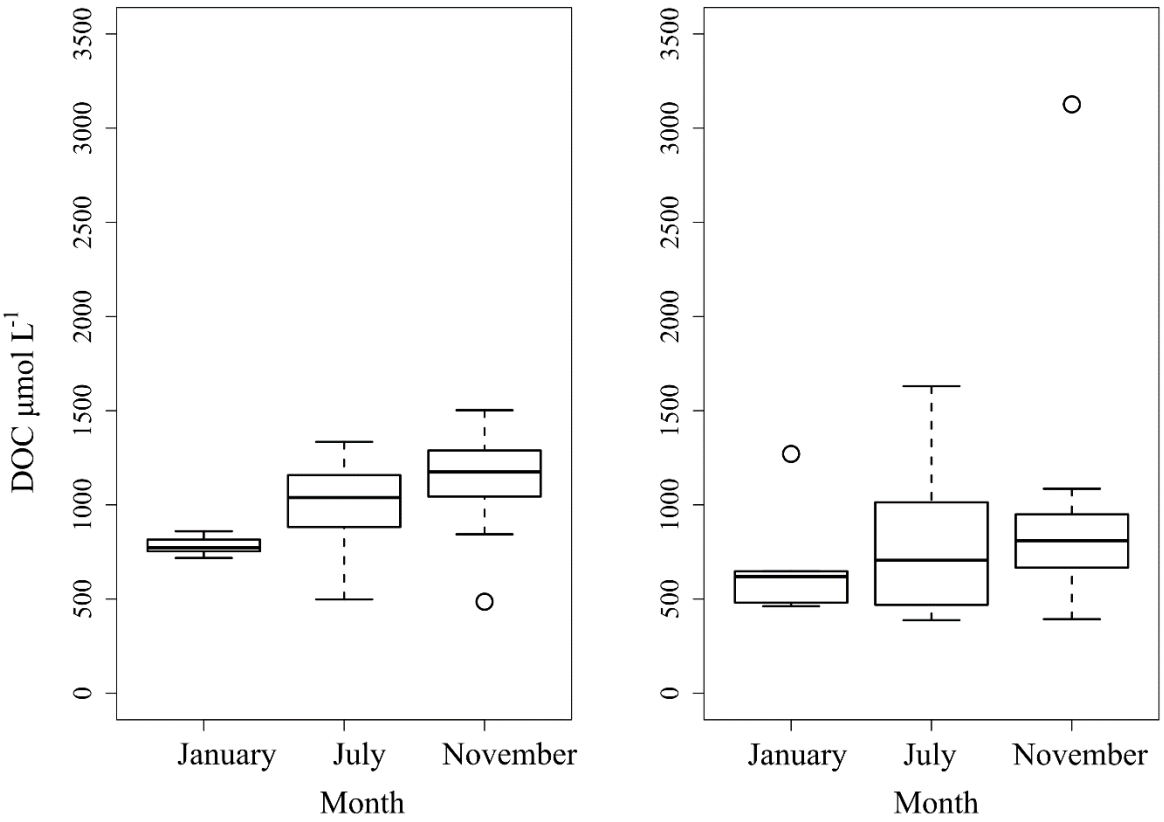

Figure 16: DOC concentrations for combined surface and bottom water (left) and porewater (right) in Baffin Bay.

4.2.3 RADIOGENIC ISOTOPES

The highest average ^{226}Ra surface water activity was measured in July (min: 10.6 $Bq \cdot m^{-3}$, max: 22.4 $Bq \cdot m^{-3}$, $\bar{x}$: 18.4 $Bq \cdot m^{-3}$ (n=8)), while the lowest occurred in January (min: 11.9 $Bq \cdot m^{-3}$, max: 15.4 $Bq \cdot m^{-3}$, $\bar{x}$: 14.0 $Bq \cdot m^{-3}$ (n=8)) followed by November (min: 11.1 $Bq \cdot m^{-3}$, max: 18.4

Bq·m^{-3}, $\bar{x}$: 15.7 Bq·m^{-3} (n=10)) (**Figure 17, Table 1).** The highest activities of all three events were found at station 3 and the next three of the highest ^{226}Ra activities were measured at stations 5 (20.6 Bq·m^{-3}), 4 (20.1 Bq·m^{-3}) and 1 (20.6 Bq·m^{-3}) (**Figure 1, Table 1**). The lowest activities were consistently measured towards the Laguna Madre, at stations 7 (11.9-14.9 Bq·m^{-3}) and 8 (10.5-12.1 Bq·m^{-3}) (**Figure 1, Table 1**). Activities of ^{226}Ra at stations 1 through 6 were greatest in July followed by November and January. Stations 7 and 8 (closest to Laguna Madre) do not follow this pattern (**Figure 17**), likely the result of mixing with Laguna Madre waters. These larger July surface water activities are accompanied by greater porewater activities (**Table 3**), which may indicate contribution from SGD (see section 4.3.1). Porewater ^{226}Ra was higher in July (min: 14.1 Bq·m^{-3}, max: 63.3 Bq·m^{-3}, $\bar{x}$: 43.6 Bq·m^{-3}) than in November (min: 12.8 Bq·m^{-3}, max: 71.2 Bq·m^{-3}, $\bar{x}$: 35.4 Bq·m^{-3}) (**Table 2**). In addition, changes in salinity levels (see **Figure 6**) cannot explain larger activities in July in both surface- and -porewater (surface water salinity $\bar{x}$: 37.0, porewater salinity $\bar{x}$: 57.1) because the bay was more saline in the following November event (surface water salinity $\bar{x}$: 49.4, porewater salinity $\bar{x}$: 54.4) (**Figure 6, Figure 18**). In addition, radium desorption is predicted to reach a maximum after approximately 20, which all of the salinities found were well above (**Figure 6**) (Elsinger and Moore, 1980; Webster et al., 1995).

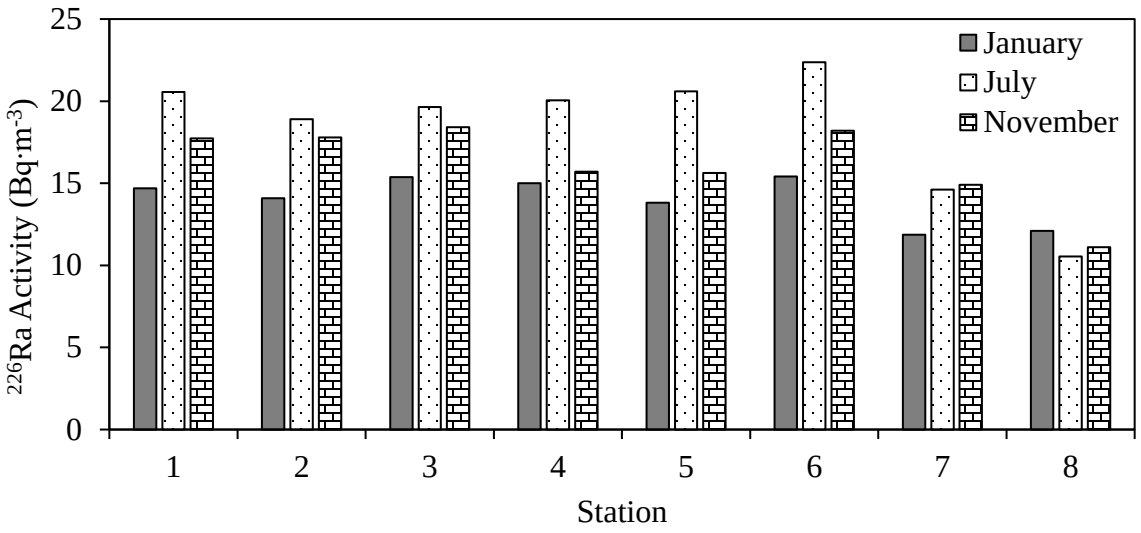

Figure 17: ^{226}Ra activities in Bq·m^{-3} for all seasons of spatial sampling. July had the highest concentrations and January the lowest on average.

Table 1: Surface water ^{222}Rn, ^{224}Ra, and ^{226}Ra activities ($Bq \cdot m^{-3}$) for each station over all spatial sampling events. Activity ratios for each station was calculated as the ratio of ^{224}Ra to ^{226}Ra activities. Age represents the radium age or the amount of time it took for a water particle since has been separated from its radionuclide source (i.e. porewater).

	Station	1	2	3	4	5	6	7	8	$\bar{x}$
Jan.	^{222}Rn	8.7±6	19.9±10	11.6±7	23.3±10	11.7±7	14.7±7	21.1±11	29.1±12	17.5±8.75
	^{224}Ra	13.5±1.35	10.8±1.08	11.5±1.15	11.0±1.10	11.0±1.10	12.9±1.29	8.7±0.87	11.2±1.12	11.3±1.13
	^{226}Ra	14.7±1.47	14.1±1.41	15.4±1.54	15.0±1.50	13.8±1.38	15.4±1.54	11.9±1.19	12.1±1.21	14.0±1.40
	AR	0.92	0.77	0.75	0.73	0.79	0.84	0.73	0.93	0.81
	Age	--	--	--	--	--	--	--	--	--
Jul.	^{222}Rn	19.3±26.64	18. 1±40.1	34.3±35.89	11.7±22.2	9.7±18.5	23.8±29.97	6.9±11.1	--	17.7±26.34
	^{224}Ra	38.6±3.86	23.4±2.34	18.6±1.86	21.0±2.10	39.0±3.90	15.9±1.59	22.6±2.26	18.4±1.84	24.7±2.47
	^{226}Ra	20.6±2.06	18.9±1.89	19.6±1.96	20.1±2.01	20.6±2.06	22.4±2.24	14.6±1.46	10.5±1.05	18.4±1.84
	AR	1.88	1.24	0.95	1.05	1.89	0.71	1.55	1.74	1.38
	Age	1	2.6	3.1	3	-1	3	1	-4	1.1
Nov.	^{222}Rn	26.7±22.9	15.9±23.68	--	--	--	--	26.5±29.23	9.0±20.72	19.5
	^{224}Ra	13.1±1.31	6.8±0.68	4.5±0.45	4.8±0.48	6.9±0.69	8.7±0.87	10.1±1.01	5.9±0.59	7.6±0.76
	^{226}Ra	17.7±1.77	17.8±1.78	18.4±1.84	15.7±1.57	15.6±1.56	18.2±1.82	14.9±1.49	11.1±1.11	16.2±1.62
	AR	0.74	0.38	0.24	0.30	0.44	0.48	0.68	0.53	0.47
	Age	6	9	11.6	6	6.2	10	9	1.4	7.4

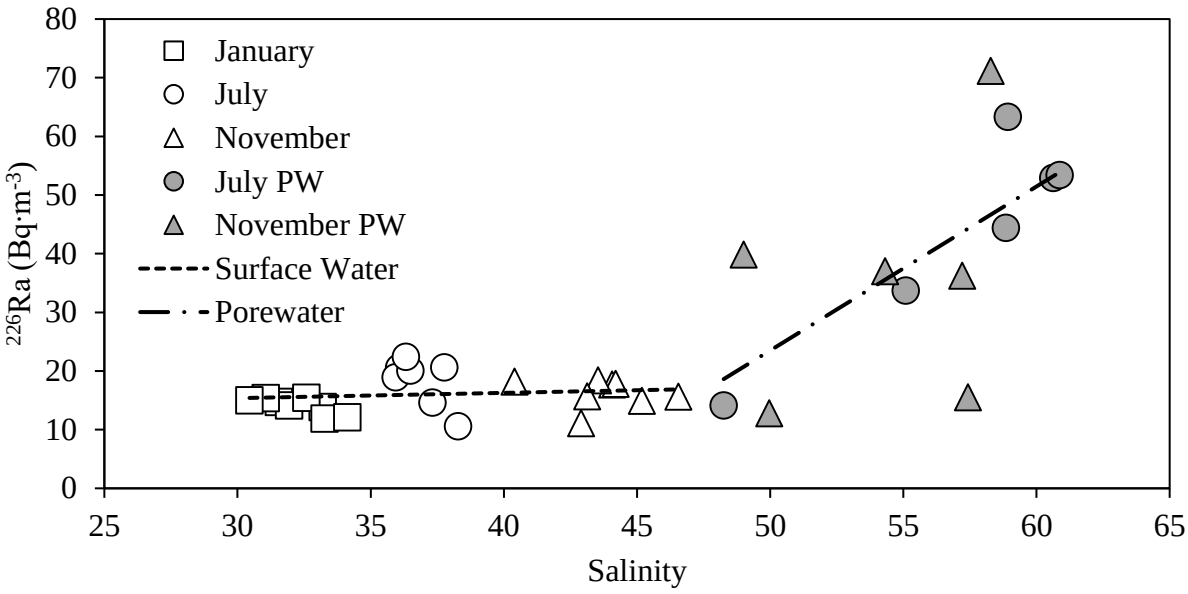

Figure 18: Graph of ^{226}Ra activity (Bq·m^{-3}) for surface and porewater versus salinity for all events. No ^{226}Ra measurements were taken in January. There is no clear relationship between salinity and surface water ^{226}Ra (R^2 = 0.02, p-value =0.5129), though porewater ^{226}Ra and salinity have a positive correlation (R^2 = 0.43, p-value = 0.01988).

The ^{224}Ra activity exhibited an overall average of 14.9±9.0 Bq·m^{-3} (n=23) across all events. The highest mean activity for a single station using all events was 21.7 Bq·m^{-3} at station 1 while the lowest of 11.5 Bq·m^{-3} was measured at station 3 (**Figure 19, Table 1**). Similar to ^{226}Ra, the event with the highest overall ^{224}Ra activity (**Figure 19, Table 1**) was July (15.9 - 39.0 Bq·m^{-3}), followed by January (8.7 - 13.5 Bq·m^{-3}) and November (4.5-13.1 Bq·m^{-3}), with some of the July ^{224}Ra activities more than double those of January and November (**Figure 19**). This large increase in the shorter-lived ^{224}Ra activities is possibly due to larger SGD inputs in July (Kelly and Moran, 2002), particularly at stations 1 (13.5 Bq·m^{-3} in January and 38.6 Bq·m^{-3} in July) and 5 (11.0 Bq·m^{-3} in January and 39.0 Bq·m^{-3} in July) (**Figure 19**).

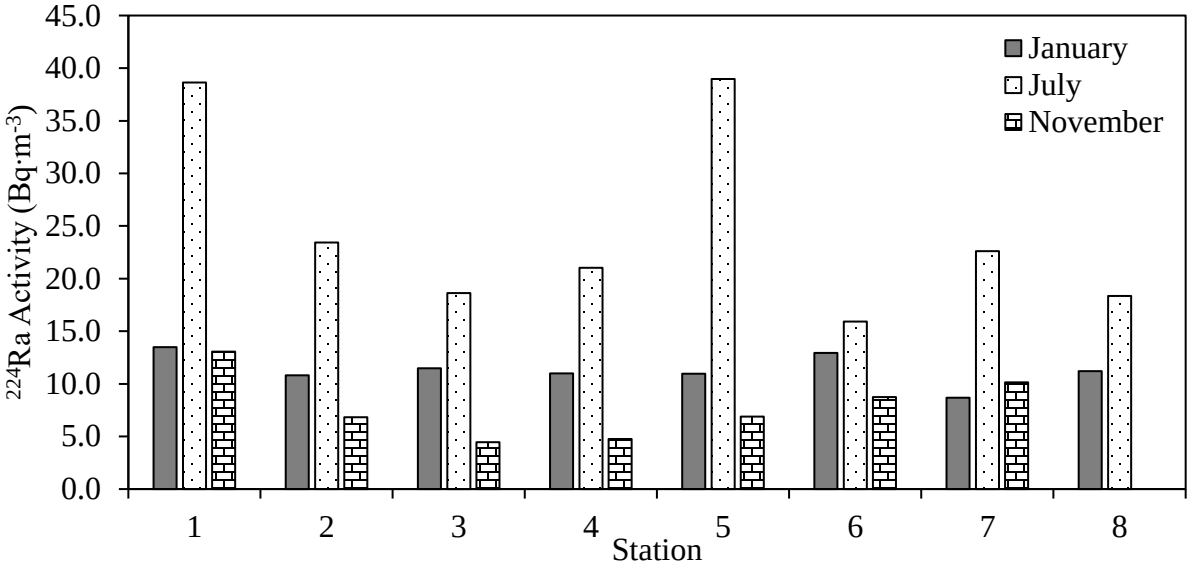

Figure 19: Surface water ^{224}Ra activities (in Bq·m^{-3}) for each station across all sampling seasons. Summer has the overall higher activity followed by spring and winter. The numerical values can be found in **Table 1**.

Similar to surface water, in average porewater activities of both ^{226}Ra and ^{224}Ra are larger in July. Porewater ^{226}Ra activities ranged from 14.1-63.3 Bq·m^{-3} in July ($\bar{x}$ of 43.6 Bq·m^{-3}) and from 12.8-71.2 Bq·m^{-3} in November ($\bar{x}$: 35.4 Bq·m^{-3}) (**Table 2**). Porewater ^{224}Ra activities ranged from 2.0-167.2 Bq·m^{-3} in July ($\bar{x}$: 72.3 Bq·m^{-3}) and from 5.3-54.5 Bq·m^{-3} in November ($\bar{x}$: 18.8 Bq·m^{-3}) (**Table 2**). In comparison, local deep groundwater ^{224}Ra and ^{226}Ra activities ranged from 3.5-269.7 Bq·m^{-3} ($\bar{x}$: 50.0 Bq·m^{-3}) and from 1.2-244.7 Bq·m^{-3} ($\bar{x}$: 46.5 Bq·m^{-3}) (

Table 3), respectively.

Well ID	8326201	8327501	8329201	8329401	8342508	8334403	($\bar{x}$)
^{222}Rn	13,135.6 ± 1085.6	4,019.0 ± 493.5	2,646.0 ± 464.8	9,254.5 ± 1300.2	11,627.3 ± 1699.4	1,883.7 ± 675.4	7094.4 ±953.2
^{224}Ra	8.4±0.84	3.5±0.35	4.3±0.43	4.8±0.48	9.3±0.93	269.7±27.0	50.0±5.0
^{226}Ra	3.2±0.32	4.8±0.48	1.2±0.12	17.7±1.77	7.5±0.75	244.7±24.5	46.5±4.65
AR	2.67	0.72	3.50	0.27	1.25	1.10	1.58
Depth	264	244	358	383	222	187	276

Table 2: Porewater ^{222}Rn, ^{224}Ra, and ^{226}Ra activities (Bq·m^{-3}) for all stations in each sampling event. AR or activity ratios are given for each station and event, where the activity ratio is the ^{224}Ra activity divided by the ^{226}Ra activity. The uncertainty of ^{222}Rn is the 2-sigma error (2σ) as derived from Capture while for Ra (224 and 226), the presented uncertainty is the maximum expected of 10% efficiency for RaDeCC measurements. However, much lower uncertainties were observed as all counts exceeded 100.

	Station	1	2	3	4	5	6	7	8	$\bar{x}$
Jan.	^{222}Rn	1.5±2.5	0±0	0.98±1.6	--	--	49.1±55	--	25.2±39	76.8±19.6
	^{224}Ra	--	--	--	--	--	--	--	--	--
	^{226}Ra	--	--	--	--	--	--	--	--	--
	AR	--	--	--	--	--	--	--	--	--
Jul.	^{222}Rn	0±37.7	57.7±78.4	160.1±129.9	153.1±130.2	--	266.1±171.3	--	56.0±68.1	693.0±102.6
	^{224}Ra	2.03±0.2	30.5±3.1	164.4±16.4	167.2±16.7	--	61.0±6.1	--	8.7±0.9	72.3±7.2
	^{226}Ra	52.9±5.3	33.7±3.4	63.3±6.3	53.4±5.3	71.2±7.1	44. 4±4.4	--	14.1±1.4	47.6±4.8
	AR	0.04	0.91	2.60	3.13	--	1.37	--	0.62	1.44
Nov.	^{222}Rn	169.5±67.7	643.4±111	0±0	789.6±111	1557.5±222.4	448.1±131.0	--	187.3±68.1	333.4±101.6
	^{224}Ra	12.2±1.2	--	54.5±5.4	9.6±0.9	5.25±0.5	--	--	12.6±1.3	18.8±1.9
	^{226}Ra	15.5±1.6	37.0±3.7	39.9	36.3±3.6	--	--	--	12.8±1.3	28.3±2.9
	AR	0.79	--	1.37	0.26	0.07	--	--	0.98	0.69

4.3 SUBMARINE GROUNDWATER DISCHARGE

4.3.1 ^{222}RN-DERIVED SGD ESTIMATES

All, but one of the radon measurements were conducted during times with no recorded precipitation in July and November (Texas Water Development Board, Water Data for Texas website (NAAS, 2017; TWDB, 2016)). Time-series sampling at station 12 in July was performed within 24 hours of a precipitation event (total rainfall: 51 mm (NAAS, 2017)).

4.3.1.1 POREWATER AND GROUNDWATER RADON ACTIVITIES

Porewater ^{222}Rn activities were measured at a minimum of five locations every sampling event (i.e. January, July, and November). These porewater grab samples did not always exceed the supported ^{222}Rn activity derived from sediment equilibration experiments (**Table 2**Error! Reference source not found.). In January and July, porewater ^{222}Rn activities ranged from 1.5 Bq·m^{-3} to 49.10 Bq·m^{-3} ($\bar{x}$=19.2 Bq·m^{-3}, n=4) and 56.0 Bq·m^{-3} to 266.1 Bq·m^{-3} ($\bar{x}$=138.6 Bq·m^{-3}, n=5), respectively (Table 2Error! Reference source not found.). Porewater ^{222}Rn activities in November ranged from 169.5 Bq·m^{-3} to 1557.5 Bq·m^{-3} ($\bar{x}$=632.7 Bq·m^{-3}, n=6) (**Table 2**Error! Reference source not found.). Wells available for sampling within the area surrounding Baffin Bay were screened at depths ranging from 186.8-383.4 m. ^{222}Rn activities in these wells vary from 1,884 Bq·m^{-3} to 13,136 Bq·m^{-3} ($\bar{x}$=7094.4 Bq·m^{-3}, n=6). (Error! Reference source not found.).

Well ID	8326201	8327501	8329201	8329401	8342508	8334403	($\bar{x}$)
^{222}Rn	13,135.6 ± 1085.6	4,019.0 ± 493.5	2,646.0 ± 464.8	9,254.5 ± 1300.2	11,627.3 ± 1699.4	1,883.7 ± 675.4	7094.4 ±953.2
^{224}Ra	8.4±0.84	3.5±0.35	4.3±0.43	4.8±0.48	9.3±0.93	269.7±27.0	50.0±5.0
^{226}Ra	3.2±0.32	4.8±0.48	1.2±0.12	17.7±1.77	7.5±0.75	244.7±24.5	46.5±4.65
AR	2.67	0.72	3.50	0.27	1.25	1.10	1.58
Depth	264	244	358	383	222	187	276

Table 3: Groundwater Well ^{222}Rn, ^{224}Ra, ^{226}Ra activities ($Bq \cdot m^{-3}$) including the AR which is the ^{224}Ra activity divided by the ^{226}Ra activity and well depth (m).

4.3.1.2 SGD ESTIMATES AND THE CHOICE OF ENDMEMBER

Previous studies have shown that selection of a representative groundwater endmember for estimation of SGD fluxes is challenging (Burnett and Dulaiova, 2003; Cerdà-Domènech et al., 2017; Garcia-Orellana et al., 2013; Lamontagne et al., 2008; Urquidi-Gaume et al., 2016) as it can result in a large range of magnitudes. Similar to the Murgulet et al. (2018) study, to account for these possible uncertainties, we used three ^{222}Rn groundwater endmembers to estimate SGD rates: 1) the greatest porewater ^{222}Rn activity (1,557 $Bq \cdot m^{-3}$), 2) the average of six select groundwater sample activities ($\overline{x}$ = 7,094 $Bq \cdot m^{-3}$) and 3) the highest groundwater ^{222}Rn activity (13,136 $Bq \cdot m^{-3}$). The highest ^{222}Rn in porewater for the duration of the study (1,557 $Bq \cdot m^{-3}$) was similar to the lowest groundwater activity (1,884 $Bq \cdot m^{-3}$) from the deep wells located in close proximity to the bay. The different ^{222}Rn activities in the groundwater endmembers do not result in large SGD rate variability (**Table 3**Error! Reference source not found.**, Table 4**Error! Reference source not found.**, Table 5**Error! Reference source not found.); however, using the largest porewater ^{222}Rn activity yields SGD rates that are relatively high when considering the hydroclimatic and hydrologic conditions in this area. The SGD estimates derived with the highest porewater activity are deemed as the least conservative and most unrealistic, not only when compared to the previous study by Uddameri et al. (2013), which measured rates between -15.69 $cm \cdot d^{-1}$ (submarine groundwater recharge) to 48 $cm \cdot d^{-1}$ (SGD), but given the semiarid climate with low precipitation rates and thus, reduced recharge rates to the water table aquifer.

The average groundwater endmember yields more reasonable and comparable (to previous studies and similar climates) SGD rates. Average SGD rates from continuous survey for

each of the Baffin Bay sub-bays and the Baffin Bay mouth are slightly higher in July ($\bar{x}$: 31.3 $cm \cdot d^{-1}$) when compared to November ($\bar{x}$: 26.6 $cm \cdot d^{-1}$) (**Table 4**Error! Reference source not found.**).** Average SGD rates from time series are only slightly lower with closely matching July ($\bar{x}$: 22.9 $cm \cdot d^{-1}$) and November ($\bar{x}$: 26.6 $cm \cdot d^{-1}$) rates (**Table 4**Error! Reference source not found.**, Table 5**Error! Reference source not found.).

The highest groundwater endmember results in more conservative SGD estimates with rates about half lower than those determined using the average groundwater, but with the same trends as described above. Time-series SGD rates ranged from 6.3 $cm \cdot d^{-1}$ to 31.3 $cm \cdot d^{-1}$ over the course of this study. Continuous SGD rates for each of the sub-bays ranged from 4.6 $cm \cdot d^{-1}$ to 21.5 $cm \cdot d^{-1}$.

Event	Endmember	Cayo del Grullo	Alazan Bay	Laguna Salada	Baffin Bay Mouth	Average
July	Avg. gw	33.9±11.4	34.7±18.0	25.4±13.4	33.9±9.7	31.3±13.1
	Max. gw	18.3±6.1	18.7±9.7	13.7±7.2	18.3±5.2	16.9±7.05
	Max. pw	154.6±51.8	158.1±82.0	115.6±60.9	154.4±44.1	142.8±59.7
November	Avg. gw	39.8±5.0	35.3±10.0	22.9±2.1	8.5±2.4	26.6±4.88
	Max. gw	21.5±2.7	19.1±5.4	12.0±1.2	4.6±1.3	14.3±18.3
	Max. pw	181.2±22.7	161.0±45.6	101.6±9.8	38.8±10.8	120.7±22.2

Table 4: SGD rates (in $cm \cdot d^{-1}$) calculated from continuous ^{222}Rn measurements for July and November sampling events for the Baffin Bay inlets and mouth. The SGD uncertainty is derived from the standard deviation (σ) of all measurements for the different areas of the bay. Included are SGD rates calculated using the average and maximum groundwater (Avg. gw and Max. gw) ^{222}Rn and the maximum porewater (Max. pw) ^{222}Rn.

Table 5: SGD rates (in $cm \cdot d^{-1}$) calculated from time-series ^{222}Rn measurements for July and November sampling events. Included are SGD rates calculated using the average groundwater (Avg. gw) ^{222}Rn and the maximum groundwater (Max. gw) ^{222}Rn. The SGD uncertainty is derived from the standard deviation (σ) of all measurements during each time-series event.

Event	Endmember	Station 9	Station 10	Station 11	Station 12	Average
July	Avg. gw	19.6±10.0	11.7±5.9	31.2±11.5	29.0±15.3	22.9±10.7
	Max. gw	10.6±5.4	6.3±3.2	16.9±6.2	15.7±8.3	12.4±5.78
November	Avg. gw	18.2±15.5	15.5±11	58.0±32.9	14.6±8.1	26.6±16.9
	Max. gw	9.8±8.4	8.4±5.9	31.3±17.8	7.9±4.4	16.3±9.13

Overall, SGD rates derived from the time-series measurements do not show a trend similar to those from continuous/bay-wide estimates. To note, however, is that the rates are within the same order of magnitude and SGD rates are lower than 60 $cm \cdot d^{-1}$ in both instances. Time-series rates are an average of a large number of ^{222}Rn 30-minute integrations in-situ (n= 16), thus increasing the potential of capturing variations in SGD throughout the day (i.e. higher or lower rates of SGD). Continuous measurements, which are a snapshot of ^{222}Rn activities within a relatively small area, capture larger areas that could include more significant SGD rates, as well as variable wind conditions. Commonly, in the study area, calm wind conditions occur in the first part of the day and start picking up in the afternoon (**Figure 2**). Wind conditions also vary in a day-by-day basis. The increased wind speed causes more wave action and degassing of ^{222}Rn from the water column at rates greater than during calm conditions (Wanninkhof, 1992), especially in shallow water bodies such as Baffin Bay. This variation in wind conditions, throughout one survey or between two survey days, could lead to ^{222}Rn degassing rates captured in some parts of the bays and not in others. In this study, we find that wind speed and ^{222}Rn activity are inversely correlated (R^2:0.4; p-value: <<0.001) (**Figure 20**Error! Reference source not found.). Losses of ^{222}Rn due to persistent wind gusts have been also observed by Spalt et al. (2018) in Copano Bay.

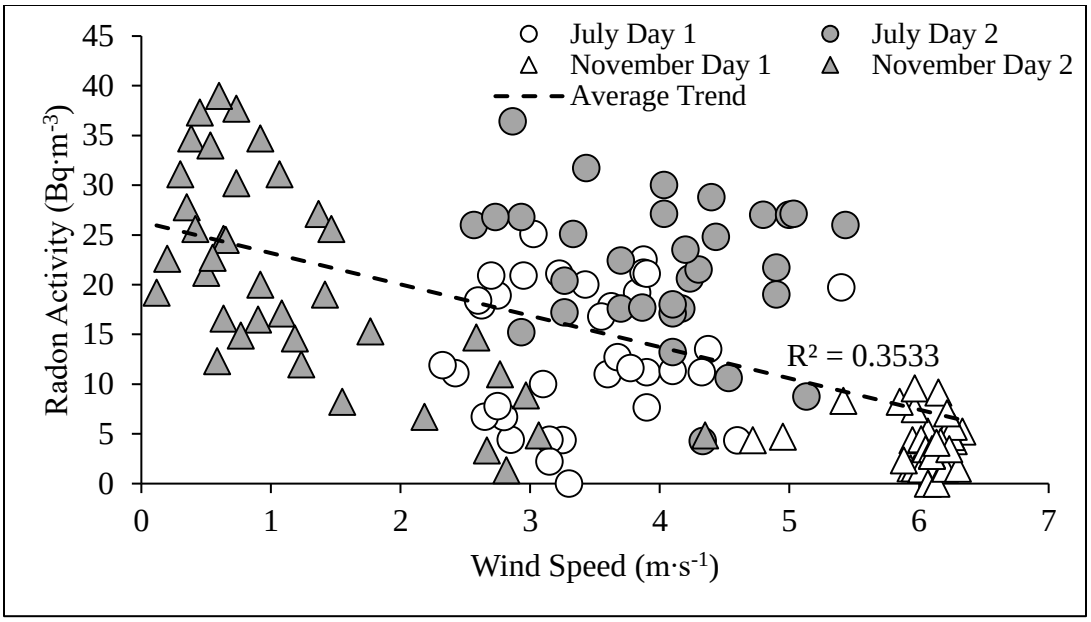

Figure 20: Wind speed ($m \cdot s^{-1}$) versus ^{222}Rn activity ($Bq \cdot m^{-3}$) in the water column during the continuous surveys.

During the first survey day in November, a large majority of ^{222}Rn activities (n=51) were below those supported by the ^{226}Ra in the water column (11.1 to 18.5 $Bq \cdot m^{-3}$). These measurements are associated with the maximum wind speeds for all surveys (min: 0.12 $m \cdot s^{-1}$, max: 6.33 $m \cdot s^{-1}$) (**Figure 20**Error! Reference source not found.). As long-term high winds may lead to degassing of ^{222}Rn and lower activities in the water (Wanninkhof, 1992), beyond those accounted for in the mass-balance, the resulting SGD rates will likely be underestimated. In this study, the lowest ^{222}Rn was measured along the transect going from the Baffin Bay mouth to the Laguna Salada. Mixing of bay waters with more isotopically lighter water coming from the Laguna Madre is expected to also lead to lower SGD rates if not accurately accounted for in the ^{222}Rn inventory. However, ^{226}Ra activity, measured at each of the eight sampling stations within the bay, at the mouth of the bay going into Laguna Madre was accounted for. Thus, there is a strong indication that ^{222}Rn degassing due to prolonged high-wind speeds and gusts in the days leading up to sampling is unaccounted for in the atmospheric evasion term of the mass-balance,

which leads to lower SGD rates for the season. To partially account for this loss due to degassing, SGD rates for November were calculated using the lowest observed surface water ^{222}Rn activity as an estimate of the expected background ^{222}Rn activity. All ^{222}Rn activities measured during the continuous mobile survey in July were above those supported by the ^{226}Ra in the water column and the wind speeds in the days prior to sampling were lower than in November (average wind speed of the previous 48 hours: 4.31 $m \cdot s^{-1}$ in July, 7.36 $m \cdot s^{-1}$ in November), thus wind effects were significantly lower in July.

The most outstanding difference in SGD estimated using the time-series ^{222}Rn assessment between July and November was at station 11 (Laguna Salada). SGD rates are lower in July (31.2±11.5 $cm \cdot d^{-1}$) at station 11 (Error! Reference source not found.**)**, which could be explained by the above observations related to wind effects and Laguna Madre input. In contrast, in November, SGD rates at station 11 are higher (58.0±32.9 $cm \cdot d^{-1}$), almost double compared to July (Error! Reference source not found.). This is the largest SGD rate measured during time-series events and exceeds the average rates from continuous mobile surveys (31.3, and 26.6 $cm \cdot d^{-1}$ for July and November, respectively). For all other stations, change in rates of SGD is much smaller from July to November, particularly using the time-series method.

4.3.2 ^{226}RA-DERIVED SGD ESTIMATES

The ^{224}Ra/^{226}Ra AR measured from local groundwater wells and porewater samples were compared to those of surface water to derive radium water ages (Knee et al., 2011b). With the average AR of local deep groundwater identified as the endmember advecting fluid, the estimated ages ranged from 5.2 to 7.9 days in January ($\bar{x}$=6.8±1.0 days, n=8), 0.7 to 5.6 days in July ($\bar{x}$=3.8±1.8 days, n=7), and 12.8 to 40.6 days in November ($\bar{x}$=29.1±8.2 days, n=8). Negative ages are a likely indication that deep groundwater is not an appropriate end-member at

this location, as it expected given the existence of a large cone of depression extending in close proximity to the bay (i.e., Kingsville) (Shafer and Baker, 1973). In comparison, using the porewater AR as the advecting fluid endmember results in overall lower ages: July: 1.0 to 3.1 days ($\bar{x}$=2.1 days, n=6), excluding stations 5, and 8, which resulted in negative ages; and November: 1.4 to 11.6 days ($\bar{x}$=7.4 days, n=8). The resulting negative ages combined with the lower overall estimated average ages could be evidence of terrestrial input in July at some locations not captured in the sampling. On the other hand, in November the sampled porewater seems to be more representative of the SGD input. Nevertheless, porewater activities were used as the representative endmember in SGD calculations, given that it likely captures the terrestrial as well as local (i.e. sediment) inputs.

The average daily SGD rates for the Baffin Bay in July and November, using the average ^{226}Ra activity of porewater as the groundwater endmember, averaged 14.9±1.49 cm·d^{-1}. Available porewater ^{224}Ra and ^{226}Ra indicate a significant decrease in activities from July to November (**Table 2**). Using the seasonal porewater ^{226}Ra endmembers and corresponding surface water radium ages, SGD rates were 16.6±1.7 cm·d^{-1} for July, and 13.2±1.3 cm·d^{-1} for November. This small variability is mainly related to changes in the porewater and surface water activities (**Table 1, Table 2**) as they influence the water ages, the ^{226}Ra inventory, and the conversion to a final bay wide SGD (Charette et al., 2001). Although, ^{226}Ra activities were greater in July in surface water, SGD rates are only slightly more elevated given that the porewater endmember activity is also greater. These large differences in porewater activities are indicative of either changes in inputs and/or changes in redox conditions to and within the subterranean estuary (see sections 5.1)

4.3.3 SGD COMPARISON

The different methods resulted in SGD rates of same order of magnitude, however of slightly different intensities (**Figure 21**). Average SGD rates derived from time-series and mobile continuous ^{222}Rn measurements estimates, using the average deep groundwater activities as the endmember ranged from 22.9 cm·d^{-1} in July to 26.6 cm·d^{-1} in November and 31.4 cm·d^{-1} in July to 30.0 cm·d^{-1} in November, respectively (**Table 4, Table 5**). In comparison, radium-derived SGD rates were about half, ranging from 16.6 cm·d^{-1} to 13.2 cm·d^{-1} in July and November, respectively.

For the entire bay, an SGD rate can most reliably be estimated from the mobile continuous ^{222}Rn and ^{226}Ra methods as they provide greater (i.e. bay wide) spatial coverage and a more spatially integrated signal, respectively. Although different in intensity, both ^{222}Rn and ^{226}Ra inventories estimate similar SGD rates for July (mobile continuous ^{222}Rn: 31.4 cm·d^{-1} and radium: 16.6 cm·d^{-1}) and November (mobile continuous ^{222}Rn: 30.0 cm·d^{-1} and ^{226}Ra: 13.2 cm·d^{-1}), though July is slightly higher than November (**Figure 21**). The different intensity of SGD derived from the two methods is within the associated errors as presented in this work (**Figure 21**). Furthermore, using the highest groundwater activity endmember, the SGD rates derived using ^{222}Rn as a tracer are in-line with the Ra estimates (**Table 4, Table 5).** For instance, time-series average SGD are 12.4 and 16.3 cm·d^{-1} in July and November, respectively and the continuous/bay-wide average rates are 16.9 and 14.3 in July and November, respectively. However, given the limited likelihood of groundwater discharge from deeper aquifers and the lower ^{222}Rn activities measured in porewater, a choice of the most conservative endmember should not be used. This is in addition to the inability of radium estimates to represent both fresh- and salt-water SGD forms, but rather represent the salty component of SGD.

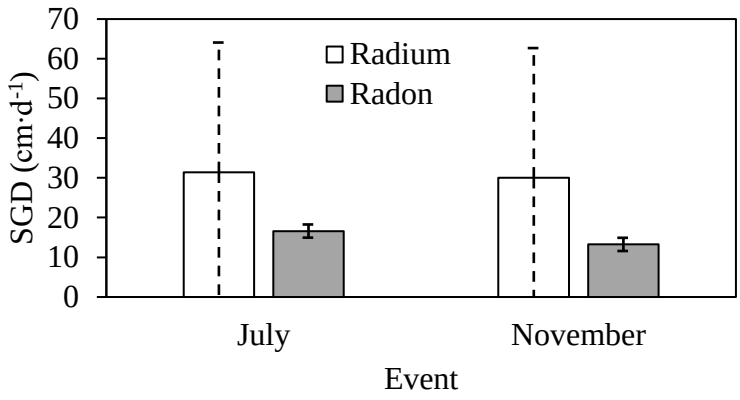

Figure 21: Graph of ^{226}Ra based SGD rate vs ^{222}Rn based continuous radon SGD rate with associated errors.

While ^{222}Rn is unreactive and capable of reliably measuring total SGD (including fresh terrestrial groundwater, saline porewater, and recirculating seawater) (Burnett and Dulaiova, 2003), ^{226}Ra requires that the SGD be saline enough to keep the ^{226}Ra in solution and not adsorbed to the sediment. Thus, ^{226}Ra reliably accounts for saline groundwater discharge or seawater recirculation, but likely misses fresher SGD (Moore, 2006). Nevertheless, while potentially higher total SGD rates may occur at some locations within the bay (i.e. 58.0±32.9 cm·d^{-1} at station 11 in November using time-series ^{222}Rn and the average of the groundwater wells endmember, **Table 5**), given the potentially larger than reported uncertainties associated with ^{222}Rn-derived rates (i.e. propagation error throughout the mass balance and end-member), an argument of saline versus fresh input of SGD cannot be supported. The close agreement between the two methods are more likely to reflect the relative dominance of saline SGD in Baffin Bay.

4.4 NUTRIENT FLUXES

Nutrient fluxes were calculated as the product of porewater nutrient concentrations (**Table 6**) and the ^{222}Rn-derived SGD rates estimated from the continuous/bay-wide measurements derived using the average groundwater endmember.

4.4.1 NITRATE

The average flux of NO_3^- in Baffin Bay across all events was 64.6 μmol per day (μmol·d^{-1}) (n=11) for the spatial sampling stations (1-6, 8) (**Table 7**). No nutrient fluxes were calculated for station 7, as extraction of porewater samples at this location was not successful. The only measurable NO_3^- flux ($7.1x10^2$ μmol·d^{-1}) was at station 8, near the mouth of Baffin Bay, in July. For all other stations there were no measurable nitrate fluxes (0.00 μmol·d^{-1}: stations 1-4, 6)). In November, all porewater NO_3^- concentrations were below the mean detection limit resulting in no measurable fluxes (**Table 6, Table 7**).

Table 6: Porewater nutrient concentrations (μM) for each of the spatial sampling sites by season. Samples where no nutrients were measured are denoted by "--" and DON concentrations that are derived from DIN concentrations larger than TDN, leading to negative DON, are denoted by "==". Porewater NO_3^- below the method detection limit (MDL) are included as "<0.11".

Station	Event	NO_3^-	NO_2^-	NH_4^+	HPO_4^{2-}	$HSiO_3^-$	DOC	TDN	DIN	DON
1	Jan.	<0.11	0.8	816.0	19.5	234.3	1270.5	1860.2	816.8	1043.4
	Jul.	<0.11	7.1	5531.3	43.7	559.0	1630.2	3224.9	5538.5	==
	Nov.	<0.11	0.6	1011.0	14.2	407.9	3126.4	3226.7	1011.6	2215.1
2	Jan.	0.6	0.3	658.9	9.8	183.4	480.6	420.2	659.7	==
	Jul.	<0.11	6.1	1394.9	43.0	511.6	850.9	841.7	1401.1	==
	Nov.	<0.11	0.7	744.1	11.0	205.9	814.1	818.5	744.8	73.7
3	Jan.	0.8	0.2	38.6	1.6	56.7	647.4	384.2	39.5	344.7
	Jul.	<0.11	4.8	1563.6	38.0	550.0	469.2	911.3	1568.4	==
	Nov.	<0.11	0.5	788.1	11.9	205.9	810.2	729.2	788.6	==
4	Jan.	--	--	--	--	--	--	--	--	--
	Jul.	<0.11	5.2	1833.4	33.5	257.8	1013.7	1007.7	1838.6	==
	Nov.	<0.11	0.7	716.4	7.7	201.3	1085.7	856.7	717.1	139.6
5	Jan	--	--	--	--	--	--	--	--	--
	Jul.	--	--	--	--	--	--	--	--	--
	Nov.	<0.11	0.6	553.6	6.7	207.4	737.1	543.5	554.2	==
6	Jan.	0.5	0.4	426.3	4.5	169.7	619.5	183.4	427.2	==
	Jul.	<0.11	5.4	523.8	27.0	204.1	387.8	328.1	529.2	==
	Nov.	<0.11	0.7	348.8	2.8	230.0	393.1	282.7	349.6	==
7	Jan.	--	--	--	--	--	--	--	--	--
	Jul.	--	--	--	--	--	--	--	--	--
	Nov.	--	--	--	--	--	--	--	--	--
8	Jan.	0.3	0.2	824.6	3.3	135.5	462.0	241.7	825.1	==
	Jul.	2.0	0.4	2501.7	4.9	259.7	560.6	1408.6	2504.1	==
	Nov.	<0.11	0.4	937.8	4.4	376.4	596.3	1093.8	938.2	155.6

4.4.2 NITRITE

The average flux of NO_2^- in Baffin Bay across all events was $9.5 \cdot 10^2$ μmol·d^{-1} (n=11) for the spatial sampling sites (**Table 7**). The highest NO_2^- flux (2.4×10^3 μmol·d^{-1}) was calculated at stations 2 and 6, near the mouth of the three bay inlets and upstream of the mouth of Alazan Bay in July and the lowest (0.4×10^2 μmol·d^{-1}), at station 8 in November (**Figure 1,** Error! Reference source not found.). Lower average NO_2^- fluxes in November are driven mostly by the lower porewater NO_2^- concentration measured at all stations except 8. In some instances, SGD rates are

also lower in November, such as at stations 5, 7 and 8. The larger flux at station 6 is driven mostly by the SGD rate, which is the highest, measured during each event (**Table 7**). At station 2, both larger SGD flux and larger NO_2^- concentrations lead to one of the largest NO_2^- fluxes in July.

4.4.3 AMMONIUM

The average flux of NH_4^+ in Baffin Bay for the July and November events was $4.2x10^5$ $\mu mol \cdot d^{-1}$ (n=11). The largest NH_4^+ fluxes ($8.8x10^5$ $\mu mol \cdot d^{-1}$) were calculated at stations 1 and 8, in the Laguna Salada and near the mouth of Baffin Bay in July (**Table 7**). The lowest flux of NH_4^+ ($8.5x10^4$ $\mu mol \cdot d^{-1}$) was measured at station 8 in November. The highest porewater NH_4^+ measured each event occurred at station 8 and station 1. In July, the largest NH_4^+ fluxes measured at stations 8 are a combination of larger SGD fluxes and higher NH_4^+ concentrations while the lower measured SGD rates and porewater NH_4^+ in November lead to lower NH_4^+ fluxes. While average SGD rates are similar between July and November, porewater concentrations of NH_4^+ (as well as NO_2^-, HPO_4^{2-}, and $HSiO_3^-$) are significantly decreasing from July to November (**Table 6**). As a result, the solute flux was lower in November at all stations within the bay (**Table 7**).

A negative, inverse relationship ($p<0.05$ when outlier included) between porewater NH_4^+ concentrations and SGD in July (**Figure 22**), indicates that NH_4^+ is accumulating in the sediments where SGD rates are lower. Increasing SGD in the form of porewater recirculation may remove NH_4^+ from porewater sediments (Santos et al., 2012). On the other hand, in November, although a negative relationship appears visible, the correlation is statistically insignificant ($p>0.05$). As discussed in the SGD section, in November, degassing of radon due to

high winds, preceding the mobile continuous survey, may have lowered SGD rates unevenly throughout the bay, potentially skewing the relationship discussed above.

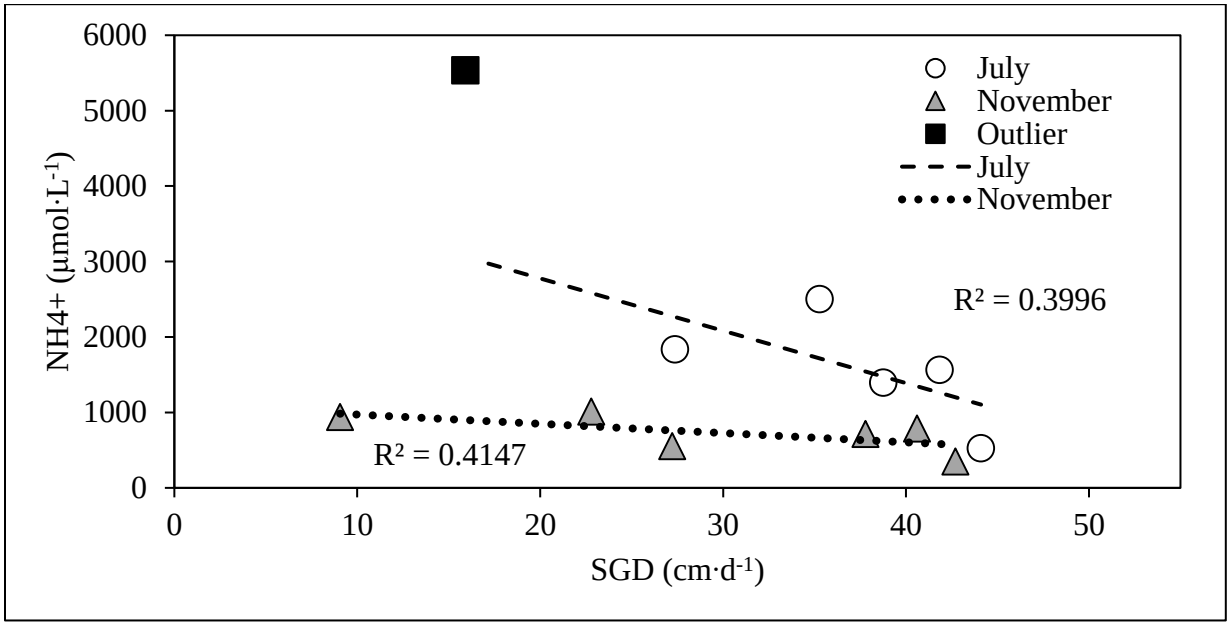

Figure 22: SGD rates, calculated using the mobile continuous ^{222}Rn method, versus porewater NH_4^+ concentration. The July event negative correlation is not significant (R^2: 0.4; p-value: 0.2518). If the outlier of Station 1 is included in July the relationship is significant (R^2: 0.82; p-value: 0.01347). In November, the correlation is slightly negative but not statistically significant (R^2: 0.38; p-value of 0.1676).

4.4.4 ORTHOPHOSPHATE

The average flux of HPO_4^{2-} in Baffin Bay across all events was $6.7x10^3$ µmol·d^{-1} (n=11) (**Table 7**). The highest HPO_4^{2-} fluxes were measured at stations 2 and 3 ($17x10^3$ and $16x10^3$ µmol·d^{-1}, respectively) in July near the location where Cayo del Grullo meets Laguna Salada, while the lowest ($0.4x10^3$ µmol·d^{-1}) at station 8 in November. In July, the lowest HPO_4^{2-} flux occurred at station 8 (**Table 7 and Figure 23A**). The highest measured HPO_4^{2-} concentrations for July and November occurred at stations 1, 2, and 3. Thus, higher HPO_4^{2-} fluxes measured at stations 2 and 3 in both months are the result of larger porewater concentrations and higher SGD rates (**Table 6, Table 7**). On the other hand, at station 1, HPO_4^{2-} fluxes are lower due to lower

measured SGD. Seasonal trends are similar to NH_4^+, with decreasing fluxes of HPO_4^{2-} from July to November.

Table 7: SGD rates ($cm \cdot d^{-1}$) determined from the mobile continuous ^{222}Rn survey and nutrient fluxes ($x10^3$ μmol d^{-1}) for the bay determined as the product of SGD and the porewater nutrient concentrations. The SGD uncertainty is derived from the standard deviation (σ) of all measurements for the different areas of the bay and nutrient flux uncertainty is the product of the SGD uncertainty and the nutrient concentration.

Station	Event	SGD	NO_3^-	NO_2^-	NH_4^+	HPO_4^{2-}	$HSiO_3^-$	DOC	TDN	DIN	DON
1	Jul.	15.9± 18.6	0.0± 0.0	1.1± 1.33	881.2± 1027.5	7.0± 8.12	89.1± 103.8	259.7± 302.8	513.8± 599.1	882.3± 1028.9	==
	Nov.	22.8± 4.3	0.0± 0.0	0.1± 0.02	230.5± 43.36	3.2± 0.61	93.0± 17.5	712.8± 134.1	735.7± 138.4	230.6± 43.4	505.0 ±95.0
2	Jul.	38.8± 16.3	0.0± 0.0	2.4± 1.00	540.7± 227.6	16.7± 7.02	198.3± 83.5	329.8± 138.8	326.3± 137.3	543.1± 228.6	==
	Nov.	--	--	--	--	--	--	--	--	--	--
3	Jul.	41.8± 14.3	0.0± 0.0	2.0± 0.69	654.3± 224.2	15.9± 5.45	230.1± 78.9	196.3± 67.3	381.3± 130.7	656.3± 224.9	==
	Nov.	40.6± 8.9	0.0± 0.0	0.2± 0.04	320.0± 69.8	4.8± 1.05	83.6± 18.2	329.0± 71.8	296.1± 64.6	320.2± 69.9	==
4	Jul.	27.4± 26.9	0.0± 0.0	1.4± 1.41	502.1± 493.9	9.2± 9.03	70.6± 69.5	277.6± 273.1	276.0± 271.5	503.5± 495.3	==
	Nov.	37.8± 10.8	0.0± 0.0	0.3± 0.07	270.7± 77.2	2.9± 0.83	76.1± 21.7	410.3± 116.9	323.7± 92.3	271.0± 77.3	52.8 ±15.0
5	Jul.	39.0± 36.2	--	--	--	--	--	--	--	--	--
	Nov.	27.2± 9.0	0.0± 0.0	0.2± 0.05	150.7± 49.9	1.8± 0.60	56.4± 18.7	200.6± 66.5	147.9± 49.0	150.8± 50.0	==
6	Jul.	44.1± 29.3	0.0± 0.0	2.4± 1.59	231.0± 153.4	11.9± 7.91	90.0± 59.8	171.0± 113.5	144.7± 96.1	233.4± 155.0	==
	Nov.	42.7± 12.4	0.0± 0.0	0.3± 0.09	148.9± 43.4	1.2± 0.35	98.2± 28.6	167.8± 48.9	120.7± 35.2	149.3± 43.5	==
7	Jul.	17.2± 22.2	--	--	--	--	--	--	--	--	--
	Nov.	9.9± 6.8	--	--	--	--	--	--	--	--	--
8	Jul.	35.3± 0.07	0.7± 0.0	0.1± 0.0	882.8± 1.84	1.7± 0.0	91.6± 0.19	197.8± 0.41	497.1± 1.03	883.7± 1.84	==
	Nov.	9.1± 4.9	0.0± 0.0	0.0± 0.02	85.0± 45.5	0.4± 0.22	34.1± 18.3	54.0± 28.9	99.1± 53.1	85.0± 45.5	14.1± 7.55

4.4.5 HYDROGEN SILICATE

The average flux of $HSiO_3^-$ in Baffin Bay for July and November was $1.0x10^5$ μmol d^{-1} (n=11) with the highest ($2.3x10^5$ μmol·d^{-1}) measured at station 3 in July and the lowest ($0.34x10^5$ μmol·d^{-1}) at station 8 in November (**Table 7, Figure 23**). In July, the largest $HSiO_3^-$ fluxes were measured at stations 2 and 3 ($2.0x10^5$ and $2.3x10^5$ μmol·d^{-1}, respectively) and the smallest at station 4 ($0.7\ x10^5$ μmol·d^{-1}) (**Figure 23A**). In November, the highest flux of $HSiO_3^-$ was measured at station 6 ($1\ x10^5$ μmol·d^{-1}) and the lowest ($0.34x10^5$ μmol·d^{-1}) at station 8 (**Figure 23B**).

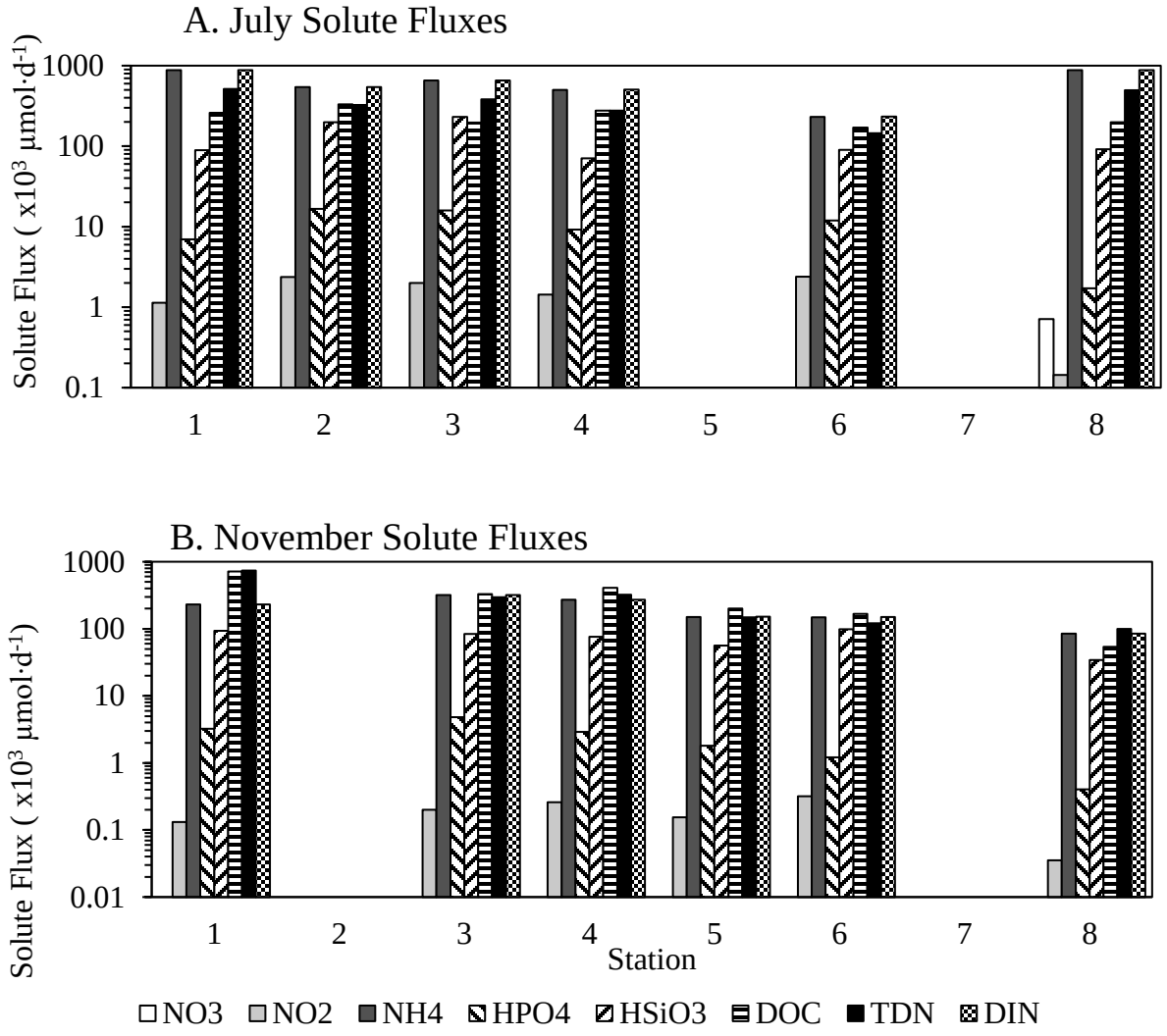

Figure 23: Graphical representation of solute fluxes derived as the product of porewater solute concentrations and SGD rates from the continuous mobile ^{222}Rn surveys.

The highest $HSiO_3^-$ measured each event occurred at stations 1, 2 and 3 with the July concentrations larger than the November. At station 8, $HSiO_3^-$ is also high, but concentrations are higher in November than in July. Thus, the larger $HSiO_3^-$ flux, a product of concentration and SGD, is at station 3, while at station 8 lower SGD rates in November lead to the lowest $HSiO_3^-$ flux for both seasons. As discussed in the SGD section, these may be the result of radon degassing and underestimated SGD rates.

4.4.6 COMPARISON OF SUBSURFACE AND SURFACE FLUXES OF SOLUTES

The surface water inflows modeled by (TWDB, 2016) were used to estimate fluxes of nutrients to the bay from surface runoff in January, June and July (**Table 8**). These modeled surface inflows include surface runoff from the three creeks that discharge into Baffin Bay and any land runoff resulting from precipitation within each of the watersheds. The fluxes were determined as the product of modeled surface inflows and the solute concentrations collected from each respective creek, at locations close to the discharge mouth to the bay. It is assumed that the concentrations of solutes in the creeks remained the same for each surveyed month. The average fluxes presented in this section are derived from the full months of January, July, and November and for all three creeks discharging into Baffin Bay.

The average input of NO_3^- was 2.9×10^8 μmol·d^{-1}. The maximum and minimum fluxes were both estimated to occur from Los Olmos Creek in January (17×10^8 μmol·d^{-1}) and November (0.18×10^8 μmol·d^{-1}), respectively. The average input of NO_2^- was 0.11×10^8 μmol·d^{-1} with a maximum of 0.26×10^8 μmol·d^{-1} in January and a minimum of 0.0052×10^8 μmol·d^{-1} in July, both from Los Olmos. The three-month average flux of NH_4^+ was 2.7×10^8 μmol·d^{-1} and while the maximum of 17×10^8 μmol·d^{-1} occurred from Los Olmos Creek in January, the minimum of

$0.13x10^8$ μmol·d^{-1} was estimated from the San Fernando Creek in January and November. The resulting average DIN flux was $5.7x10^8$ μmol·d^{-1} with the maximum and minimum of $34x10^8$ and $0.4x10^8$ μmol d^{-1} in January and November, respectively, both from Los Olmos Creek. This is mainly related to higher freshwater inflows that, based on our field observations, are likely to be overestimated by the model.

The average HPO_4^{2-} flux was $2.0x10^8$ μmol·d^{-1} with a maximum of $4.3x10^8$ μmol·d^{-1} from Petronila Creek in January and a minimum of $0.043x10^8$ μmol·d^{-1} from Los Olmos in November. The average $HSiO_3^-$ flux was $95x10^8$ μmol·d^{-1} with a maximum of $270x10^8$ μmol·d^{-1} from Petronila Creek in January and a minimum of $1.3x10^8$ μmol·d^{-1} from Los Olmos Creek in November.

Average flux of DOC for the creeks was estimated to be $320x10^8$ μmol·d^{-1} with maximum and minimum inputs from San Fernando Creek in January ($2,100x10^8$ μmol·d^{-1}) and November ($11x10^8$ μmol·d^{-1}). The average TDN flux was $89x10^8$ μmol·d^{-1} with a maximum of $640x10^8$ μmol·d^{-1} from Los Olmos Creek in January and a minimum of $2.9x10^8$ μmol·d^{-1} from San Fernando Creek. The DON flux was similar to the TDN flux, with an average of $84x10^8$ μmol·d^{-1} and a maximum of $610x10^8$ μmol·d^{-1} from Los Olmos Creek in January and a minimum of $1.7x10^8$ μmol·d^{-1} from San Fernando Creek in January and November.

Nutrient fluxes were also estimated using the USGS stream gauge daily discharge data for the San Fernando and Los Olmos Creeks (the Petronila Creek is ungauged) (

Table 9). The streamflow data used is from the Los Olmos stream gauge (USGS, 2017b), the San Fernando stream gauge (USGS, 2017a), and from the Tranquitas Creek, a tributary of the San Fernando that joins the San Fernando Creek south of the previously mentioned stream gauge (USGS, 2018).

Creek	Month	NO_3^-	NO_2^-	NH_4^+	HPO_4^{2-}	$HSiO_3^-$	DOC	TDN	DIN	DON
Los Olmos	Jan.	17.0	0.26	1.7	4.0	120.0	2100	640	34	610
	Jul.	0.3	0.005	0.33	0.08	2.3	42	13	0.7	12
	Nov.	0.2	0.003	0.18	0.04	1.3	23	6.9	0.4	6.6
San Fernando	Jan.	11.1	0.04	0.13	0.63	4.3	111	28.9	1.2	1.7
	Jul.	2.8	0.1	0.33	1.6	11	28	7.5	3.2	4.3
	Nov.	1.1	0.04	0.13	0.63	4.3	11	2.9	1.2	1.7
Petronila	Jan.	1.6	0.2	2.4	4.3	270.0	230	51	4.2	47
	Jul.	1.4	0.2	2.1	3.7	240.0	200	44	3.6	40
	Nov.	1.2	0.16	1.8	3.1	200.0	170	37	3.1	34
Total watershed	Jan.	19.7	0.5	19.5	8.9	394.3	2341	693.9	39.4	658.7
	Jul.	4.5	0.3	2.8	5.4	253.3	270	64.5	7.5	56.3
	Nov.	2.9	0.2	2.1	3.8	205.6	204	46.8	4.7	42.3

Table 8: Freshwater inflow fluxes ($\mu mol \cdot d^{-1} x10^8$) of NO_3^-, NO_2^-, NH_4^+, HPO_4^{2-}, $HSiO_3^-$ for July and November derived as the product of creek water nutrient concentration multiplied by creek discharge into Baffin Bay from TWDB (2016).

During the period of the study, the Los Olmos Creek stream gauge measured zero discharge; therefore, it is assumed that there was no solute input from Los Olmos Creek. In addition, no streamflow discharge data are available for Petronila Creek, leaving only the San Fernando Creek for comparison of solute flux rates with those derived from the modeled inflow. The average flux rate of NO_3^- across all events for the San Fernando Creek is $8.8x10^8$ µmol d^{-1} with the lowest output estimated for July ($2.3x10^8$ µmol d^{-1}) and the highest in January ($10x10^8$ µmol d^{-1}). The input of NO_2^- was on average $0.36x10^8$ µmol d^{-1} with the highest estimated input in November ($0.57x10^8$ µmol d^{-1}) and the lowest in July ($0.09x10^8$ µmol d^{-1}). The average input of NH_4^+ was approximately $1.1x10^8$ µmol d^{-1} with the highest input being in November ($1.7x10^8$ µmol d^{-1}) and the lowest in July ($0.27x10^8$ µmol d^{-1}). The resulting input of DIN from the San Fernando Creek ($\bar{x}$: $10.5x10^8$ µmol d^{-1}) is larger than that derived from the modeled inflows (1.9

x10^8 μmol d-1). The highest input from stream gauge estimates is estimated to have occurred in November (17x10^8) and the lowest in January (2.6x10^8 μmol d^{-1}), while the estimates from the

Creek	Month	NO_3^-	NO_2^-	NH_4^+	HPO_4^{2-}	$HSiO_3^-$	DOC	TDN	DIN	DON
Los Olmos	Jan.	0	0	0	0	0	0	0	0	0
	Jul.	0	0	0	0	0	0	0	0	0
	Nov.	0	0	0	0	0	0	0	0	0
San Fernando	Jan.	10	0.41	1.2	6.1	41	110	28	12	16
	Jul.	2.3	0.090	0.27	1.3	9.0	23	6.1	2.6	3.5
	Nov.	14	0.57	1.7	8.4	57	150	39	17	22
Petronila	Jan.	--	--	--	--	--	--	--	--	--
	Jul.	--	--	--	--	--	--	--	--	--
	Nov.	--	--	--	--	--	--	--	--	--

modeled inflows are the largest in January (**Table 8 and**

Table 9).

The average HPO_4^{2-} flux was 5.3x10^8 μmol d^{-1} with the highest estimated rate in November (8.4x10^8 μmol d^{-1}) and the lowest in July (1.3x10^8 μmol d^{-1}). The average $HSiO_3^-$ flux was 35.7x10^8 μmol d^{-1}, with the highest estimated rate in November (57x10^8 μmol d^{-1}) and the lowest in July (9.0x10^8 μmol d^{-1}). The average flux of TDN from the San Fernando Creek was 24.4x10^8 μmol d^{-1} with the highest rate in November (39x10^8 μmol d^{-1}) and the lowest in July (6.1x10^8 μmol d^{-1}). The average DON input was 41.5x10^8 μmol d^{-1}, with an estimated maximum in November (22x10^8 μmol d^{-1}) and minimum in July (3.5x10^8 μmol d^{-1}). DOC fluxes were on average 94.3x10^8 μmol d^{-1} with the highest rate in November (150x10^8 μmol d^{-1}) and the lowest in July (23x10^8 μmol d^{-1}).

Overall, the estimated solute fluxes using the two surface inflows for the San Fernando Creek are in the same order of magnitude. Differences are noted among the months when the minimum or maximum are expected. However, given the close agreement among the two different estimates (i.e. using the modeled inflow and the stream gauge data), we believe that the modeled inflow estimates may be used as substitutes for the gauged streamflow. As most gauges

are in general located a considerable distance upstream from the discharge mouth to the bay, the estimated solute fluxes may be overestimated as we observe in this study for San Fernando

Creek	Month	NO_3^-	NO_2^-	NH_4^+	HPO_4^{2-}	$HSiO_3^-$	DOC	TDN	DIN	DON
Los Olmos	Jan.	0	0	0	0	0	0	0	0	0
	Jul.	0	0	0	0	0	0	0	0	0
	Nov.	0	0	0	0	0	0	0	0	0
San Fernando	Jan.	10	0.41	1.2	6.1	41	110	28	12	16
	Jul.	2.3	0.090	0.27	1.3	9.0	23	6.1	2.6	3.5
	Nov.	14	0.57	1.7	8.4	57	150	39	17	22
Petronila	Jan.	--	--	--	--	--	--	--	--	--
	Jul.	--	--	--	--	--	--	--	--	--
	Nov.	--	--	--	--	--	--	--	--	--

Creek. However, large solute fluxes were estimated from the Los Olmos Creek using the ungagged flow (modeled), while there was no measurable discharge at the gauge. Thus, the estimates from the ungagged inflow rates may be overestimating the flux of solutes into the bay in times with no rain or observed streamflow discharge to the bay.

Table 9: Solute fluxes ($\mu mol \cdot d^{-1} x 10^8$) for July and November derived as the product of porewater nutrient concentration by sampling stations multiplied by *streamflow discharge from USGS water gauges.* No streamflow data are available for the Petronila Creek, denoted as "--".

Given that SGD was measured spatially, across the entire Baffin Bay system, we applied a bay-wide seasonal average SGD rate to determine the bay-wide flux rate of solutes (**Table 10, Figure 24**). This, together with the average solute concentration of porewater, measured each season, indicates that a DIN contribution from the subsurface of $1{,}533.5 x 10^8$ $\mu mol \cdot d^{-1}$ is expected in July, while an almost three times lower rate of $479 x 10^8$ $\mu mol \cdot d^{-1}$, may occur in November. Similarly, phosphate (HPO_4^{2-}) and silicate ($HSiO_3^-$) are also larger bay-wide in July ($22 x 10^8$ and $268 x 10^3$ $\mu mol \cdot d^{-1}$, respectively) than in November ($5.5 x 10^3$ and $172 x 10^3$ $\mu mol \cdot d^{-1}$, respectively), but of lower magnitudes overall than DIN. Average bay-wide DOC fluxes from SGD are larger in November ($710 x 10^8$ $\mu mol \cdot d^{-1}$) than July ($563 x 10^3$ $\mu mol \cdot d^{-1}$).

To estimate the overall importance of SGD in the bay-wide nutrient budget, surface runoff inputs were estimated using the Texas Water Development Board's Water Data for Texas modeled coastal freshwater inflows for the sub-watersheds feeding into the Baffin Bay system. Solute concentrations from the three creeks discharging into Baffin Bay were used as the representative concentrations for the surface inflow fluxes (**Table 10, Figure 24**). Assuming that the solute concentration is constant across the seasons, a DIN of $39.4x10^8$ $\mu mol \cdot d^{-1}$ is expected in January, $7.5x10^8$ $\mu mol \cdot d^{-1}$ in July and $4.7x10^8$ $\mu mol \cdot d^{-1}$ in November. Orthophosphate (HPO_4^{2-}) and hydrogen silicate ($HSiO_3^-$) are also larger in January with a flux rates of ($8.9x10^8$ and $394x10^8$ $\mu mol \cdot d^{-1}$) followed by July ($5.4x10^8$ and $253x10^8$ $\mu mol \cdot d^{-1}$) and November ($3.8x10^8$ and $206x10^8$ $\mu mol \cdot d^{-1}$). Average DOC fluxes from surface runoff are larger January ($2{,}341x10^8$ $\mu mol \cdot d^{-1}$), followed by July ($270x10^8$ $\mu mol \cdot d^{-1}$) and November ($204x10^3$ $\mu mol \cdot d^{-1}$).

A comparison of bay-wide solute fluxes (**Figure 24**) indicates that DIN inputs, mainly in the form of ammonium, are almost two orders of magnitude higher in the SGD component than the surface runoff. DOC inputs are also larger in the SGD component in July and November. Inorganic nitrogen in the form of nitrate is likely to enter Baffin Bay from surface inputs while SGD may have larger contributions of nitrite. Orthophosphate and silicate (in the form of hydrogen silicate ion) are very similar in magnitudes.

Average solute flux	Event	NO_3^-	NO_2^-	NH_4^+	HPO_4^{2-}	$HSiO_3^-$	DOC	TDN	DIN	DON
SGD flux: in $\mu mol \cdot d^{-1}x10^3$ per *1 m^2 area*	July	0.1	1.5	698.6	10.0	122.6	257.1	404.1	700.2	==
	Nov.	0	0.2	218.6	2.5	78.6	324.1	323.6	218.7	193.8
SGD flux: in **$\mu mol \cdot d^{-1}x10^8$** per *bay area*	July	0.2	3.3	1529.9	21.8	268.4	563.01	885.1	1533.5	==
	Nov.	0	0.4	478.7	5.5	172.2	709.8	708.7	479.1	424.4
Total watershed flux: in **$\mu mol \cdot d^{-1}x10^8$**	Jan.	19.7	0.5	19.5	8.9	394.3	2341	693.9	39.4	658.7
	Jul.	4.5	0.3	2.8	5.4	253.3	270	64.5	7.5	56.3
	Nov.	2.9	0.2	2.1	3.8	205.6	204	46.8	4.7	42.3

Table 10: Average solute fluxes for July and November derived from the bay-wide mobile continuous SGD estimates in $\mu mol \cdot d^{-1}x10^3$ per 1 m^2 and in $\mu mol \cdot d^{-1}x10^8$ per bay area 2.19 $x10^8$

m^2 along with a total watershed flux (using modeled inflows) in $\mu mol \cdot d^{-1} x 10^8$. DON concentrations affected by analytical limitations of TDN measurements in porewater, are denoted by "==".

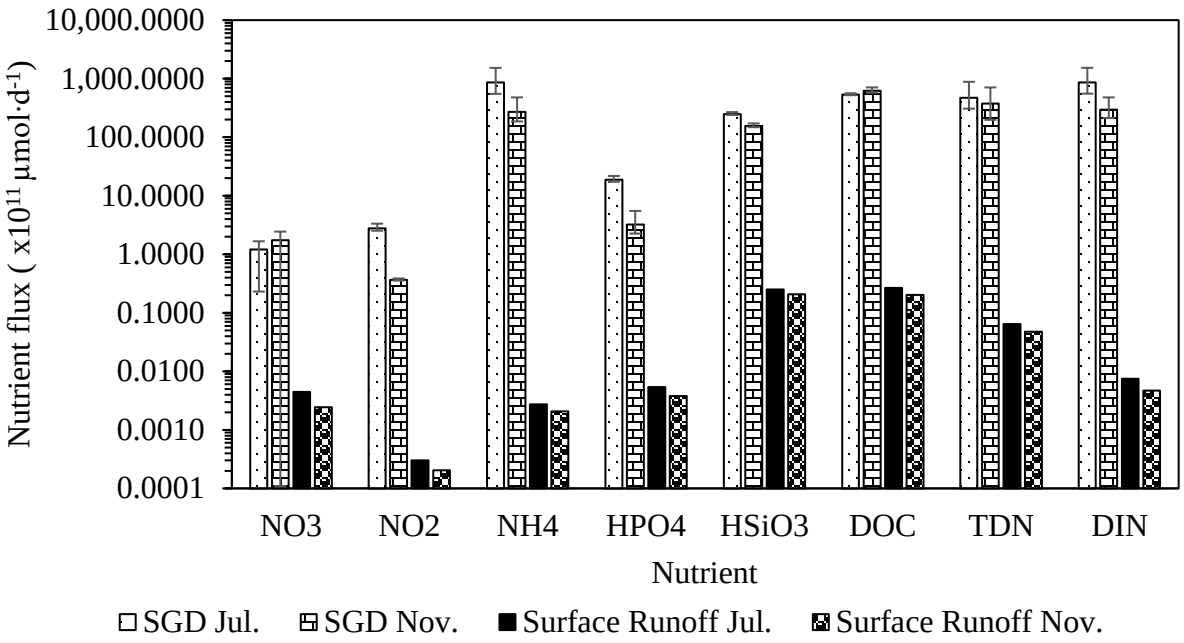

Figure 24: Comparison of solute fluxes derived from SGD and modeled surface runoff inflows. Error bars represent the maximum fluxes derived using the deep porewater nutrient concentration and the minimum fluxes determined using the shallow porewater depth range (**Tables 16, 19**).

5. RESIDENCE TIMES, SGD AND PW NUTRIENT FATE

5.1 SGD TRENDS

July discharge rates were determined to be only slightly higher than those in November by the ^{226}Ra and the continuous Rn methods, and considering the errors associated with each of the methods, these differences are not deemed significant. July had higher ^{226}Ra activities in the porewater and surface water, which could suggest that higher SGD rates are to be expected (Garcia-Orellana et al., 2014; Moore, 1996). Salinity levels in the porewater throughout the study (ranging from 31.0-65.6 in January, 48.3-60.9 in July, and 49.0-59.3 in November, see **Figure 6**) have been consistently above the maxima reported in the literature of 10 to 20, to enhance desorption from sediments (Elsinger and Moore, 1980; Webster et al., 1995). Thus, at these

salinities, almost all adsorbed radium would likely be in solution, in both the porewater and surface water (Webster et al., 1995). Even with an increase in salinity, if above 20, desorption of radium from sediment should no longer occur, yet a positive relationship is observed between porewater salinity (above 45) and ^{226}Ra (R^2 = 0.43, p-value = 0.01988) (**Figure 18**).

Based on Ra-derived water ages, the shortest bottom sediment flushing time was in July while the longest in November. Longer flushing times are expected to be associated with lower SGD and surface water-porewater mixing rates. Though the flushing rates as estimated in this study are dependent on ^{226}Ra activities of both porewater and surface water that were higher in July and could have been caused by changes in porewater chemistry conditions (ORP, pH) (Kadko et al., 1987), rather than larger terrestrial inputs of groundwater. For instance, organic matter decomposition and remineralization, that may be significant during warm seasons when phytoplankton activity is expected to be higher, could enhance ^{226}Ra desorption leading to an increase in porewater activity (Kadko et al., 1987), and thus in surface water (see discussion below related to estuary productivity and SGD). In our study, enrichment of surface water accompanied by a similar trend in porewater (see section 4.2.3 and 4.3.2) does not lead to larger Ra-derived SGD rates in July. This strongly suggests that changes in the end-member signature with time should be considered in SGD calculations.

Although SGD rates are similar throughout the bay, some locations along the northern shoreline may be subject to larger magnitudes of SGD rates, especially following rain events and changes in hydrologic gradients. Some of the sampling sites chosen for the investigation with the aid of the CRP imagery are associated with locations of remnants serpulid reefs in Baffin Bay (Dalrymple (1964) (**Figure 3, Figure 4**). Many of the reefs were located on sandy substrates (Simms et al., 2010) that would be excellent conductors of SGD and preferential flow paths for

any kind of groundwater discharge (Fetter, 2001). Sites 6 and 3 are expected to overlie serpulid reefs (6) or lie close to reefs (3), as indicated by the elevated bathymetry and higher subsurface resistivity (**Figure 3, Figure 4, Figure 5**) and the serpulid reef-rock found in the sediment core at one of these locations (**Figure 5**). As expected, these locations are associated with higher than average (July SGD $\bar{x}$: 32.4±20.5 cm·d^{-1}, November SGD $\bar{x}$: 27.2±8.1 cm·d^{-1}) continuous ^{222}Rn SGD rates (Fetter, 2001; Simms et al., 2010) as measured during spatial surveys, both in July and November at stations 6 (44.1±29.3 and 42.7±12.4 cm·d^{-1}, respectively) and 3 (41.8±14.3 and 40.6±8.9 cm·d^{-1}, respectively) (**Table 7**). In addition, porewater at station 3 (extracted from depths ranging from 1-1.8 m depths) had salinities similar to the surface water in January and November; all other porewaters had regularly maintained a salinity at least 10 greater than the surface water.

5.1.2 SGD AND SURFACE WATER BIOLOGICAL PRODUCTIVITY

The best indicator of biological productivity from this dataset is the measurement of chl-α in the surface and bottom water. The average January chl-α concentration for spatial samples (surface and bottom combined) is 13.7 μg·L^{-1}, the average for July was 14.9 μg·L^{-1}, and the average for November was 12.2 μg·L^{-1}. The increased SGD fluxes of nutrients across the bay concurs with higher overall production. However, overall no significant relationship between SGD and chl-α concentration is observed (R^2 of 0.03, p-value of 0.5176). Nevertheless, the slightly higher chl-α in July is expected due to increases in temperature and sunlight in July, while the data shows that nutrient inputs were to remain the same across the sampled seasons.

The increase in biomass may have implications on the porewater chemistry, beyond levels of nutrients. For instance, the increase in chl-α leads to increased OM in the sediments, which, when degraded, leads to more reducing conditions that facilitate the release of ^{226}Ra to

porewater and, consequently, the water column (Windom and Niencheski, 2003), along with production of NH_4^+, PO_4^{3-}, and $HSiO_3^-$ (Buskey et al., 2001; Weston et al., 2006) as observed in this study. However, due to its short half-life, ^{224}Ra ($t_{½}$: 3.63 days) is unlikely to contribute significantly via desorption as any adsorbed ^{224}Ra during oxic conditions would have decayed while bound to the sediment (Windom and Niencheski, 2003). In this system, ^{224}Ra and ^{226}Ra increased in activity in July with activity ratios larger than in November ($\overline{x}$ AR for July and November: 1.38, 0.47 respectively, **Table 1**). These enrichment of the short-lived isotope over the long-lived ^{226}Ra ($t_{½}$: 1,600 years) indicates that some input of ^{224}Ra (and ^{226}Ra) is likely associated with a shallow groundwater source, as also indicated by Spalt et al. (2018) to occur in Copano Bay. Shallow transport of groundwater enriched in nutrients in July could be the result of a wet spring season that recharged the water table aquifer and increased hydraulic gradients towards the coast. A shift towards more terrestrial input rather than seawater intrusion, not necessarily associated with a change in SGD magnitude, within the subterranean estuary leading to July sampling, may be a source of nutrients, which when combined with OM degradation leads to the significant increase in porewater nutrient concentrations when compared to January and November.

5.2 FACTORS CONTROLLING POREWATER ACCUMULATIONS

5.2.1 SEDIMENT FLUSHING RATES AND SGD

Longer sediment flushing time conditions and/or lower SGD rates have been associated with the accumulation of salts, production of ammonia and reduced or low dissolved oxygen in porewaters (Fetter, 2001; Gardner et al., 2006; Kadko et al., 1987). In this study, the limited exchange between surface water and porewater as it leads to higher concentrations of NH_4^+ in porewater (and other nutrients, salts, etc.), in orders of magnitudes higher than the surface water

($\overline{x}$ NH_4^+: 1178.5 vs 6.15 μM, $\overline{x}$ $HSiO_3^-$: 275.4 vs 101.2 μM, $\overline{x}$ salinity: 54.7 vs 40.3, $\overline{x}$ alkalinity:14,271.6 vs 3191.6 μM, and $\overline{x}$ DIC: 13,401.9 vs 2,666.8 μM for porewater and surface water respectively), is observed to some extent spatially each season. Lower porewater nutrient concentrations were observed in November (July $\overline{x}$ and November $\overline{x}$ concentrations: 390 vs 262 μM $HSiO_3^-$, 2,225 vs 729 μM NH_4^+, 13,838 vs 13,622 μM of TA, etc.), when bottom flushing rates (July, excluding negatives: min. 1 day, max. 3.1 days, $\overline{x}$ 1.1 days; November: min. 1.4 days, max. 11.6 days, $\overline{x}$ 7.4 days) and SGD (July: min. 15.9±18.6, max. 44.1±29.3, $\overline{x}$ 32.4±20.5 $cm \cdot d^{-1}$; November: min. 9.1±4.9, max. 42.7±12.4, $\overline{x}$ 27.2±8.1 $cm \cdot d^{-1}$) are only slightly lower, but within the associated errors.

Although, overall there is no relationship between SGD and NH_4^+, as discussed in section 4.4.3, there is an inverse relationship between SGD and NH_4^+ when analyzed by season, with the most significant correlation in July (including the outlier, **Figure 22**) when fluxes of SGD are more variable. Nevertheless, some relationships between one sampling season to another have been identified for two stations. For instance, a sharp decrease in the concentration of NH_4^+ at station 11 in porewater was observed from July to November ($\overline{x}$: 1,908.9 μM and 488.2 μM, respectively). This has been associated with an almost doubling of SGD rate from July to November, as shown from the time-series SGD measurements. In addition, during spatial sampling, the highest NH_4^+ concentration ($5.5x10^3$ μM) was measured in close proximity to station 11 (i.e. station 1), also associated with an increase in SGD rate from 15.9±18.6 $cm \cdot d^{-1}$ in July to 22.8±4.3 $cm \cdot d^{-1}$ in November leading to a lower porewater NH_4^+ concentration in November ($1.0x10^3$ μM). Thus, at this station SGD may have a significant influence in the buildup of NH_4^+, possibly leading to observed lower NH_4^+ in November.

Another observation of possible influences of SGD on porewater nutrient accumulation are the areas that overlie (station 6) or lie close to serpulid reefs (station 3) (**Figure 1, Figure 3**). As discussed in section 5.1, these stations are characterized by higher than average SGD rates and have generally lower nutrient concentrations in porewaters (**Table 6**), which are also of salinities similar to surface water such as station 3, during January and November (January, July, and November porewater 31.0, 58.9, 49.0 and surface water: 31.1, 35.0, 44.1, respectively). In addition, when compared to any other porewater samples, with the exception of station 8 in July, higher NO_x and lower NH_4^+ concentrations (station 3 in January, July, and November 1.0, 4.8, 0.5 μM of NO_x, 38.6, 1563.6, 788.1 μM of NH_4^+ and bay-wide 0.82, 5.17, 0.6 μM of NO_x, 552.9, 2224.8, 728.5 μM of NH_4^+, respectively where NO_3^- <0.11 is considered as a zero) were also measured at station 3 (**Table 6**), likely the result of faster exchange and mixing between surface- and pore-water due to more permeable substrates (see section 5.1). The transformation of NH_4^+ to NO_x is likely to have happened rapidly here (Schiavo et al., 2009) as more exchange with surface water leads to oxidizing conditions leading to coupled nitrification-denitrification (Brandes et al., 2007). During more active wind and wave conditions, enhanced mixing of porewater and surface water at this station could increase fluxes of nutrients to the bay. In this study, a high-enough temporal resolution sampling of porewater chemistry was not conducted to observe rapid changes in ORP, salinity, or nutrients, but the presence of highly permeable sediments and the observed similarities in the water chemistry between surface and subsurface water for the three seasons indicate the more rapid exchange between subsurface and bay waters.

The July observed significant increases in porewater nutrients, other than NH_4^+ (up to $5.5x10^3$ μM) and NO_2^- (up to 7.1 μM), such as HPO_4^{2-} and $HSiO_3^-$, may be associated with terrestrial sources, in addition to remineralization. High porewater NH_4^+ concentrations in the

1,000-5,000 μM range have been measured in anoxic porewater sediments by Abdulla et al. (2018) at depths between 0.5-4 m in the Santa Barbara Basin where it was likely produced by organic matter remineralization. In this study however, the larger ^{224}Ra and ^{226}Ra porewater activities and lower residence times in July may also be indicative of larger terrestrial inputs which when coupled with remineralization may lead to the observed buildup of nutrients. Thus, changes in accumulation rates of nutrients in porewater from one season to another may be related to varying extents of remineralization and input of external sources through the subterranean estuary (e.g., groundwater). However, within each season, and, in particular July, the inverse relationship between SGD and NH_4^+ (R^2: 0.82; p-value: 0.01347, **Figure 22**) do suggest that SGD magnitudes can affect accumulation of nutrients in porewater when flushing rates are lower (see section 4.4.3).

As indicated above, similar to the nutrients, alkalinity is also highest in July porewaters. Production of alkalinity in sediments has been associated with increased anaerobic remineralization of organic matter from larger phytoplankton production (i.e. chl-a) (**Figure 7, Figure 8**) (Chaillou et al., 2014) such as observed and expected to occur during summer months (see section 3.2.2). Nitrogen cycling can have small effects on alkalinity in porewater (Gardner et al., 2006). For instance, nitrification, when occurring at a rate similar to denitrification, consumes alkalinity faster than denitrification can produce it (Li and Irvin, 2007). However, nitrification occurs in oxidizing conditions which do not pervade reducing sediments such as is shown in this study by the largely negative ORP values across all sampling events ($\bar{x}$: -311.8 mV). Therefore, the observed reducing conditions associated with increases in alkalinity (Gardner et al., 2006) are indicative of denitrification processes. In addition, an increase in porewater alkalinity with NH_4^+ can be observed (**Figure 14**) (R^2: 0.34; p-value: 0.01336). The

prevailing reducing conditions of most porewaters (ORP $\bar{x}$: -229.6, -345.8, -341.3 mV for January, July, and November, respectively), and the positive correlation between NH_4^+ and alkalinity indicate that organic matter remineralization is likely occurring as well as DNRA.

The absence of measurable NO_3^- in porewater associated with large amounts of NH_4^+, in July and November, further suggest low nitrification activity and the rapid consumption or reduction to NH_4^+ (DNRA). Measurable amounts of NO_3^- in January at four out of five stations, accompanied by some of the lowest NH_4^+, could result from lower reduction rates as ambient temperatures are lower. Dong et al. (2011) suggests that, at lower temperatures and higher NO_3^- concentrations, estuaries in temperate environments exhibit proportionately greater levels of anammox and benthic denitrification. In July, the likely source of the NO_2^-, which is in higher concentrations than in November (0.38, 4.83, 0.60 μM of NO_2^- in January, July, and November respectively, **Table 6**), is denitrification facilitated by the increased availability of NO_3^- and NH_4^+ from either OM remineralization or groundwater input.

5.2.2 SALINITY EFFECTS

In Baffin Bay surface water salinities increased significantly from event to event ranging from 30.45 to 57.51 ($\bar{x}$: 39.6). Porewater samples show a slight increase from January ($\bar{x}$: 52.26) to July ($\bar{x}$: 56.52) and slightly decrease to November ($\bar{x}$:54.77) (**Figure 6**). Salinity has been shown to have inhibitory effects on nitrogen cycling processes such as nitrogen fixation, nitrification, denitrification, and DNRA. Salinities effects on remineralization (i.e. organic matter decomposition) have been found to be contradictory and poorly understood (Ardón et al., 2013; Gardner et al., 2006; Rysgaard et al., 1999). While some studies found increases in remineralization rates with salinities (Gardner et al., 2006; Giblin et al., 2010; Santoro, 2010), others found the opposite (Steinke and Charles, 1986) or that depending on other conditions,

increasing salinity may enhance or diminish rates of remineralization (Stagg et al., 2017). However, these studies are limited to salinity ranges below those observed in Baffin Bay (2-17 (Mendelssohn et al. (1999)) and 0-30 (Steinke and Charles (1986)), respectively) and may not be applicable to the studied environment.

Nitrogen fixation was found to decrease with increasing salinities and in some environments it is not observed in salinities above 8 to 10 (Ardón et al., 2013; Gardner et al., 2006; Rysgaard et al., 1999). Nitrification has also been found to decrease with increasing salinity and the associated increase in sulfide concentrations (Gardner et al., 2006; Giblin et al., 2010; Santoro, 2010). Denitrification has been shown to decrease with salinity as well through effects on microorganism physiology, hydrogen sulfide toxicity to denitrifiers, and reduced availability of NO_3^- (Ardón et al., 2013; Rysgaard et al., 1999). DNRA has been shown to increase with increases in salinity likely due to enhancement by sulfate-reducing bacteria which provides sulfide as an electron donor and creates reducing conditions (Gardner et al., 2006). Assimilation of N has also been shown to decrease with increasing salinities (du Plooy et al., 2015). The large difference in the relative abundances of porewater NH_4^+ and NO_3^- in this study seem to agree with the literature (Ardón et al., 2013; Gardner et al., 2006; Rysgaard et al., 1999), which suggests that the increased salinity levels in Baffin Bay may have facilitated the buildup of NH_4^+ in the sediment porewater. The concentration of NH_4^+ in the surface water is higher than the concentration of NO_3^-, likely due to the decrease in nitrification, denitrification, and increase in DNRA (Ardón et al., 2013; Gardner et al., 2006; Giblin et al., 2010). A conceptual model of processes that may govern the nutrient fate in porewater in Baffin Bay are included in **Figure 25**.

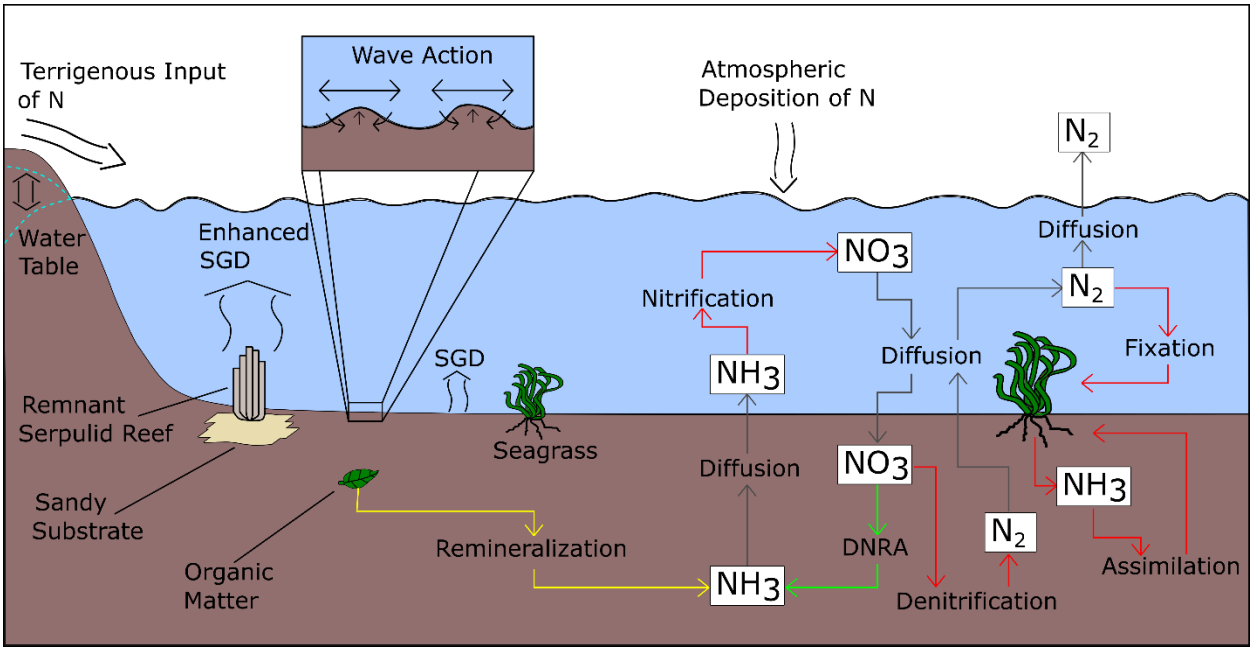

Figure 25: Conceptual diagram of N cycling processes in Baffin Bay and examples of SGD. Red arrows indicate processes slowed by increasing salinity, green arrows indicate processes aided by increasing salinity, whereas yellow arrows indicate processes where the effects of salinity are not well constrained.

6. CONCLUSION

A key goal of this study is to understand the role of SGD on nutrient transport to Baffin Bay in order to shed light on the driving forces of harmful algal bloom occurrences. SGD rates are expected to change across the hydroclimatic gradient in response to changes in precipitation rates, aquifer recharge rates, hydraulic gradients, and riverine inputs. Five of the seven bays along the Texas Gulf Coast have been classified as being potentially affected (≥67%) by increased salinization and decreases in water quality, productivity, sediment, and nutrient transport due to reductions in freshwater inflow. These adverse conditions have major impacts on the life cycles and health of many marine species, with potential repercussions throughout the food web. Although, SGD has been recognized as an important component of the hydrologic and biogeochemical system cycles that link terrestrial waters to marine environments in many coastal areas, there is a lack of understanding about its role in alleviating or contributing to these

problems. Due to the exceptionally high concentrations of nutrients and organic matter accumulated in aquifers, and subterranean estuaries, SGD may fuel bacterial respiration, leading to hypoxic conditions in estuaries.

In Baffin Bay, SGD rates vary slightly spatially and by season at a few locations with rates ranging from 9.1±4.9 to 44.1±29.3 cm·d^{-1} ($\bar{x}$: 30.0±14.7 cm·d^{-1}) for the continuous ^{222}Rn method (**Table 7**). However, the average SGDs for July and November derived from continuous mobile ^{222}Rn surveys (31.4±32.7, 30.0±30.9 cm·d^{-1}, respectively) and from the ^{226}Ra inventory (16.6±1.66, 13.2±1.32 cm·d^{-1}, respectively) across the entire bay system are in very close agreement given the uncertainties associated with each measurement and the choice of endmember. On the other hand, nutrient concentrations measured in the interstitial porewater varies significantly both spatially and temporally. Consequently, in the Baffin Bay system, SGD-derived nutrient fluxes are not so much a function of changes in hydrologic conditions spatially and across seasons (i.e. changes in SGD rates), but rather vary significantly with changes in nutrient concentrations in the porewater. Even though, SGD rates are lower when compared to the other South Texas estuaries, the associated nutrient fluxes are much more elevated. In particular, NH_4^+ concentrations were found to be largely elevated (by one or two orders of magnitude), with the largest measured concentrations in porewater in July (5,531 µmol·L^{-1}) and a minimum in January (538.6 µmol·L^{-1}) compared to other bays such as Aransas Bay (porewater NH_4^+ $\bar{x}$: <1 µM) (Douglas et al., 2017), and Corpus Christi Bay (porewater NH_4^+ $\bar{x}$: <250 µM) (Murgulet et al., 2015).

A comparison of bay-wide solute fluxes indicates that DIN inputs, mainly in the form of ammonium, are almost two orders of magnitude higher in the SGD component than the surface runoff. DOC inputs are also larger in the SGD component in July and November. Inorganic

nitrogen in the form of nitrate is likely to enter Baffin Bay from surface inputs while SGD may have larger contributions of nitrite. Orthophosphate and silicate (in the form of hydrogen silicate ion) are very similar in magnitudes. Therefore, the nutrient input associated with SGD, regardless of its nature (i.e. fresh or saline; groundwater or recirculated saline), is likely significant in this shallow bay system. The characteristic persistent winds in this area are likely the dominant driver of seawater recirculation, while episodic rain events may enhance the fresher SGD input in this bay. Both scenarios can lead to diffusion of porewater solutes into the water column.

The fate of porewater nutrients in Baffin Bay is predetermined by their source (i.e. internal versus external) and the bay conditions (both hydrogeologic and biogeochemical). The majority of nutrient sources in the porewater, as observed in the contrast between July and November, is likely to be from degradation of OM from phytoplankton during warm months. OM deposited on the surface sediments is remineralized leading to production of NH_4^+, HPO_4^{2-}, $HSiO_3^-$ and carbon (which contributes to alkalinity). In addition, the nitrogen cycling bacterial community is affected by the hypersaline conditions in the porewater and surface water inhibiting processes such as the coupled nitrification and denitrification and leading to reduced nitrogen fixation and uptake and increased DNRA. These conditions are likely a major cause of the observed significant buildup of NH_4^+, particularly in the hot months such as July. On the other hand, the higher porewater ^{224}Ra and ^{226}Ra activities and greater $^{224}Ra/^{226}Ra$ activity ratios measured in July in both surface water and the porewater when combined with the increase in porewater NO_2^- is an indication that input through the subterranean estuary may have changed from July to November. A shift from seawater intrusion to a terrestrial input as a result of increased in hydraulic gradients could explain not only the enrichment of ^{224}Ra over ^{226}Ra, but a

supply of nitrate. Therefore, both a different source of groundwater as well as an increase in the OM degradation are considered sources of nutrients to Baffin Bay during the warm season, following spring wet conditions.

REFERENCES

Advanced Geosciences, I., (2017) SuperSting Marine Resistivity. Advanced Geosciences, Inc.

Alaniz, R.T., Goodwin, R.H. (1974) Recent sediments of a hypersaline estuarine bay: Gulf Coast Association of Geological Societies. Transactions 24, 308-313.

Ardón, M., Morse, J.L., Colman, B.P., Bernhardt, E.S. (2013) Drought-induced saltwater incursion leads to increased wetland nitrogen export. Global Change Biology 19, 2976-2985.

Ashworth, J.B., Hopkins, J., (1995) Major and minor aquifers of Texas, in: Board, T.W.D. (Ed.), p. 69.

Behrens, E.W. (1963) Buried Pleistocene river valleys in Aransas and Baffin bays, Texas. Publications of the Institute of Marine Science, University of Texas 9, 7-18.

Behrens, E.W. (1966) Surface salinities for Baffin Bay and Laguna Madre, Texas, April 1964-March 1966. Publications of the Institute of Marine Science, University of Texas 11, 168-179.

Brandes, J.A., Devol, A.H., Deutsch, C. (2007) New developments in the marine nitrogen cycle. Chem Rev 107, 577-589.

Breier, J.A., Breier, C.F., Edmonds, H.N. (2010) Seasonal dynamics of dissolved Ra isotopes in the semi-arid bays of south Texas. Marine Chemistry 122, 39-50.

Breuer, J.P. (1957) An ecological survey of Baffin and Alazan Bays, Texas: Publ., Inst. Mar. Sci 4, 134-155.

Brock, D. (2001) Uncertainties in Individual Estuary N-Loading Assessments. Nitrogen Loading in Coastal Water Bodies: An Atmospheric Perspective, 171-185.

Brown, R.M., McClelland, N.I., Deininger, R.A., Tozer, R.G. (1970) A Water Quality Index - Do We Dare.

Burnett, W.C., Dulaiova, H. (2003) Estimating the dynamics of groundwater input into the coastal zone via continuous radon-222 measurements. Journal of Environmental Radioactivity 69, 21-35.

Burnett, W.C., Taniguchi, M., Oberdorfer, J. (2001) Measurement and significance of the direct discharge of groundwater into the coastal zone. Journal of Sea Research 46, 109-116.

Buskey, E.J., Liu, H., Collumb, C., Bersano, J.G.F. (2001) The Decline and Recovery of a Persistent Texas Brown Tide Algal Bloom in the Laguna Madre (Texas, USA). Estuaries 24, 337-346.

Cerdà-Domènech, M., Rodellas, V., Folch, A., Garcia-Orellana, J. (2017) Constraining the temporal variations of Ra isotopes and Rn in the groundwater end-member: Implications for derived SGD estimates. Science of the Total Environment 595, 849-857.

Chaillou, G., Couturier, M., Tommi-Morin, G., Rao, A.M. (2014) Total alkalinity and dissolved inorganic carbon production in groundwaters discharging through a sandy beach. Procedia Earth and Planetary Science 10, 88-99.

Charette, M.A., Buesseler, K.O., Andrews, J.E. (2001) Utility of radium isotopes for evaluating the input and transport of groundwater-derived nitrogen to a Cape Cod estuary. Limnology and Oceanography 46, 465-470.

Conley, D.J., Paerl, H.W., Howarth, R.W., Boesch, D.F., Seitzinger, S.P., Havens, K.E., Lancelot, C., Likens, G.E. (2009) Controlling Eutrophication: Nitrogen and Phosphorus. Science 323, 1014-1015.

Corbett, D.R., Dillon, K., Burnett, W., Chanton, J. (2000) Estimating the groundwater contribution into Florida Bay via natural tracers, 222Rn and CH4. Limnology and Oceanography 45, 1546-1557.

Cyronak, T., Santos, I.R., Erler, D.V., Eyre, B.D. (2013) Groundwater and porewater as major sources of alkalinity to a fringing coral reef lagoon (Muri Lagoon, Cook Islands). Biogeosciences 10, 2467-2480.

Dalrymple, D.W., (1964) Recent Sedimentary Facies of Baffin Bay, Texas, Geology. Rice University, University Microfilms, Inc., Ann Arbor, Michigan.

Dickson, A.G., Sabine, C.L., Christian, J.R. (2007) Guide to best practices for ocean CO2 measurements.

Dimova, N., Burnett, W., Horwitz, E., Lane-Smith, D. (2007) Automated measurement of 224Ra and 226Ra in water. Applied radiation and isotopes 65, 428-434.

Dimova, N.T., Burnett, W.C., Speer, K. (2011) A natural tracer investigation of the hydrological regime of Spring Creek Springs, the largest submarine spring system in Florida. Continental Shelf Research 31, 731-738.

Dimova, N.T., Swarzenski, P.W., Dulaiova, H., Glenn, C.R. (2012) Utilizing multichannel electrical resistivity methods to examine the dynamics of the fresh water–seawater interface in two Hawaiian groundwater systems. Journal of Geophysical Research: Oceans 117.

Dong, L.F., Sobey, M.N., Smith, C.J., Rusmana, I., Phillips, W., Stott, A., Osborn, A.M., Nedwell, D.B. (2011) Dissimilatory reduction of nitrate to ammonium, not denitrification or anammox, dominates benthic nitrate reduction in tropical estuaries. Limnology and Oceanography 56, 279-291.

Dortch, Q. (1990) The interaction between ammonium and nitrate uptake in phytoplankton. Marine Ecology Progress Series, 183-201.

Douglas, A., Murgulet, D., Wetz, M.S., Spalt, N., (2017) Evaluating Groundwater Inflow and Nutrient Transport to Texas Coastal Embayments Phase II. Texas General Land Office, Texas General Land Office.

Driese, S.G., Nordt, L.C., Lynn, W.C., Stiles, C.A., Mora, C.I., Wilding, L.P. (2005) Distinguishing climate in the soil record using chemical trends in a Vertisol climosequence from the Texas Coast Prairie, and application to interpreting Paleozoic paleosols in the Appalachian Basin, USA. Journal of Sedimentary Research 75, 339-349.

du Plooy, S., Perissinotto, R., Smit, A., Muir, D. (2015) Role of salinity, nitrogen fixation and nutrient assimilation in prolonged bloom persistence of Cyanothece sp. in Lake St Lucia, South Africa. Aquatic Microbial Ecology 74, 73-83.

Dulaiova, H., Burnett, W.C., Chanton, J.P., Moore, W.S., Bokuniewicz, H.J., Charette, M.A., Sholkovitz, E. (2006) Assessment of groundwater discharges into West Neck Bay, New York, via natural tracers. Continental Shelf Research 26, 1971-1983.

Elsinger, R.J., Moore, W.S. (1980) 226Ra behavior in the pee Dee River-Winyah Bay estuary. Earth and Planetary Science Letters 48, 239-249.

EPA, U., (2011) 40 CFR APPENDIX B TO PART 136 - DEFINITION AND PROCEDURE FOR THE DETERMINATION OF THE METHOD DETECTION LIMIT-REVISION 1.11. U.S. Government Publishing Office.

Fetter, C.W. (2001) Applied Hydrogeology, Fourth Edition ed. Prentice-Hall, Inc., Upper Sadle River, New Jersey.

Fisk, H.N. (1959) Padre Island and the Laguna Madre flats, coastal south Texas. 2nd Coastal Geography COnfer, 103-151.

Folk, R.L., Siedlecka, A. (1974) The “schizohaline” environment: its sedimentary and diagenetic fabrics as exemplified by Late Paleozoic rocks of Bear Island, Svalbard. Sedimentary Geology 11, 1-15.

Garcia-Orellana, J., Cochran, J., Bokuniewicz, H., Daniel, J., Rodellas, V., Heilbrun, C. (2014) Evaluation of 224Ra as a tracer for submarine groundwater discharge in Long Island Sound (NY). Geochimica et Cosmochimica Acta 141, 314-330.

Garcia-Orellana, J., Rodellas, V., Casacuberta, N., Lopez-Castillo, E., Vilarrasa, M., Moreno, V., Garcia-Solsona, E., Masque, P. (2013) Submarine groundwater discharge: Natural radioactivity accumulation in a wetland ecosystem. Marine Chemistry 156, 61-72.

Gardner, W.S., McCarthy, M.J., An, S., Sobolev, D., Sell, K.S., Brock, D. (2006) Nitrogen fixation and dissimilatory nitrate reduction to ammonium (DNRA) support nitrogen dynamics in Texas estuaries. Limnology and Oceanography 51, 558-568.

George, P.G., Mace, R., Petrossian, R., (2011) Aquifers of Texas: Texas Water Development Board Report 380, p. 182.

Giblin, A.E., Gaines, A.G. (1990) Nitrogen inputs to a marine embayment: the importance of groundwater. Biogeochemistry 10, 309-328.

Giblin, A.E., Weston, N.B., Banta, G.T., Tucker, J., Hopkinson, C.S. (2010) The effects of salinity on nitrogen losses from an oligohaline estuarine sediment. Estuaries and Coasts 33, 1054-1068.

Glass, C., Silverstein, J. (1999) Denitrification of High-Nitrate, High-Salinity Wastewater. Water Resources Research 33, 223-229.

Holmes, R.M., Peterson, B.J., Deegan, L.A., Hughes, J.E., Fry, B. (2000) Nitrogen biogeochemistry in the oligohaline zone of a New England estuary. Ecology 81, 416-432.

Hu, C., Muller-Karger, F.E., Swarzenski, P.W. (2006) Hurricanes, submarine groundwater discharge, and Florida's red tides. Geophysical Research Letters 33.

Jolly, I.D., McEwan, K.L., Holland, K.L. (2008) A review of groundwater-surface water interactions in arid/semi-arid wetlands and the consequences of salinity for wetland ecology. Ecohydrology 1, 43-58.

Kadko, D., Cochran, J.K., Lyle, M. (1987) The effect of bioturbation and adsorption gradients on solid and dissolved radium profiles in sediments from the eastern equatorial Pacific. Geochimica et Cosmochimica Acta 51, 1613-1623.

Kattner, G. (1999) Storage of dissolved inorganic nutrients in seawater: poisoning with mercuric chloride. Marine Chemistry 67, 61-66.

Kelly, R., Moran, S. (2002) Seasonal changes in groundwater input to a well-mixed estuary estimated using radium isotopes and implications for coastal nutrient budgets. Limnology and Oceanography 47, 1796-1807.

Khalil, M.K., Rifaat, A.E. (2013) Seasonal fluxes of phosphate across the sediment-water interface in Edku Lagoon, Egypt. Oceanologia 55, 219-233.

Kim, G., Burnett, W., Dulaiova, H., Swarzenski, P., Moore, W. (2001) Measurement of 224Ra and 226Ra activities in natural waters using a radon-in-air monitor. Environmental science & technology 35, 4680-4683.

Knee, K.L., Garcia-Solsona, E., Garcia-Orellana, J., Boehm, A.B., Paytan, A. (2011a) Using radium isotopes to characterize water ages and coastal mixing rates: A sensitivity analysis. Limnology and Oceanography-Methods 9, 380-395.

Knee, K.L., Garcia-Solsona, E., Garcia-Orellana, J., Boehm, A.B., Paytan, A. (2011b) Using radium isotopes to characterize water ages and coastal mixing rates: A sensitivity analysis. Limnology and Oceanography: Methods 9, 380-395.

Kristensen, G.H., Jepsen, S. (1991) Biological Denitrification of Waste Water from Wet Lime–Gypsum Flue Gas Desulphurization Plants. Water Science and Technology 23, 691-700.

Kroeger, K.D., Swarzenski, P.W., Greenwood, W.J., Reich, C. (2007) Submarine groundwater discharge to Tampa Bay: Nutrient fluxes and biogeochemistry of the coastal aquifer. Marine Chemistry 104, 85-97.

Lambert, M.J., Burnett, W.C. (2003) Submarine groundwater discharge estimates at a Florida coastal site based on continuous radon measurements. Biogeochemistry 66, 55-73.

Lamontagne, S., La Salle, C.L.G., Hancock, G.J., Webster, I.T., Simmons, C.T., Love, A.J., James-Smith, J., Smith, A.J., Kämpf, J., Fallowfield, H.J. (2008) Radium and radon radioisotopes in regional groundwater, intertidal groundwater, and seawater in the Adelaide Coastal Waters Study area: implications for the evaluation of submarine groundwater discharge. Marine Chemistry 109, 318-336.

Lee, J.-M., Kim, G. (2006) A simple and rapid method for analyzing radon in coastal and ground waters using a radon-in-air monitor. Journal of environmental radioactivity 89, 219-228.

Li, B., Irvin, S. (2007) The comparison of alkalinity and ORP as indicators for nitrification and denitrification in a sequencing batch reactor (SBR). Biochemical Engineering Journal 34, 248-255.

Loáiciga, H.A. (2006) Modern-age buildup of CO2 and its effects on seawater acidity and salinity. Geophysical Research Letters 33.

Lohse, E.A., (1955) Dynamic geology of the modern coastal region, northwest Gulf of Mexico, in: Hough, J.L. (Ed.), Finding Ancient Shorelines: A Symposium with Discussions. Society of Economic Paleontologists and Mineralogists Special Publication, pp. 99-104.

Matson, E.A. (1993) Nutrient flux through soils and aquifers to the coastal zone of Guam (Mariana Islands). Limnology and Oceanography 38, 361-371.

Mendelssohn, I.A., Sorrell, B.K., Brix, H., Schierup, H.-H., Lorenzen, B., Maltby, E. (1999) Controls on soil cellulose decomposition along a salinity gradient in a Phragmites australis wetland in Denmark. Aquatic Botany 64, 381-398.

Militello, A., (1998) Hydrodynamics of wind-dominated, shallow embayments. Florida Institute of Technology, Melbourne, FL, p. 232.

Millero, F.J. (1993) What is PSU? Oceanography 6, 67-67.

Minor, E., Pothen, J., Dalzell, B., Abdulla, H., Mopper, K. (2006) Effects of salinity changes on the photodegradation and ultraviolet—visible absorbance of terrestrial dissolved organic matter. Limnology and Oceanography 51, 2181-2186.

Moore, W., (1996) Large groundwater inputs to coastal waters revealed by 226Ra enrichments.--p. 612-614. En: Nature (London)(United Kingdom).--Vol. 380, no. 6575 (1996).

Moore, W.S. (2006) Radium isotopes as tracers of submarine groundwater discharge in Sicily. Continental Shelf Research 26, 852-861.

Moore, W.S. (2010) The effect of submarine groundwater discharge on the ocean. Annual review of marine science 2, 59-88.

Murgulet, D., Murgulet, V., Spalt, N., Douglas, A., Hay, R.G. (2016) Impact of hydrological alterations on river-groundwater exchange and water quality in a semi-arid area: Nueces River, Texas. Sci Total Environ 572, 595-607.

Murgulet, D., Wetz, M.S., Douglas, A., McBee, W., Spalt, N., Linares, K., (2015) Evaluating Groundwater Inflow and Nutrient Transport to Texas Coastal Embayments. Texas General Land Office, Corpus Christi, TX.

NAAS, K., (2017) Kingsville, TX - Global Summary of the Month, in: NOAA (Ed.). NOAA, https://www.ncdc.noaa.gov/cdo-web/datasets/GSOM/stations/GHCND:USC00414810/detail.

NOAA, (2014) National Weather Service.

Nyquist, J.E., Freyer, P.A., Toran, L. (2008) Stream bottom resistivity tomography to map ground water discharge. Groundwater 46, 561-569.

Paerl, H.W. (1997) Coastal eutrophication and harmful algal blooms: Importance of atmospheric deposition and groundwater as "new" nitrogen and other nutrient sources. Limnology and Oceanography 42, 1154-1165.

Peterson, R.N., Burnett, W.C., Taniguchi, M., Chen, J., Santos, I.R., Ishitobi, T. (2008) Radon and radium isotope assessment of submarine groundwater discharge in the Yellow River delta, China. Journal of Geophysical Research 113.

Price, W.A. (1936) Reynosa problem of South Texas, and origin of caliche.

Prokopenko, M., Sigman, D., Berelson, W., Hammond, D., Barnett, B., Chong, L., Townsend-Small, A. (2011) Denitrification in anoxic sediments supported by biological nitrate transport. Geochimica et Cosmochimica Acta 75, 7180-7199.

RCRA SOP, (2009) Protocol for Groundwater/Surface Water Interface Sampling Using a Pore Water Sampler, in: Beneski, B., Bonenfant, E. (Eds.), Standard Operating Procedure Change Record. Department of Environmental Protection Bureau of Remediation and Waste Management RCRA Program.

Rebich, R.A., Houston, N.A., Mize, S.V., Pearson, D.K., Ging, P.B., Evan Hornig, C. (2011) Sources and Delivery of Nutrients to the Northwestern Gulf of Mexico from Streams in the South-Central United States. JAWRA Journal of the American Water Resources Association 47, 1061-1086.

Rusnak, G.A., (1960) Sediments of Laguna Madre, Texas, in: Shepard, F.P., Phleger, F.B., Van Andal, T.H. (Eds.), Recent Sediments, Northwest Gulf of Mexico. American Association of Petroleum Geologists, Tulsa OK, pp. 153-196.

Rysgaard, S., Thastum, P., Dalsgaard, T., Christensen, P.B., Sloth, N.P. (1999) Effects of salinity on NH4+ adsorption capacity, nitrification, and denitrification in Danish estuarine sediments. Estuaries 22, 21-30.

Santoro, A.E. (2010) Microbial nitrogen cycling at the saltwater–freshwater interface. Hydrogeology Journal 18, 187-202.

Santos, I.R., Cook, P.L., Rogers, L., Weys, J.d., Eyre, B.D. (2012) The "salt wedge pump": Convection-driven pore-water exchange as a source of dissolved organic and inorganic carbon and nitrogen to an estuary. Limnology and Oceanography 57, 1415-1426.

Schiavo, M., Hauser, S., Povinec, P. (2009) Stable isotopes of water as a tool to study groundwater–seawater interactions in coastal south-eastern Sicily. Journal of Hydrology 364, 40-49.

Schulz, H.D., Dahmke, A., Schinzel, U., Wallmann, K., Zabel, M. (1994) Early diagenetic processes, fluxes, and reaction rates in sediments of the South Atlantic. Geochimica et Cosmochimica Acta 58, 2041-2060.

Shafer, G.H., Baker, E.T. (1973) Ground-water resources of Kleberg, Kenedy, and southern Jim Wells counties, Texas.

Simms, A.R., Aryal, N., Miller, L., Yokoyama, Y. (2010) The incised valley of Baffin Bay, Texas: a tale of two climates. Sedimentology 57, 642-669.

Smith, C.G., Robbins, L.L., (2012) Surface-Water Radon-222 Distribution along the Western-Central Florida Shelf. U.S. Geological Survey, p. 26.

Spalt, N., Murgulet, D., Hu, X. (2018) Relating estuarine geology to groundwater discharge at an oyster reef in copano bay, TX. Journal of Hydrology.

Stagg, C.L., Schoolmaster, D.R., Krauss, K.W., Cormier, N., Conner, W.H. (2017) Causal mechanisms of soil organic matter decomposition: deconstructing salinity and flooding impacts in coastal wetlands. Ecology.

Steinke, T., Charles, L. (1986) In vitro rates of decomposition of leaves of the mangrove Bruguiera gymnorrhiza as affected by temperature and salinity. South African Journal of Botany 52, 39-42.

Sun, Y., Torgersen, T. (1998) The effects of water content and Mn-fiber surface conditions on 224Ra measurement by 220Rn emanation. Marine Chemistry 62, 299-306.

Swarzenski, P. (2007) U/Th series radionuclides as coastal groundwater tracers. Chemical Reviews 107, 663-674.

Swarzenski, P.W., Reich, C., Kroeger, K.D., Baskaran, M. (2007) Ra and Rn isotopes as natural tracers of submarine groundwater discharge in Tampa Bay, Florida. Marine Chemistry 104, 69-84.

Takahashi, T., Broecker, W.S., Bainbridge, A.E. (1981) The alkalinity and total carbon dioxide concentration in the world oceans. Carbon cycle modelling, SCOPE 16, 271-286.

TCEQ, (2012) Surface Water Quality Monitoring Procedures, Volume 1: Physical and Chemical Monitoring Methods, Austin, TX.

TCOON, (2016) Historical Standard Meteorological Data - Station BABT2 - 8776604 - Baffin Bay, TX, in: Network, T.C.O.O. (Ed.). National Oceanic and Atmospheric Administration, National Data Buoy Center.

TWDB, (2016) Hydrology for the Laguna Madre Estuary Watershed, in: Studies, C.f.W.S. (Ed.).

Uddameri, V., Singaraju, S., Hernandez, E.A. (2013) Temporal variability of freshwater and pore water recirculation components of submarine groundwater discharges at Baffin Bay, Texas. Environmental Earth Sciences 71, 2517-2533.

Urquidi-Gaume, M., Santos, I.R., Lechuga-Deveze, C. (2016) Submarine groundwater discharge as a source of dissolved nutrients to an arid coastal embayment (La Paz, Mexico). Environmental earth sciences 75, 1.

USDA, (2012) National Soil Survey Handbook, Title 430-VI.

USGS, (2017a) USGS 08211900 San Fernando Ck at Alice, TX, in: Inquiries, U.T.W.S.C.W.-D. (Ed.). National Water Information System: Web Interface.

USGS, (2017b) USGS 08212400 Los Olmos Ck nr Falfurrias, TX, in: Center, U.T.W.S. (Ed.). National Water Information System: Web Interface.

USGS, (2018) USGS 08212300 Tranquitas Ck at Kingsville, TX, in: Inquiries, U.T.W.S.C.W.-D. (Ed.). National Water Information System: Web Interface.

Wanninkhof, R. (1992) Relationship between wind speed and gas exchange over the ocean. Journal of Geophysical Research: Oceans 97, 7373-7382.

Ward, G.H., Armstrong, N.E. (1997) Current Status and Historical Trends of Ambient Water, Sediment, Fish and Shellfish Tissue Quality in the Corpus Christi Bay National Estuary Program Study Area: Summary Report. Natural Resources Center, TAMU-CC.

Waterstone, Parsons, (2003) Groundwater availability of the central Gulf Coast aquifer--Numerical simulations to 2050, Central Gulf Coast, Texas.

Webster, I.T., Hancock, G.J., Murray, A.S. (1995) Modelling the effect of salinity on radium desorption from sediments. Geochimica et Cosmochimica Acta 59, 2469-2476.

Welschmeyer, N.A. (1994) Fluorometric analysis of chlorophyll a in the presence of chlorophyll b and pheopigments. Limnology and Oceanography 39, 1985-1992.

Weston, N.B., Dixon, R.E., Joye, S.B. (2006) Ramifications of increased salinity in tidal freshwater sediments: Geochemistry and microbial pathways of organic matter mineralization. Journal of Geophysical Research: Biogeosciences 111.

Wetz, M.S., (2015) Baffin Bay Volunteer Water Quality Monitoring Study: Synthesis of May 2013-July 2015 Data. Coastal Bend Bays & Estuaries Program, pp. 1-28.

Wetz, M.S., Cira, E.K., Sterba-Boatwright, B., Montagna, P.A., Palmer, T.A., Hayes, K.C. (2017) Exceptionally high organic nitrogen concentrations in a semi-arid South Texas estuary susceptible to brown tide blooms. Estuarine, Coastal and Shelf Science 188, 27-37.

Windom, H., Niencheski, F. (2003) Biogeochemical processes in a freshwater–seawater mixing zone in permeable sediments along the coast of Southern Brazil. Marine Chemistry 83, 121-130.

Winn, C.D., Li, Y.-H., Mackenzie, F.T., Karl, D.M. (1998) Rising surface ocean dissolved inorganic carbon at the Hawaii Ocean Time-series site. Marine Chemistry 60, 33-47.

Wood, W.W., (1976) Guidelines for collection and field analysis of ground-water samples for selected unstable constituents. US Geological Survey.